ADVANCED FUNCTIONAL MATERIALS
www.afm-journal.de

Biodegradable Piezoelectric Materials: Powering the Future of Bioelectronic Medicine

Zijian Wang, Changxu Chen, Hongyu Meng, He Lian, Xi Cui,* Chao Zhang,* and Zhou Li**

Piezoelectric materials have become a research hotspot in bioelectronic medicine due to their excellent electromechanical conversion properties. In particular, biodegradable piezoelectric materials can avoid the risk of secondary removal surgeries, revealing great potential in clinical applications. This review summarizes the types, mechanisms, and properties of representative degradable piezoelectric materials, including amino acids, peptides, polysaccharides, and synthetic polymers. The processing strategies and the progress of their application in biomedical applications are further demonstrated. Finally, challenges and perspectives of the development of degradable piezoelectric materials are also discussed.

1. Introduction

Endogenous bioelectric fields play fundamental roles in orchestrating biological processes, including embryonic development, tissue regeneration, and metabolic regulation. These intrinsic electrical cues are dynamically generated through ion channel activity and mechanical forces within living systems, serving as critical regulators of cellular behaviors such as migration, differentiation, and apoptosis. Piezoelectric materials, characterized by their inherent ability to convert mechanical stimuli (e.g., ultrasound waves, physiological motion, cellular traction forces) into electrical signals through the piezoelectric effect, have emerged as promising tools to mimic or amplify these endogenous bioelectric patterns. By delivering localized electrical stimulation without external power sources, piezoelectric platforms enable real-time, self-powered therapeutic interventions, thereby unlocking revolutionary potential in implantable medical devices, tissue engineering scaffolds, and regenerative medicine.

However, conventional piezoelectric materials face significant challenges in clinical translation due to their limited biocompatibility and non-degradable nature. For instance, lead-based piezoceramics (e.g., PZT) exhibit high piezoelectric coefficients d_{33} of ≈300–600 pC N^{-1}[1,2] but raise concerns over cytotoxicity from lead leaching and chronic inflammation risks. on the other hand, their inherent brittleness and mismatched mechanical properties (e.g., elastic modulus ≈60–100 GPa for PZT[1,3,4] vs ≈0.1–20 GPa for soft tissues[5,6]) further hinder integration with dynamic biological environments, often necessitating secondary surgical removal. Similarly, commercial piezoelectric polymers (e.g., polyvinylidene fluoride, PVDF), with mechanical flexibility, are also virtually non-degradable. Their limitations underscore the urgent need for more suitable piezoelectric biomaterials that harmonize electromechanical performance with biocompatibility and programmed degradability.

In this context, biodegradable piezoelectric materials—spanning amino acid crystals, peptide-based assemblies, and polymers—have recently gained prominence. These materials uniquely combine piezoelectricity, tunable degradation kinetics, and metabolic clearance pathways, thereby addressing the critical demands of biomedical implants. For example, piezoelectric polymers such as poly(L-lactic acid) (PLLA) and copolymer systems have been engineered to degrade into non-toxic byproducts (e.g., lactic acid) over weeks to months, aligning with tissue repair timelines.[7] Concurrently, bioinspired materials such as glycine-rich peptide nanowires and cellulose-based composites demonstrate

Z. Wang, H. Lian
School of Medical Instrumentation
Shenyang Pharmaceutical University
Shenyang 110016, China
E-mail: lianhe@syphu.edu.cn
Z. Wang, C. Chen, H. Meng, X. Cui, Z. Li
Beijing Institute of Nanoenergy and Nanosystems
Chinese Academy of Sciences
Beijing 101400, China
E-mail: cuixi@binn.cas.cn; li_zhou@tsinghua.edu.cn
C. Chen
School of Nanoscience and Engineering
University of Chinese Academy of Sciences
Beijing 100049, China
Z. Wang, X. Cui, C. Zhang
School of Biomedical Engineering
Shenzhen Campus of Sun Yat-Sen University
Shenzhen 518107, China
E-mail: zhchao9@mail.sysu.edu.cn
Z. Li
Tsinghua Changgung Hospital
School of Clinical Medicine
Tsinghua University
Beijing 100084, China
Z. Li
School of Biomedical Engineering
Tsinghua University
Beijing 100084, China

The ORCID identification number(s) for the author(s) of this article can be found under https://doi.org/10.1002/adfm.202519501

DOI: 10.1002/adfm.202519501

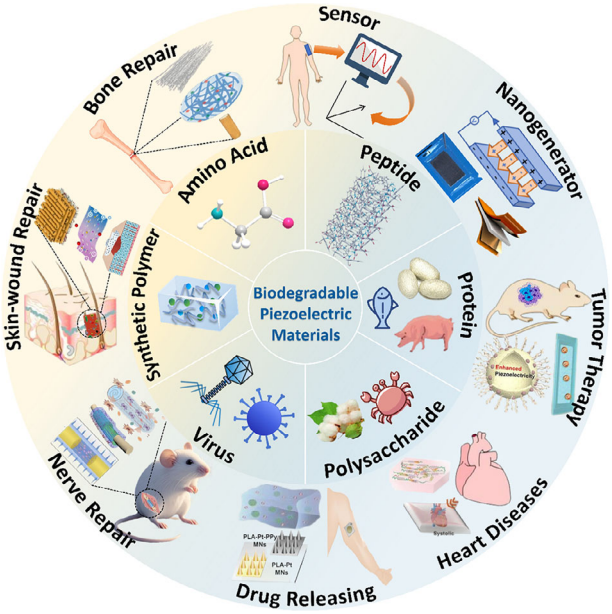

Figure 1. Classification and Applications of Piezoelectric Materials. Advancements in biodegradable piezoelectric biomaterials and emerging applications in the medical field, such as bone repair, skin-wound repair, nerve repair, drug releasing, heart disease therapy, tumor therapy, nanogenerator, and flexible sensor.

piezoelectric responses derived from their hierarchical crystalline structures,[8,9] offering enhanced integration with biological systems. Recent advances in material synthesis and processing—including molecular alignment techniques,[10] hybridization with bioactive agents,[11] and structural optimization[12]—have further expanded their functionality for targeted applications in bone remodeling, neural regeneration, and wound healing.

This review systematically examines the evolving landscape of biodegradable piezoelectric biomaterials. We first elucidate the classification of piezoelectric materials based on their crystallographic origins and electromechanical coefficients, establishing a foundation for understanding performance benchmarks. Subsequently, we analyze degradable piezoelectric materials. As shown in **Figure 1**, we first classified biodegradable piezoelectric materials into amino acids, peptides, proteins, polysaccharides, viruses, and synthetic polymers. And then we emphasize their molecular design principles, physicochemical properties, and biomedical relevance. These devices based on biodegradable piezoelectric materials can be used for bone repair, skin wound healing, nerve repair, drug release, heart disease treatment, tumor therapy, power generation, and as sensors to monitor human movement. A dedicated section discusses advanced fabrication strategies (e.g., electrospinning,[13] 3D printing,[14] and solvent casting[15]) to tailor material architectures for specific therapeutic needs. Finally, we highlight persisting challenges in balancing piezoelectric output with degradation profiles, scaling up production, and ensuring long-term biosafety, while outlining future directions in computational material design, closed-loop therapeutic systems, and clinical validation protocols.

2. Classification of Piezoelectric Materials: Crystallographic Origins and Electromechanical Coefficients

2.1. Fundamentals of the Piezoelectric Effect

The piezoelectric phenomenon was first discovered in 1880 by the Curie brothers, who observed the generation of electric charges in natural single-crystal α-quartz and Rochelle salt ($NaKC_4H_4O_6{\cdot}4H_2O$) under mechanical stress.[16] This unique property originates from the non-centrosymmetric crystal structure of materials, where mechanical deformation disrupts the spatial symmetry of atoms/ions, leading to the displacement of positive and negative charge centers and the formation of electric dipoles. Since its discovery, diverse piezoelectric materials have been extensively studied and applied in technologies such as ultrasonic transducers,[17] vibration sensors,[18] and pressure detectors.[19] In response to the toxicity and environmental concerns associated with Pb^{2+} ions, the development of lead-free piezoelectric ceramics began in 1962.[20] Key lead-free systems include (Bi, Na)TiO_3 (BNT), (Na, K)NbO_3 (NKN), Li-modified (Na, K)NbO_3, and tungsten bronze (TB) structures. A significant milestone was achieved in 2006 when Wang et al.[21] introduced the concept of self-powered piezoelectric devices using ZnO nanowire arrays to enable nanoscale conversion between mechanical and electrical energy.

In inorganic piezoelectric materials, the alignment of dipoles arises from the non-centrosymmetric arrangement of constituent atoms or ions. As illustrated in **Figure 2a**, the wurtzite structure of ZnO exhibits a hexagonal lattice symmetry that lacks inversion centers. Mechanical strain distorts this lattice, generating surface charges proportional to the applied stress. For organic piezoelectric polymers (Figure 2b), dipolar moments stem from differences in electronegativity between backbone atoms (e.g., carbon and fluorine in PVDF) and functional groups arranged in asymmetric conformations (e.g., chiral chains, helical structures, or hydrogen-bonded networks). The piezoelectric response of such polymers is highly dependent on crystallinity, as aligned molecular chains enhance dipole orientation.

The piezoelectric constant d_{ij} quantifies a material's ability to convert mechanical stress into electrical charge, and it is commonly expressed in units of pC/N (charge coefficient) or pm/V (strain coefficient). A higher d_{ij} value indicates greater charge displacement per unit stress. Relationships between applied stress, strain, and induced voltage are governed by a 3D tensor system. As shown in Figure 2c, the directionality of piezoelectric responses varies with the mode of stress application. For example, the "33-mode" describes voltage generation along the same axis as the applied compressive stress, while shear-induced responses are classified as "14-mode," "15-mode," or others. Notably, materials often exhibit the highest piezoelectric coefficients along specific crystallographic orientations.[22]

2.2. Classification Based on Crystallographic Origins

The electromechanical response of piezoelectric materials is intrinsically governed by their crystallographic symmetry. Among the 32 crystallographic point groups, only the 20

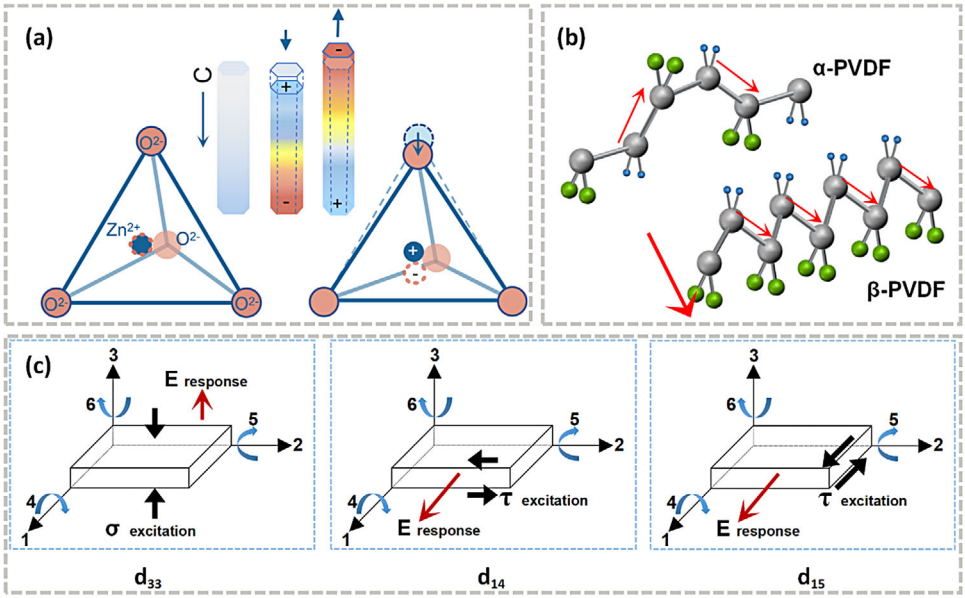

Figure 2. Piezoelectric mechanisms and different modes in inorganic and organic piezoelectric materials. a) Piezoelectric properties of inorganic piezoelectric materials exemplified by zinc oxide. b) The piezoelectric properties of organic piezoelectric materials—exemplified by the synthetic polymer PVDF (poly(vinylidene fluoride)) in its α-phase and β-phase—are illustrated as follows: small arrows stand for intrachain dipole moments, and large arrows stand for net dipole moments. The upper one corresponds to the α-phase of PVDF, where the intrachain dipole moments are arranged in a helical structure; because of this helical arrangement, their dipole moments cancel each other out, resulting in no net dipole moment at the macroscopic level. The lower one corresponds to the β-phase of PVDF, where the intrachain dipole moments are arranged in-phase; due to this in-phase arrangement, a distinct net dipole moment is generated at the macroscopic level. c) Relationship between piezoelectricity and stress direction in different piezoelectric modes.

non-centrosymmetric classes lack inversion centers, enabling strain-induced polarization.[23] Perovskites (e.g., PZT, $BaTiO_3$) adopt tetragonal (P4mm) or rhombohedral (R3m) phases under external fields, where cooperative oxygen octahedron tilting creates switchable spontaneous polarization. In contrast, the hexagonal wurtzite structure of ZnO allows piezoelectricity through ionic displacement along the polar *c*-axis, while orthorhombic PVDF relies on aligned C-F dipoles in β-phase crystallites. Natural biomaterials like collagen exhibit weak piezoelectricity due to limited long-range order of polar amino acid residues, highlighting the role of lattice periodicity in optimizing electromechanical coupling.″

2.3. Classification by Electromechanical Performance and Degradability

From a translational perspective, piezoelectric materials are classified into three categories based on the interplay between electromechanical output and biodegradability: 1) High-performance inorganics: Compounds like PZT and AlN achieve exceptional piezoelectric coefficients via rigid ionic lattices, yet their non-degradability and non-biocompatibility (e.g., Pb^{2+} leaching) restrict chronic implantation. 2) Engineered organics: Semi-crystalline polymers (e.g., PVDF, PLLA) balance flexibility (modulus 2–4 GPa) and hydrolytic degradation by tailoring chain conformation. For instance, stretched β-phase PVDF films attain d_{33} ≈20–30 pC N^{-1}[24–27] through aligned C-F dipoles, whereas shear piezoelectricity in PLLA d_{14} ≈10 pC N^{-1} originates from helical chain packing. However, their incomplete degradation (decadal timescales for PVDF) and byproduct toxicity necessitate molecular redesign. 3) Biomolecule: Natural polymers such as chitin and cellulose exhibit intrinsic biocompatibility but display weak piezoelectric responses, necessitating structural hybridization (e.g., nanocomposites, chemical grafting) to amplify electromechanical performance. Emerging biohybrid systems bridge this gap by integrating biodegradability with enhanced piezoelectricity. For instance, γ-phase glycine crystals achieve inorganic-like piezoelectric coefficients while degrading into non-toxic amino acids within weeks. Similarly, β-sheet nanofibrils self-assembled from diphenylalanine dipeptides demonstrate bone-mimetic mechanical compliance and a programmable degradation window, though challenges persist in maintaining piezoelectric stability under humid environments and scaling up crystallographic uniformity during synthesis.

3. Degradable Piezoelectric Materials

While traditional piezoelectric ceramics and synthetic polymers dominate in electromechanical performance, their limited biodegradability and potential biotoxicity hinder sustainable biomedical applications. Then, since the discovery of the first semi-organic ferroelectric—Rochelle salt, lead-free dot materials have become another focus of research.[28] Recent advancements highlight piezoelectric biomolecules (e.g., proteins, cellulose, chitosan(CS)) as emerging alternatives that uniquely integrate biocompatibility, tunable degradation kinetics, and minimal environmental footprint. These natural polymers inherently

avoid chronic immune rejection risks due to their biomimetic composition, while enzymatic/chemical degradation pathways ensure complete resorption into metabolic byproducts (e.g., amino acids, glucose).[29–31] Additionally, their low dielectric constants reduce energy dissipation in dynamic physiological environments, significantly enhancing charge transfer efficiency in bioelectronic interfaces. From a chemical design perspective, degradable piezoelectric polymers can be systematically classified into two categories based on their structural origins.

3.1. Natural Piezoelectric Materials

Nature itself offers an inspirational solution: piezoelectricity is not merely a synthetic phenomenon but an evolutionary strategy widely exploited by biological systems (from DNA deformation to bone remodeling) for mechanoelectrical signal transduction. Due to the inherent asymmetry within the structure of natural biological small molecule crystals, many of them exhibit piezoelectricity,[32] and scientists have already taken the viruses, fish bladders, and prawn shells as piezoelectric materials to manufacture piezoelectric materials, and various piezoelectric coefficient of different degradable piezoelectric materials are summarized in **Table 1**. Since then, more and more researchers have worked on the investigation of piezoelectric biodegradable materials. These organic biological materials like proteins, collagen, and chitin are easily available and possess excellent piezoelectricity. Hence, we will discuss these materials comprehensively.

3.1.1. Amino Acids, Peptides, and Proteins

Amino acids, the fundamental constituents of peptides and proteins, emerge as a unique class of naturally piezoelectric materials, combining intrinsic biocompatibility with the ability to convert mechanical energy into electricity. Their inherent molecular asymmetry, arising from diverse functional side chains (—COOH, $-NH_2$, and others) and directional intermolecular interactions (hydrogen bonds, π–π stacking), facilitates non-centrosymmetric crystal packing—a critical requirement for piezoelectric activity. For instance, glycine, a representative amino acid, relies on specific stabilization strategies to maintain its piezoelectric phases[22,33] while diphenylalanine peptides, typical of piezoelectric peptides, achieve ordered structures via self-assembly for performance optimization.[16,34] Vasilescu et al.[35] conducted the first experiment about investigating the piezoelectricity of amino acids and demonstrated its piezoelectricity in many samples which attributed to their zwitterionic character and polar crystal lattices. These materials underpin innovative biomedical devices—from glycine-embedded chitosan sensors monitoring physiological signals to self-assembled peptide nanogenerators driving localized cancer therapies.

Glycine: Among the 20 kinds of common amino acids, glycine has a non-chiral structure, and it's the simplest amino acid among the piezoelectricity biomaterials. Moreover, glycine is an essential precursor in numerous biosynthetic pathways, such as the synthesis of glutathione, purines, and heme.[36] When glycine materials are implanted into the body as devices, water-soluble glycine will be absorbed by peripheral cells or enter the blood circulation to participate in subsequent protein synthesis or energy metabolism after contact with body fluids, and finally be metabolized to water, carbon dioxide, and urea. Glycine is a polymorphic crystal which has three crystal polymorphs including α, β, and γ crystal structures[32] (**Figure 3a**). The α-glycine is a centrosymmetric crystal so that it does not show any piezoelectricity. And the β-glycine and γ-glycine are predicted to be with piezoelectricity due to their non-centrosymmetric structure. Lemanov et al.[37] tested the piezoelectric response of crystalline powders under high-frequency (≈10 MHz) electric pulses and noticed that β-glycine and DL-alanine possess the best piezoelectric performance which is compared to or even exceeds quartz crystals. Guerin et al.[22] measured a strong shear piezoelectric coefficient d_{16} of ≈178 pC N^{-1} in β-glycine guided by quantum mechanical calculations and the γ-glycine is predicted to show a high longitudinal piezoelectric coefficient d_{33} of ≈10.4 pC N^{-1}. Under ambient conditions, the relative thermo-dynamic stabilities of three glycine following the order $\gamma > \alpha > \beta$, which means β-glycine easily tends to transform into α- or γ-glycine phase and is challenging to obtain in kinetics and maintain its stability under ambient conditions. Thus, the strategies of active self-assembly,[38] growing on the substrate,[39] simple solution-casting technique[40] and electrospinning[41] are proposed to obtain stable β-glycine with excellent piezoelectric performances.

Inspiring by the researches on piezoceramics within a century, Zhang et al.[38] proposed an active self-assembly methodology to manufacture piezoelectric β-glycine films resembling the inorganic polycrystalline morphology. They adopted the electrohydrodynamic spray method which strategically coupled nanoconfinement effects with electric fields to mimic two critical processes in conventional piezoceramic fabrication: high-temperature sintering and electrical poling. During crystallization, the applied fields served for two purposes—directing the nucleation of β-glycine nanocrystals while simultaneously inducing in situ dipole alignment across the growing crystalline domains. This synergistic control yielded continuous, densely packed films (Figure 3b) and enabled such film to exhibit exceptional piezoelectricity and thermodynamic stability. Structural characterization revealed a piezoelectric strain coefficient of 11.2 pm V^{-1} and the thermostability is effectively improved before melting (192 °C). Based on this film, they further fabricated a 10 μF capacitor with an average charging speed of 90 nC s^{-1}, demonstrating its ability to serve as a stable power source for implanted devices. Moreover, after 24 000 compression cycles, its output performance remains almost unchanged, demonstrating its excellent stability.

A lot of studies have focused on the stability of polycrystalline technology so far. Like crystal growth in nanoscale crystallization chambers, on patterned substrate or Pt-coated Sing substrate,[44–46] and in the recent work, Seyedhosseini et al.[39] reported a quite stable self-assembled β-glycine with piezoelectricity grown on the Si substrate. However, it's extremely rigid while in contact with the rigid silicon substrate, and small size makes it hard to use it to fabricate any flexible devices. For solving this problem, Hosseini et al.[40] prepared β-glycine/chitosan (β-Gly/CS) films (Figure 3c-i) by dissolving glycine powder in chitosan polymer solution via a simple solution-casting technique. They successfully synthesized the oriented and stable β-glycine crystals within chitosan through regulating the composition of glycine and chitosan. The sensors based on such film can be

Table 1. Piezoelectric coefficients of representative degradable materials.

Type	Piezoelectric materials	Piezoelectric coefficient	Degradation rate	Mechanical modulus	Refs.
Amino acid	Alanine	$d_{24} = 17.75$ pC N^{-1}	–	–	[132]
	Cysteine	$d_{22} = 11$ pC N^{-1}	–	E = 6GPa	[22]
	β-Glycine	$d_{16} = 178$ pC N^{-1}	–	E = 26GPa	[22]
		$d_{33} = 7.2$ pC N^{-1}	In vitro: Gly-Alg-Glycerol composite membrane fully dissolved within 2 h Poly(lactic acid) (PLA) + beeswax encapsulation extends stability to 5 days In vivo: Complete disappearance within 1 day; encapsulation extends stability to >5 days	E ≈50MPa (1% glycerol and Gly/Alg = 1:1)	[42]
		$d_{33} = 19$ pC N^{-1}	Pure crystals in PBS solution fully degrade within 120 days. PCL encapsulation (90μm thickness) fails within 10 days. PCL encapsulation (260μm thickness) fails within 25 days.	E = 32MPa	[41]
		$d_{33} = 4.15$ pm V^{-1}	Fully degrades within 6 weeks	>25GPa	[43]
		–	Without encapsulation, it degrades within days in PBS solution. After PLGA encapsulation, it can last up to 30 days.	1.5–15GPa	[40]
		$d_{33} = 11.2$ p.m. V^{-1}	–	–	[38]
	γ-Glycine	$d_{33} = 10.4$ pC N^{-1}	–	E = 49GPa	[22]
		$d_{33} = 5.3$ pC N^{-1}	In vitro: Complete dissolution within 5 min; PLA encapsulation leads to failure after 6 days and degradation within 10 weeks. In vivo: Complete disappearance within 1 day; encapsulation results in failure after 3–5 days.	Gly:PVA = 2:1 Young's modulus ≈4.0 GPa Tensile strength ≈10 MPa	[48]
		$d_{33} = 6.13 \pm 1.13$ pC N^{-1}	–	–	[49]
		$d_{33} = 8.2$ pC N^{-1}	10min	Composite film<2*10^{3}MPa	[50]
	DL-alanine	$d_{33} = 5$ pC N^{-1}	–	–	[52]
	Proline	$d_{25} = 27.75$ pC N^{-1}	–	E = 23.95 GPa	[133]
Peptide	Diphenylalanine (FF)	$d_{15} = 80$ pC N^{-1}	–	E = 10–31 GPa	[134]
		$d_{33} = 10.025 \pm 0.33$ pC N^{-1}	–	E = 0.409 ± 0.031 MPa	[65]
	Poly (γ-benzyl α,L-glutamate) (PBLG)	$d_{33} = 25$ pC N^{-1}	–	E = 3 GPa	[33]
		$d_{33} = 23$ pC N^{-1}	–	–	[67]
Protein	Collagen	$d_{14} = 12$ pC N^{-1}	–	–	[78]
	Keratin	$d_{14} = 1.8$ pC N^{-1}	–	–	[135]
	Silk	$d_{14} = 1.5$–5 pC N^{-1}	No change observed after 10 weeks in the PBS environment. Half-life ≈39.8 days in 1 mg mL^{-1} protein environment.	–	[136]
Polysaccharides	Cellulose	$d_{33} = 19.3 \pm 2.9$ pm V^{-1}	–	–	[137]
		$d_{33} = 27.2$ pm V^{-1}	It degrades completely in PBS (37 °C) within 100 days and degrades by half at 74 °C within 14 days.	–	[73]
		$d_{33} = 31$ pm V^{-1}	–	E = 8.2 GPa	[74]
	Chitosan	$d_{33} = 18.4$ pC N^{-1}	–	–	[138]
	Chitin	$d_{33} = 9.49$ pC N^{-1}	No attenuation for one year after encapsulation.	Pure CNF: Y = 187.5 N mm^{-2} CNF/PVDF composite film: Y = 538 N mm^{-2}	[139]
Polyester	Poly (D-lactic acid) PDLA	$d_{14} = 2.28$ pC N^{-1}	–	–	[140]

(*Continued*)

Table 1. (Continued)

Type	Piezoelectric materials	Piezoelectric coefficient	Degradation rate	Mechanical modulus	Refs.
	Poly (L-lactic acid) PLLA	d_{14} = 10 pC N^{-1}	–	Modulus of elasticity c = 2 GN m^{-2} (50 °C)	[135]
	2,2,3,3,4,4-hexafluoropentane-1,5-diol (HFPD)	d_{33} = 138 pC N^{-1}	Complete degradation within 1 h in vitro. Reduced to 21.1% within 24 h in vivo.	(100) plane E = 6.14 GPa (010) plane E = 8.85 GPa (001) plane E = 4.3 GPa	[141]
Composite	Glycine-polyvinyl Alcohol(PVA)	d_{33} = 5.3 pC N^{-1}	In vitro: Unencapsulated degradation within 5 min; Encapsulated degradation within 10 weeks. In vivo: Unencapsulated degradation within 1 day.	Composite membrane E = 4–9 GPa Pure component E = 30 Gpa Pure component E = 0.2 Gpa	[48]

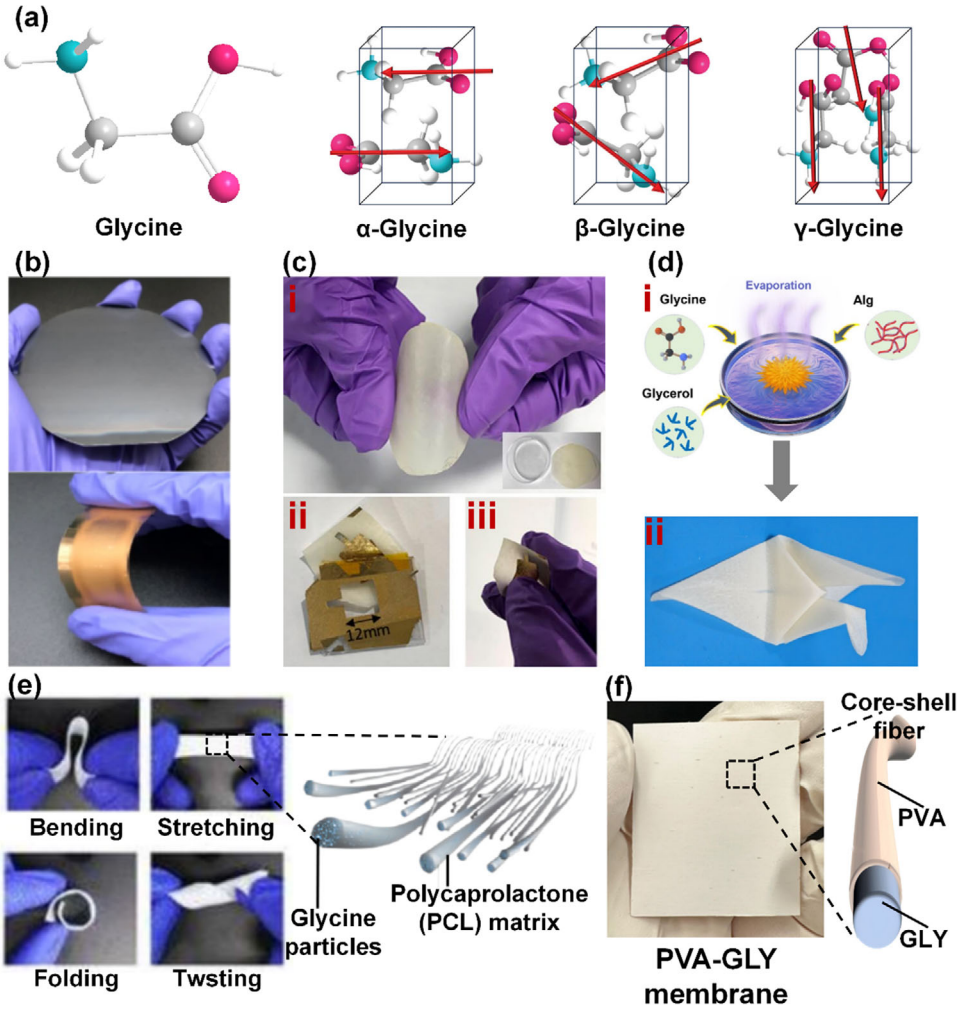

Figure 3. Piezoelectric Device Based on β-Glycine. a) The chemical structure of glycine and the crystal structures of glycine in three conformations. Reproduced with permission.[32] Copyright 2024, Wolters Kluwer Health, Inc. b) Photographs of a film on a 4-inch silicon wafer (up) and film on a flexible gold-coated polyethylene terephthalate (PET) substrate (down). Reproduced with permission.[38] Copyright 2023, Springer Nature c-i) Optical images of the glycine/chitosan (Gly/CS) film and c-ii) film with gold-coated electrodes and c-iii) the fabricated flexible Gly/CS sensor. Reproduced with permission.[40] Copyright 2020, American Chemical Society d-i) Schematic illustration of the synthetic approach for the Gly-Alg-Glycerol piezoelectric films. d-ii) An origami pigeon made of a piece of Gly-Alg-Glycerol film. Reproduced with permission.[42] Copyright 2024, Oxford University Press. e) Optical images of Gly-PCL films in various forms(left) and schematic illustration of Gly-PCL nanofibers(right). Reproduced with permission.[41] Copyright 2023, The American Association for the Advancement of Science. f) The optical image of PVA-GLY nanofiber membrane(left) and the schematic illustration of the PVA-GLY nanofiber(right). Reproduced with permission.[43] Copyright 2024, Elsevier.

completely degraded within a few days in phosphate-buffered saline (PBS) solution (pH = 7.4), and the degradation cycle of the sensor can be adjusted by using different materials for encapsulation. For example, when poly(L-lactide-co-glycolide) (PLGA) is used, the degradation cycle can reach 30 days. Notably, compared to the nondegradable commercial piezoelectric materials, this developed biodegradable β-glycine/chitosan-based piezoelectric film exhibited a high sensitivity (≈2.82 ± 0.2 mV kPa^{-1}). However, due to multiple spherulite domains in such glycine-chitosan film that have different polarization orientations, leading to partially canceling out and weaking macroscopic piezoelectricity.

Meanwhile, Lin et al.[42] embedded the pure β-glycine crystals in alginate (Alg) and glycerol matrix to fabricated piezoelectric films by a simple solvent-casting method as well (Figure 3d-i). Unlike the previous researches, in Lin's work, the β-glycine formed a single, monolithic spherulite, instead of multiple spherulites, resulted in endowing the Gly-Alg-Glycerol piezoelectric films with outstanding piezoelectricity, including a high piezoelectric constant (7.2 pC N^{-1}) and a high piezoelectric sensitivity (1.97 mV kPa^{-1}). In vivo experiments have demonstrated such Gly-Alg-Glycerol films could serve as a sensor to detect the physiological pressure signals. However, due to its excellent water solubility, once the device came into contact with body fluids, it would dissolve, and the output voltage would drop sharply. Therefore, it needed to be sealed with degradable materials such as polylactic acid (PLA). Moreover, the Gly-Alg-Glycerol films were flexible enough to be easily processed into complex shapes like an origami pigeon (Figure 3d-ii). Solvent-casting methods acted as a relatively simple way to effectively harvest the piezoelectricity of β-glycine. But lacking the control over crystal growth direction leaded to the random orientations of crystal domain/dipole moments which resulted in a phenomenon that though every single glycine crystal exhibited a high piezoelectricity, the overall film possessed a low piezoelectric output. Thus, there is an urgent need for a newly flexible, and easy method to make oriented glycine crystals.

For overcoming the limitations of solvent casting in crystal orientation control, researchers have explored new strategies. Chorsi et al.[41] adopted the electrospinning technology to manufacture glycine-PCL nanofibers possessed (Figure 3e-ii) highly oriented glycine crystals at a large scale. And they found that, compared with the glycine crystal films generated by conventional solvent-cast, such glycine-PCL nanofibers exhibit a more excellent ability to produce a high actuation performance (i.e., the ability to transform electricity into movement). Moreover, it had a high piezoelectric coefficient d_{33} of 19 pC N^{-1} and a high ultrasound (US) output of 334 kPa which is superior to the most advanced transducers. And they make this material into an ultrasound transducer as a novel treatment platform for glioblastoma therapy. Finally, they determined that the working life of the transducer in PBS solution (37 °C) was 10 to 25 days, and indicated that this depended on the thickness of the PLA encapsulation layer. Also, take advantage of the benefits of electrospinning technology, Wang et al.[43] successfully fabricated the polyvinyl alcohol (PVA)-Gly nanofiber membrane (Figure 3f-ii) through the electrospinning of the mixed PVA-Gly solution, and these fabricated PVA-Gly fibers showed high piezoelectricity (≈4.15 pm V^{-1}). Subsequently, they used it as the filter layer in the mask which could achieve a filtration efficiency of 97% for 0.3 µm particles. They conducted a continuous filtration experiment on the mask for up to 10h. The results showed that the filtration effect of the mask only decreased by 1.1%, demonstrating superior durability. Moreover, to simulate the normal breathing process, the mask was moistened with a humidifier. After drying, its filtration performance was measured to have only decreased by 4.7%, eliminating the interference of water vapor produced during human breathing on the mask's performance. Briefly, β-glycine crystals are a kind of outstandingly piezoelectric materials, and how to effectively obtain the stable β-glycine is still the focus of current researches.

Unlike β-glycine, γ-glycine possesses great piezoelectricity and stability at the same time so that it represents a more suitable alternative. However, glycine crystals are typically brittle and exhibit poor mechanical properties, and commonly referred to as ceramics. Moreover, the requirement for an extremely high electric field to align glycine domains presents a significant challenge in achieving macroscopic piezoelectricity in polycrystalline films. Several strategies have been explored, including incorporating γ-glycine into polymers, utilizing self-assembly, controlling nucleation site position, and employing co-dissolution-evaporation at hydrophobic interfaces.

As an application of the strategy of incorporating γ -glycine into polymers, Ukasi et al.[47] incorporated γ-glycine into fully organic γ-glycine/chitosan composites (**Figure 4a**) and processed a comprehensive exploration of improving the electric output of flexible hybrid piezoelectric-triboelectric nanogenerators (P-TENG). In their study, they determined that when doping 50% γ-glycine into composites, the P-TENG would achieve the optimal electrical output, turning in an open-circuit voltage (V_{OC}) of 79 V and a short-circuit current (I_{SC}) of 64 µA.

Based on the self-assembly strategy and with an eye on further optimizing performance, Wang et al.[48] developed a self-assembly protocol for producing wafer-scale heterostructured piezoelectric films through a polyvinyl alcohol (PVA)-Gly-PVA laminate architecture (Figure 4b). Interfacial hydrogen bonding between the polymeric layers and glycine mediates directional crystallization, inducing epitaxial growth of γ-glycine polymorphs with uniform crystallographic orientation throughout the composite matrix. According to their experiments, this synthesized film showed superb, stable, and uniform piezoelectricity as well as profound flexibility and biocompatibility. When unencapsulated devices were implanted into rats, they can be completely degraded within one day without causing any inflammatory response. Compared to pure glycine crystals, the mechanical flexibility of heterostructured PVA-glycine films improved nearly an order of magnitude, and the films exhibited a piezoelectric coefficient of 5.3 pC N^{-1}. However, there is still an obvious gap between the piezoelectric coefficient of glycine-PVA composite film and the nature γ-glycines' theoretical piezoelectric coefficient d_{33} ≈10.4 pC N^{-1}. Based on this work, Wang et al.[49] further demonstrated that the orientation of glycine crystal nuclei could determine the crystal orientation of the as-synthesized film. They successfully moved the nucleation site from the edge to the middle of the liquid film to align the <001> direction vertically, via surface curvature tuning. And the result turned out that such PVA-Gly-PVA sandwich films showed the highest average piezoelectric coefficient d_{33} of 6.13 ± 1.13 pC N^{-1} which presented a promising kinetic method to realize crystallization and property control.

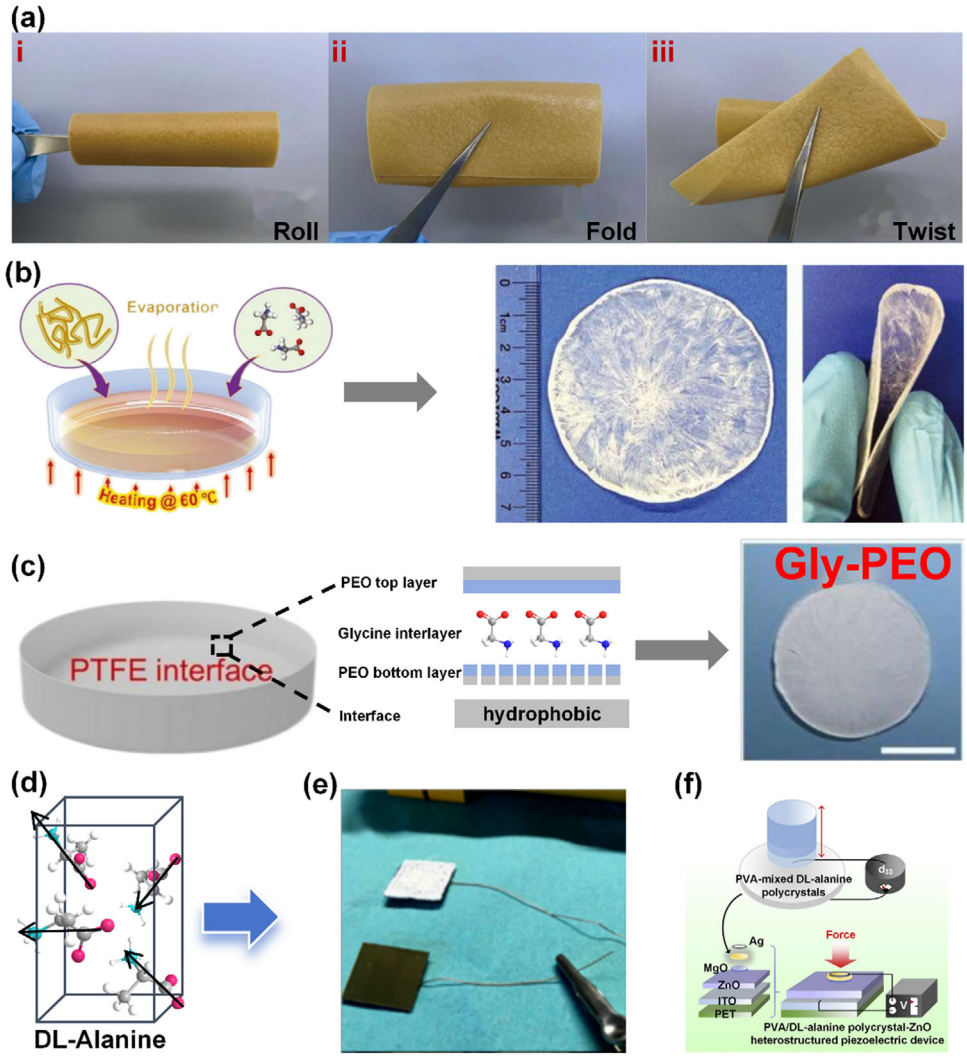

Figure 4. Piezoelectric devices based on γ-glycine and DL-alanine. a) Digital photographs of γ-glycine/chitosan films in a-i) Roll, a-ii) Fold and a-iii) Twist states to verify their flexibility. Reproduced with permission.[47] Copyright 2023, Elsevier. b) Schematic synthesis approach of piezoelectric glycine-PVA films over a large area. The right images are digital photographs of a wafer-sized as-grown film (left) and a largely curved film showing the flexibility (right). Reproduced with permission.[48] Copyright 2021, The American Association for the Advancement of Science. c) Schematic illustration demonstrates the interface-induced orientation between the PEO layer at the bottom of the Gly-PEO composite film and γ-glycine crystals, and the digital image of GLY-PEO film. Reproduced with permission.[50] Copyright 2023, Elsevier Ltd. d) The crystal structures of the DL-Alanine. e) Energy harvester fabricated from racemic amino acid thin films grown on copper electrodes. Reproduced with permission.[51] Copyright 2019, American Physical Society. f) Schematic illustration of PVA/DL-alanine polycrystal-ZnO heterostructured piezoelectric devices. Reproduced with permission.[52] Copyright 2022, Elsevier.

To further enhance the piezoelectric performance of γ-glycine, Yu et al.[50] prepared glycine-PEO composite film (Figure 4c) through the co-dissolution-evaporation method on the hydrophobic PTFE interface. As a result, this film showed a higher piezoelectric coefficient d_{33} of ≈8.2 pC N^{-1} which is closer to the piezoelectric coefficient d_{33} of γ-glycine. From above, γ-glycine is an attractive material with outstanding piezoelectricity, but when we utilize it to make composite flexible films, its piezoelectric coefficient would reduce because it's hard to control the crystal orientation of γ-glycine. Future studies need to further focus on optimizing the nucleation dynamics and composite technology to narrow the gap between actual performance and theoretical value, and achieve a higher piezoelectric coefficient and large-scale production.

DL-Alanine: Besides glycine, DL-alanine (the D and L-alanine racemic mixtures) possess excellent piezoelectricity at the same time (Figure 4d). D-alanine can be easily and efficiently utilized and metabolized, while L-alanine can also be utilized and metabolized through special pathways within a certain limit. Through an experiment of emission of high-frequency electrical pulses on DL-Alanine crystal, Lemanov et al.[37] had confirmed the piezoelectricity of DL-Alanine. Furthermore, Guerin et al.[51] measured the piezoelectric charge and strain, and voltage tensors of the DL-alanine by using density functional theory. They also demonstrated that under simple manual compression, the DL-alanine could generate a voltage up to 0.8 V which twice as high as other amino acid crystals. In their study, they introduced the application of DL-alanine in a transducer (Figure 4e) for

temperature and force measuring. Jeon et al.[52] fabricated polyvinyl alcohol (PVA)-mixed DL-alanine (PVA/DL-alanine) polycrystals (Figure 4f) and investigated its piezoelectric characteristics in d_{33}. In this study, they found that when the weight ratio of PVA and DL-alanine was 1:3, the d_{33} of PVA/DL-alanine was ≈5 pC N^{-1}. Therefore, DL-alanine could be considered as a potential piezoelectric materials in applications of piezoelectric devices. For all this, there still needs a deeper study for the mechanism of piezoelectric development of PVA/DL-alanine polycrystals.

For further expanding its fields of application in wearable devices with stretchability and flexibility, it's necessary to overcome its inherent properties—the intrinsic rigidity and hardness of the DL-alanine crystalline phase. Wang et al.[53] presented a piezoelectric film based on the DL-alanine, and the film contained unimpaired piezoelectricity and omnidirectional stretchability which was suitable to the tissue. In this work, a truss-like microstructure which was self-assembled by controlled molecule-solvent interaction and interface tension to realize such superior stretchability. Resulting in maintaining both the structural integrity and piezoelectricity, meanwhile such a microstructure could suffer up to 40% tensile strain along different directions through controlling the opening and closing states of the truss meshes.

Peptides: Some amino acids through dehydration condensation to build up peptides, these peptides could be as another piezoelectric material with good biocompatibility and biodegradability. After being specifically and non-specifically recognized by peptidases and proteases that are abundant in the body, the peptide bonds of polypeptides are hydrolyzed and eventually metabolized and cleared. To date, such piezoelectric peptides attract more and more researchers to study it because of its high piezoelectricity and the variety of their self-assembly structures.[54,55] Some peptides like diphenylalanine (FF),[56] cyclo-glycine-tryptophan (cyclo-GW),[56] cyclo-phenylalanine-tryptophan (FW),[56] and Fmoc-FF,[57] have been found that all of them have piezoelectricity. And in particular, FF peptide is the most representative piezoelectric peptide, and the FF monomers (**Figure 5a**) could be driven by intermolecular forces, including hydrogen bonds, electrostatic interactions, π–π stacking, etc., to self-assemble into various micro-nanostructures.[58,59] Self-assembly is an interesting phenomenon and it make piezoelectric peptides with such high biocompatibility and piezoelectricity. The study on self-assembly piezoelectric peptides expands a new field of piezoelectric materials.

In traditional synthesis systems for FF-based peptide nanotubes, the commonly used solvent is the 1,1,1,3,3,3-hexafluoro-2-propanol (HFIP)-water co-solvent system. This solvent system is not only highly toxic but also expensive, significantly limiting the development of biocompatible and eco-economically friendly piezoelectric devices. To address this, Lee et al.[60] proposed a meniscus-driven self-assembly process using an ethanol-water solvent system to prepare highly oriented piezoelectric FF nanotubes. Compared to the HFIP solvent system, FF nanotubes synthesized in the ethanol solvent system exhibited unidirectional polarization and piezoelectric properties indistinguishable from those of the former. Subsequently, they fabricated a piezoelectric nanogenerator based on these FF nanotubes. Under a force of 40 N, this generator achieved a voltage of 1.66 V, a current of 19.4 nA, and a power output of 19.2 nW.

Due to FF's high solubility in water (0.76 g mL^{-1}), it degrades extremely rapidly in vivo, posing significant challenges for practical applications. Lee et al.[61] proposed an effective degradation control strategy by incorporating hydrophobic and biocompatible porphyrin into FF to regulate the degradation rate of FF-based piezoelectric nanogenerators (PENGs). Experimental results demonstrated that porphyrin-doped FF still forms well-oriented piezoelectric nanostructures through self-assembly, with piezoelectric properties comparable to pure FF. Furthermore, while FF-based PENG degraded within 5 min in PBS solution, the doped version maintains stable output for 15 min.

The piezoelectric characteristics of diphenylalanine (FF) peptide nanostructures were systematically investigated through multiphysics finite element modeling by Jenkins et al.,[62] with comparative analysis against conventional inorganic piezoelectric systems. Computational simulations revealed FF peptide nanowires exhibited enhanced voltage generation under equivalent mechanical stress compared to zinc oxide (ZnO), lead zirconate titanate (PZT), and barium titanate (BTO). Experimental validation employed vertically aligned FF microrod arrays in a flexible nanogenerator configuration (Figure 5b), demonstrating an open-circuit voltage of 0.6 V that correlated strongly with theoretical predictions. Meanwhile, Tao et al.[63] designed an eco-compatible energy harvesting system through integration of FF microrods within free-standing polylactic acid (PLA) films (Figure 5c). This biodegradable piezoelectric nanogenerator achieved peak performance metrics that the output voltage and power density of 1.78 V and 1.56 W m^{-3} respectively. Such a device could be easily and completely degraded in acidic, alkaline, and PBS solutions. After 25 days, no large components could be found in these three solutions.

Nevertheless, the main barrier in realizing a practical piezoelectric device is how to prepare a scalable unidirectionally polarized structure which can transform the external force into electric energy. As shown in Figure 5e, Lee et al.[64] addressed this limitation through meniscus-guided self-assembly techniques, producing large-area aligned diphenylalanine (FF) nanotube arrays with uniform dipole orientation. The resultant peptide-based energy harvesters exhibited peak outputs of 2.8 V, 37.4 nA, and 8.2 nW, respectively, under 42 N compressive loading. Another similar case is that Ma et al.[65] adopted a nanoconfinement self-assembly strategy to form a unique Mortise-Tenon structure with oriented styrene-block-butadiene-block-styrene molecular beams in the FF crystal fibers and finally, this hierarchical design achieved unprecedented mechanical compliance (1200% elasticity, Young's modulus: 0.409 ± 0.031 MPa) coupled with a macroscopic piezoelectric coefficient d_{33} of 10.025 ± 0.33 pC N^{-1}. Functionalization through gallium-indium (Ga-In) alloy coating and wireless transmission module integration yielded a flexible biosensing platform (Figure 5f) capable of monitoring physiological signals. This sensor could precisely capture the characteristics of human movement and has been proven to be capable of detecting typical Parkinsonian gait. Additionally, it could sensitively and accurately capture minute pressure signals within the body, such as the slight pressure changes during heartbeat and

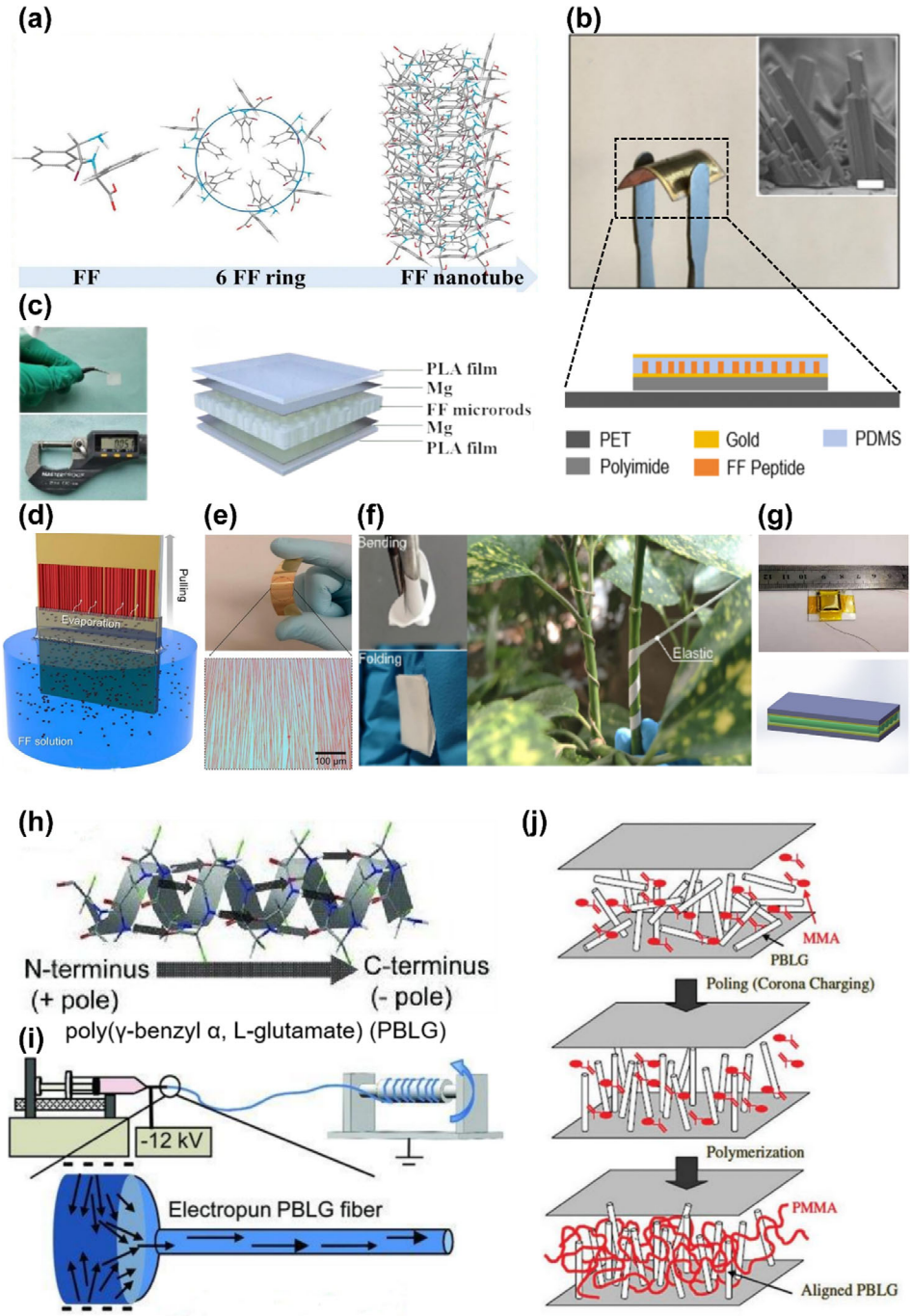

Figure 5. Various piezoelectric devices based on FF peptide and PBLG. a) The process of forming 6 FF rings and FF nanotubes from phenylalanine monomers. Reproduced with permission.[32] Copyright 2024, Wolters Kluwer Health, Inc. b) Optical image of a bendable FF polypeptide nanogenerator. The inset shows an SEM image of peptide microrods. Scale bar is 10 μm. And the schematic illustration of the FF-peptide nanogenerator structure on a PET substrate. Reproduced with permission.[62] Copyright 2018, Elsevier. c) Optical photograph(left) and schematic structural diagram(right) of the FF-based PENG device. Reproduced with permission.[63] Copyright 2021, Elsevier. d) Highly unidirectionally aligned piezopolarly polarized FF nanotubes prepared via meniscus-driven dip-coating. Reproduced with permission.[64] Copyright 2018, American Chemical Society. e) Photographs and optical microscope images of highly aligned FF nanotubes. Reproduced with permission.[64] Copyright 2018, American Chemical Society. f) Optical images of FF-CFs under bending, folding, and stretching conditions, demonstrating its flexibility and elasticity. Reproduced with permission.[65] Copyright 2024, Springer Nature. g) Optical image of a nanogenerator with dimensions (up) and schematic diagram of its sandwich structure (down). Reproduced with permission.[66] Copyright 2022, American Chemical Society. h) A simplified schematic of the α-helical molecular structure of PBLG without side chains, where small arrows along the chain represent hydrogen bonds; the long arrow beneath the helix denotes the macroscopic dipole moment. Reproduced with permission.[33] Copyright 2011, Advanced Materials. i) Schematic diagram of PBLG fiber preparation via electrospinning and polarization process. Reproduced with permission.[33] Copyright 2011, Advanced Materials. j) Polarization process of PBLG in MMA solution and PMMA polymerization process. Reproduced with permission.[67] Copyright 2011, Elsevier.

breathing. Compared with other implantable sensors, this device also demonstrated minimal immune response and has good biocompatibility. However, the strategies for fabricating the FF peptides with the requirements which we need are still lacking. Yuan et al.[66] proposed that the coassembly process of peptide-based materials could effectively control the properties of piezoelectric peptides. In their study, they figured that the coassembled peptides of diphenylalanine and phenylalanine-tryptophan (Figure 5g) exhibited a higher piezoelectric coefficient of up to 38% increasing, and the harvesting device showed nearly a three-fold increase in open-circuit voltage outputs compared to the conventional self-assembly FF peptides.

Poly (γ-benzyl α,L-glutamate) (PBLG) is a well-known rod-like α-helical polypeptide, in which the strong electric dipole moments are generated by parallel and directional alignment of hydrogen bonds along the helical axis collectively (Figure 5h), and make such peptides impressionable to electric and magnetic field. Due to these large number of hydrogen bonds, the PBLG form a macroscopic dipole which can couple synergistically with the external electric field and shear force. Although a lot of studies have tried various surface attachments and poling attempts, it's still difficult to maintain the poled helices in the solid state. Farrar et al.[33] manufactured the PBLG fibers through electrospinning (Figure 5i), and the fiber exhibited a high piezoelectric coefficient d_{33} of 25 pC N^{-1} and maintained stability even after processing 100 °C thermal treatment for over 24 h. However, to further enhance the compressive piezoelectric responses or reflective nonlinear optical signals, various attempts to pole α-helical rods in the direction normal to the film surface. But the PBLG strongly tended to orient parallel to the film surface which made it difficult to achieve a solid PBLG film with the major helical axis aligned vertically to the film surface. Hwang et al.[67] cured the mixed solution of PBLG and poly(methylmethacrylate) (PMMA) in a designed mold, which was completely contacted to the charging (Figure 5j). They demonstrated that all the PBLG could be poled vertically to the disk surface and directly influenced the piezoelectricity of the composite materials. Nevertheless, the PMMA is a kind of non-degradable polymer, and its Young's modulus is relatively high so that it would produces very small deformation when subjected to external forces, which indirectly affects the piezoelectric properties.

Protein: Proteins are made of amino acids and are one of the essential components of human cells and tissues, it has complex and various but precise structures that enable it to perform specific functions. The piezoelectric properties of silk were first discovered experimentally by Harvey et al.[68] in 1939. They rubbed a steel ball with silk inside a quartz tube filled with neon gas and observed that the quartz tube emitted a faint red glow. This indicated that the silk generated a weak electric current during friction or compression. Silk is an animal-derived materials with rich components of glycine, including silk fibroins (SF, gain from bombyx) or spider silk (SS, gain from spiders).

In the research field of silk piezoelectricity, it is an important direction to fabricate functional devices by taking advantages of its piezoelectric properties. Guo et al.[69] presented a hybrid piezoelectric-triboelectric nanogenerator (P-TENG) through sequential electrospinning of silk fibroin and poly(vinylidene fluoride) (PVDF) nanofibers onto conductive textile substrates, forming complementary triboelectric layers (**Figure** 6a-ii). Through systematic optimization of coupled piezoelectric and triboelectric effect mechanisms, the device achieved enhanced energy conversion efficiency, demonstrating peak outputs of 500 V open-circuit voltage, 12 μA short-circuit current, and 0.31 mW cm^{-2} power density, which surpassed conventional textile-based energy harvesters in power generation capacity. Chiesa et al.[70] mixed regenerated silk (RS) fibroin with a soluble plant-derived polyphenol (i.e., chestnut tannin) decorated with graphene (G-RS/T) nanoplatelets (Figure 6a-iii). Based on these materials and 3D printing technology, they fabricated a flexible self-adhesive piezoelectric device capable of gastrointestinal motility monitoring which was a bioresorbable 3D printed flexible and self-adhesive piezoelectric device. Immersing the device in PBS solution (37 °C, pH = 7.4), and the majority of the device degrades within three weeks. After seven days of degradation, the device still produced a good signal, while output performance declined on days fourteen and twenty-one, demonstrating its excellent stability.

In the human body and animal, collagen is the most common biodegradable piezoelectric protein. In recent years, some researchers have studied the piezoelectricity of collagen. Denning et al.[78] used piezoresponse force microscopy (PFM) to confirm the d_{14} of rat tail collagen is ≈12 pm V^{-1}.[15] Although we still can not reveal its exact piezoelectric mechanism. Recently, inspired by the electric eel skin, a super stretchable e-skin (electronic skin) has been developed. The fish skin is composed of collagen nanofibers and is extremely sensitive to the small variations of environmental mechanical vibration. Based on such fish skin, Ghosh et al.[71] developed an energy harvester which act as a sensor to monitor real-time physiological signals at the same time. The fish-skin-based nanogenerator (FSKNG)/pressure sensor (Figure 6b-i) possesses an ultrasensitive of ≈27 mV N^{-1} and is highly durable of 75 000 cycles. Moreover, when FSKNG is exposed to the external pressure of ≈1.8 MPa, it could generate open-circuit voltage, Voc ≈2 V, and short-circuit current, Isc ≈20 nA. Besides this, Son et al.[34] processed the pollack skin with sodium hydroxide solution to wipe out the noncollagenous substances and fabricated a pollack skin-based piezoelectric nanogenerator (PS-PENG) which possessed a flexible and simple structure by a simple process. Notably, after alkaline processing, the PS-PENG exhibited a higher voltage and current performance that was enhanced by ≈2.40 and 2.48 times, and its maximum power density could achieve ≈2.27 mW m^{-2} which proved its practical application.

3.1.2. Polysaccharides

Polysaccharides, as the most abundant natural carbohydrates, exist widely in organisms. Especially for the cellulose, which could be obtained from the cell walls of plants. The early study on piezoelectricity of cellulose was during the 1950s and 1960s, and Fukada et al.[79,80] simply measured its electromechanical response and supposed this response depends on its polar ordering of hydroxyl groups. Although limited by cognition and technology, it was unable to know the complete structure of cellulose at that time, Fukada did made a remarkable hypothesis. After inspiring by Fukada's studies, a number of researchers have devoted themselves into learning about the piezoelectricity of cellulose

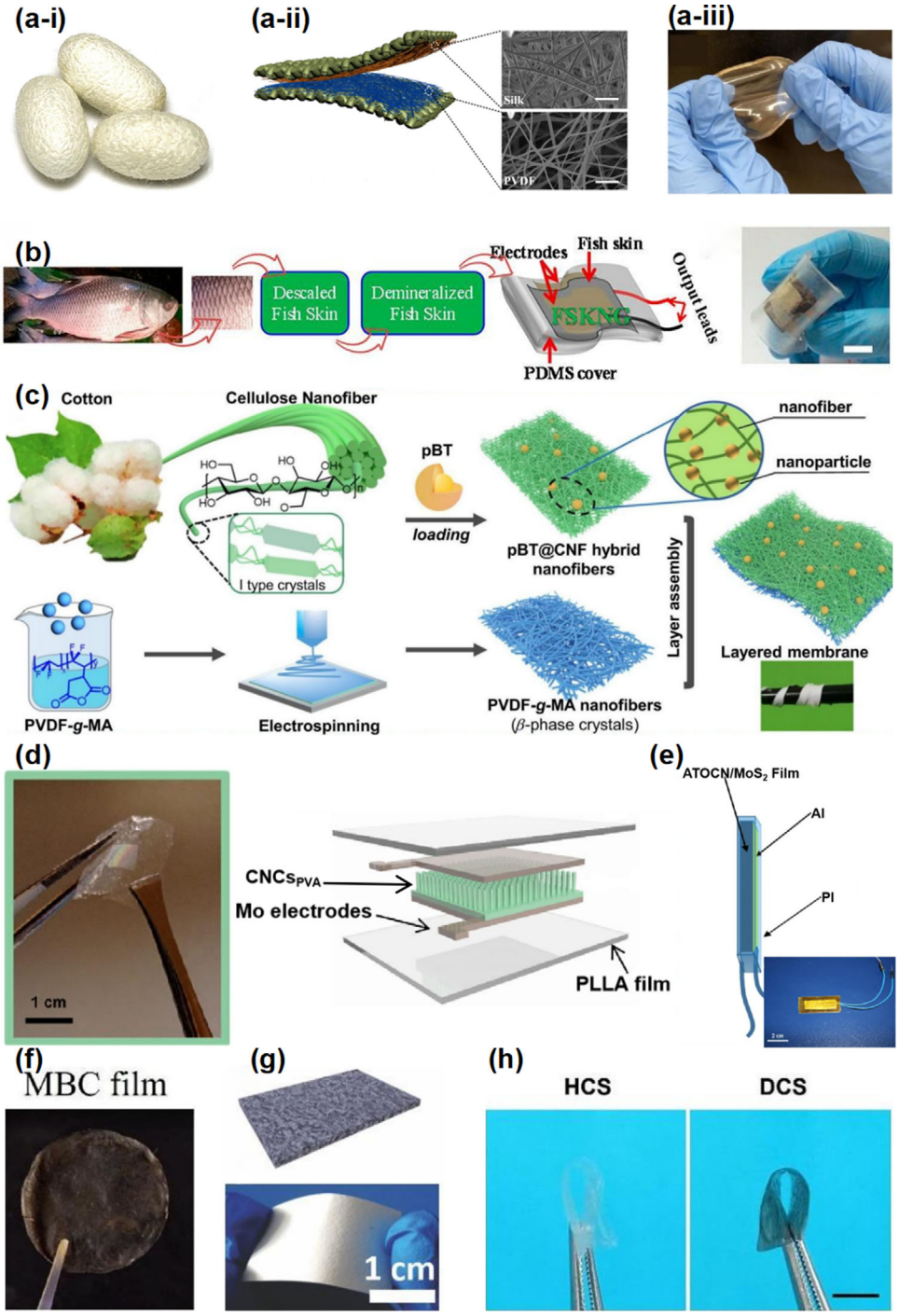

Figure 6. Various piezoelectric devices based on protein, collagen, and polysaccharides. a-i) The regenerated silk. Copyright 2022, American Chemical Society. a-ii) Schematic diagram of all-fiber hybrid-triboelectric nanogenerator: the electrode, composed of silk nanofibers prepared by electrospinning at the top and PVDF fibers at the bottom, serves as the triboelectric pair. Reproduced with permission.[70] Copyright 2018, Elsevier. a-iii) Optical image of the flexible RS/T10 composite. Copyright 2022, American Chemical Society. b) Schematic diagram of the process for manufacturing a fish skin nano generator (FSKNG) using raw fish skin (FSK). Reproduced with permission.[71] Copyright 2017, American Chemical Society. c) Schematic illustration of the preparation of layered CPNF membranes. The CPNF membrane wrapped around chopsticks in the lower right inset demonstrates its flexibility. Reproduced with permission.[72] Copyright 2021, Elsevier. d) The left image shows an optical photograph of the CNCsPVA device, while the right image depicts its structural schematic diagram. Reproduced with permission.[73] Copyright 2025, The American Association for the Advancement of Science. e) Schematic diagram and optical photograph of the TOCN/MoS_2 nanogenerator. Reproduced with permission.[74] Copyright 2020, Elsevier. f) Photograph of BC/$MnFe_2O_4$ (MBC) nanocomposite film. Reproduced with permission.[75] Copyright 2019, Elsevier. g) Schematic diagram and optical image of NG devices based on BTO/BC piezoelectric paper. Reproduced with permission.[76] Copyright 2015, John Wiley and Sons. h) The flexibility tests of the HCS and DCS films. Scale bar = 5 mm. Reproduced with permission.[77] Copyright 2024, Elsevier.

and developing novel cellulose-based biomaterials depend on its properties. However, the pure cellulose has low piezoelectricity, which a piezoelectric coefficient d_{33} of only 0.4 pC N^{-1}. To obtain higher piezoelectricity of cellulose-based materials, it could be designed with a multi-layer structure, obtain highly oriented nanofibers via electrospinning, or add some high piezoelectric materials like $MnFe_2O_4$, $BaTiO_3$, and MoS_2 act as fillers into cellulose substrates. Resulting in increasing dielectric constant and density of oriented dipoles to improve the composites' piezoelectric output.[81]

Among them, adopting a multi-layer structure design and introducing high dielectric/piezoelectric fillers is an effective way to enhance piezoelectric performance. Wang et al.[72] developed a layered piezoelectric nanogenerator (PENG) through hierarchical integration of cellulose nanofiber (CNF) matrices and poly(vinylidene fluoride) (PVDF) piezoelectric films, forming a mechanically interlocked architecture with enhanced interfacial cohesion (Figure 6c). The design incorporated advanced material modifications: 1) strategic substitution of PVDF homopolymers with maleic anhydride-grafted PVDF (PVDF-g-MA) to enable covalent bonding with CNF substrates, and 2) nanoscale interfacial engineering through deposition of core–shell polydopamine (PDA)@$BaTiO_3$ (pBT) nanoparticles on CNF surfaces, serving as molecular bridges between hydrophilic cellulose and hydrophobic polymer phases. Compared with the conventional cellulose architectures and prior hybrid systems, this multifunctional integration demonstrated unprecedented performance metrics. Quantitative characterization revealed a piezoelectric coefficient d_{33} of 27.2 pC N^{-1} and power density of 1.72 μW cm^{-2}, representing significant improvements over existing cellulose-based energy harvesters.

At the same time, Ghosh et al.[73] also focused on the strategy of adding piezoelectric fillers and assembled cellulose nanocrystals (CNCs) (Figure 6d) in multilayered piezoelectrics by a scalable method with the power density of up to 0.6 μW cm^{-2}, pressure sensitivity of 4.2 V kPa^{-1} under the 0.76 to 4.55 kPa gentle touch range, and great biocompatibility. When such a device was immersed in PBS solution (37 °C, pH = 7.4), the device exhibited a degradation cycle lasting up to 112 days. In accelerated bioresorbability testing at 74 °C, significant weight reduction becomes observable after 14 days, with only Mo fragments remaining visible after 100 days. In addition to employing multi-layer structures, composite high-performance films can also enhance the output performance of devices. Wu et al.[74] found the single-layered MoS_2 nanosheets have highly piezoelectricity with a conversion efficiency of 5.08%. Meanwhile, it is an eco-friendly piezoelectric filler because of its lead-free property. They adopted an environmentally benign pathway of aqueous dispersion to prepare 2,2,6,6-tetramethylpiperidine-1-oxyl (TEMPO)-oxidized cellulose nanofibril (TOCN)/moly-bdenum disulfide (MoS_2) nanosheet bionanocomposite piezoelectric films (Figure 6e). When the content of MoS_2 was 4 wt.%, such composite films could reach the maximum piezoelectric coefficient d_{33} of 31 pC N^{-1}. Moreover, the nanogenerator based on this TOCN/MoS_2 composite films showed a maximum output voltage and short-circuit current of 4.1 V and 0.21 μA, respectively. Subsequently, Song et al.[82] developed flexible piezoelectric aerogel architectures through integration of TEMPO-oxidized cellulose nanofibrils (TOCN) with molybdenum disulfide (MoS_2) nanosheets. The hierarchical porous structure, fabricated via controlled assembly of TOCN and 2D MoS_2 constituents, demonstrated peak electromechanical conversion efficiency at 6 wt.% MoS_2 loading when acted as piezoelectric nanogenerators (PENGs). All of these features enable it to be a promising materials in the field of harvesting.

Unlike plant cellulose, bacterial cellulose is an extracellular polysaccharide secreted by microorganisms such as Bacillus Acetococcus. Because the synthesis process does not require lignin, hemicellulose, and other companion organisms, the fiber possesses higher purity and crystallinity, which means that the molecular chain arrangement is more regular, resulting in promoting the formation of piezoelectric polarization and the effective separation of charge. Thus, enhancing the piezoelectric response. Moreover, it has a large specific surface area and high porosity. This structure not only enables the payload of functional materials (such as $BaTiO_3$, ZnO, etc.), but also provides a fast channel for ion transport, thereby improving the piezoelectric output efficiency.

Based on the structural advantages of the above-mentioned bacterial cellulose materials, researchers have achieved the loading of various functional materials to enhance their piezoelectric performance. Sriplai et al.[75] manufactured bacterial cellulose (BC)/$MnFe_2O_4$ (MBC) (Figure 6f) via co-precipitation and hot-pressing method, and made it into low-cost and highly sensitive sensors. The sensitivity of pristine BC film in the normal mode and bending mode are of ≈5 and 25 pC N^{-1}, respectively. Whereas these numerical values are improved to ≈23 and 57 pC N^{-1}, respectively. Their study demonstrated the MBC films could be a potential candidate as a highly flexible sensor. In addition to that, Zhang et al.[76] proposed a nanogenerators (NGs) with great output properties which was a type of piezoelectric paper based on $BaTiO_3$ (BTO) nanoparticles and BC (Figure 6g). Benifiting to the unique structure that BTO nanoparticles show homogeneous distribution in the BC, the BTO/BC piezoelectric paper-based NG exhibits excellent output performance with an open-circuit voltage of 14 V and short-circuit current density of 190 nA cm^{-2}. And in the bending mode, the NG device could generate an output voltage of 1.5 V to drive a liquid crystal display screen. Owing to the low cost, lightweight property, and eco-friendliness of this NG device, it has huge potential applications in energy harvesters and self-powered electronics.

Chitin and its deacetylated derivative chitosan represent a distinct class of piezoelectric polysaccharides, distinguished by their biocompatibility, biodegradability, and structural versatility. As the second most abundant natural biopolymer after cellulose, chitin occurs ubiquitously in arthropod exoskeletons, fungal cell walls, and marine biomass.[83,84] These intrinsic piezoelectric properties, coupled with non-toxic characteristics, position these materials as promising candidates for biomedical applications.

According to its biocompatibility and structural modificability, researchers have developed a variety of functional applications and modification strategies. Luo et al.[77] engineered bioinspired piezoelectric wound dressings through functionalization of chitosan matrices, developing heparin-coated (HCS) and polydopamine-coated (DCS) composite films (Figure 6h). Chitosan possesses widely recognized broad-spectrum antibacterial properties and is also a biomedical material with su-

perior bio-compatibility.[85,86] It has been verified that the antibacterial activity and biocompatibility of the prepared CS membrane not only remain unchanged but are even slightly enhanced after modification with heparin and dopamine. These dressings leveraged piezoelectric-stimulated interfacial interactions to regulate the localized release of acidic fibroblast growth factor (aFGF), demonstrating accelerated burn wound closure in murine models within a 14-day treatment cycle. Street et al.[87] fabricated a kind of nanofibers shows a 300% increase in tensile strength and 400% increase in piezoelectric response via the air gap electrospinning method with the naturally-occurring, semi-crystalline polymer chitin, which proposed a significantly method for improving the crystallinity and piezoelectricity of chitin.

3.2. Synthetic Biodegradable Piezoelectric Polymers

Unlike amino acids, proteins, polysaccharides, or bio-piezoelectric polymers derived from nature or modified from these bases, synthetic biodegradable piezoelectric polymers are chemically synthesized to meet specific human requirements. Although their origins differ, both exhibit excellent piezoelectric properties alongside biodegradability and biocompatibility. Therefore, we classify them together as biodegradable piezoelectric materials for discussion. Poly-L-lactic acid (PLLA), polyhydroxybutyrate (PHB), and piezoelectric gels (or PiezoGels) as promising candidates in the field of biomedical piezoelectric devices will be introduced.

Piezoelectric biopolymers can meet the important demands for protecting the environment, thus the market of its application is growing every year. For example, Poly-L-lactic acid (PLLA) as an organic biodegradable piezoelectric material has demonstrated excellent biocompatibility and biodegradability.[88–90] The U.S. Food and Drug Administration (FDA) has permitted its clinical utility[91] and PLLA is a noteworthy piezoelectric material in the domains of wearable[92] and biomedical[93] devices and biosensors.[94] Its raw material, lactic acid, could be easily obtained by the fermentation of polysaccharides and sugar which extracted from renewable natural resources like corn, potato, sugar-beet, etc., and owing to its electrical polarity of the carbon-oxygen double bonds (C═O) branching out from the backbone, makes PLLA possess piezoelectricity.[95–98] Therefore, PLLA is an inexpensive, easily-obtained, biodegradable, and biocompatible synthetic piezoelectric polymers and plays an important role in medical applications.

However, there are some imperfections of the PLLA-film-based force sensor, including low reproducibility, film rigidity, and modest piezoelectric constants (≈5 to 12 pC N^{-1}) and this would lead to be ineffective for transducers or highly sensitive pressure sensors.[99,100] Meanwhile, there still exists a challenge to make powder-based materials into functional films successfully with repeatable oriented crystals to obtain controllable piezoelectricity. Weak and unstable piezoelectricity is another significant challenge that hinders the practical application of PLLA. For facing and fixing such problems, researchers have proposed some strategies including structure optimization and materials composite, thermal annealing and mechanical stretching, stretch-free fabrication process, and electrospinning.

As shown in **Figure 7a**, Gong et al.[101] combined a nonpiezoelectric meso-poly (lactic acid) (meso-PLA) electret-based triboelectric nanogenerator (NG) which generated high output voltage with a double-layered poly(L-lactic acid) (PLLA)-based piezoelectric nanogenerator (PENG) which generated relatively high current to use for an e-skin device application. The output power of the hybrid NG could achieve 0.31 mW which was 11% higher than the PLLA-based PENG. In addition, under the resonance frequency of 19.7 Hz and a tip load of 4.71 g, the hybrid NG produced an output voltage of 70V and a current of 25 μA that showed great promise for future e-skin applications.

Additionally, PLA nanofibers could act as an electroactive scaffold with the capability of noninvasive in vivo electrical-stimulation (ES). Chen et al.[102] prepared a 3D biodegradable piezoelectric scaffold for wireless electrostimulation therapies, integrating polylactic acid (PLA) nanofibers with potassium sodium niobate ($K_{0.5}Na_{0.5}NbO_3$, KNN) via electrospinning (Figure 7b). This structure harnesses ultrasound-activated piezoelectric responses to generate spatiotemporally controlled electrical stimulation without invasive interfaces. Under the remote stimulus of proper programmed US irradiation, a 3D piezoelectric scaffold could generate a sustainable, adjustable timeline and strength ES and demonstrated efficacy in augmenting axonal regeneration and functional recovery in spinal cord injury models. The KNN nanowires were immersed in PBS solution (37 °C, pH = 7.4), and analyzing the leachate reveals release concentrations of Na, K, and Nb at 0.8–1 mg L^{-1}, 0.5–0.6 mg L^{-1}, and 0.01 mg L^{-1}, respectively. The insoluble Nb_2O_5 component transformed into NbO_3^- and water under neutral or alkaline conditions. During degradation, although KNN nanowires fractured into smaller fragments over time, their internal structure remains stable.

Curry et al.[103] achieved to improve the crystallinity and alignment of PLLA through thermal annealing and mechanical stretching processes respectively so that the PLLA would obtain the best piezoelectric effect and created a biodegradable and biocompatible piezoelectric force sensor made by PLLA. Figure 7c illustrates the structure of the sensor including two layers of piezoelectric PLLA which sandwiched between Mo or Mg electrodes and encapsulating layers of PLA. Their sensor can precisely detect pressure in the range of 0–18 kPa and they confirmed this sensor can be implanted into the abdominal cavity of a mouse to monitor the pressure of diaphragmatic contraction. Subsequently, they placed the sensors in PBS solution (37 °C, pH = 7.4) and calibrated the equipment every 24 h. After four days of degradation, applying the same force to the sensors yielded virtually identical output signal amplitudes. This was further proved by the structural integrity of sensors implanted in the backs of mice at 2, 4, 6, and 16 days post-implantation.

Although the improvements of crystallinity and alignment are well performed by thermal annealing and mechanical stretching, it would cause the stretched PLLA films with a low β phase ratio, poor stability, and high rigidity.[99,100,103] For this reason, Ali et al.[104] also adopted a stretch-free fabrication process to manufacture a flexible and biodegradable piezoelectric film for a pressure sensor which was based on the composition of PLLA/Gly with controlled piezoelectricity (Figure 7d). Such a film can gradually degrade completely in PBS solution (37 °C, pH = 12) within 5 days. The developed sensor showed a high sensitivity of 13.2

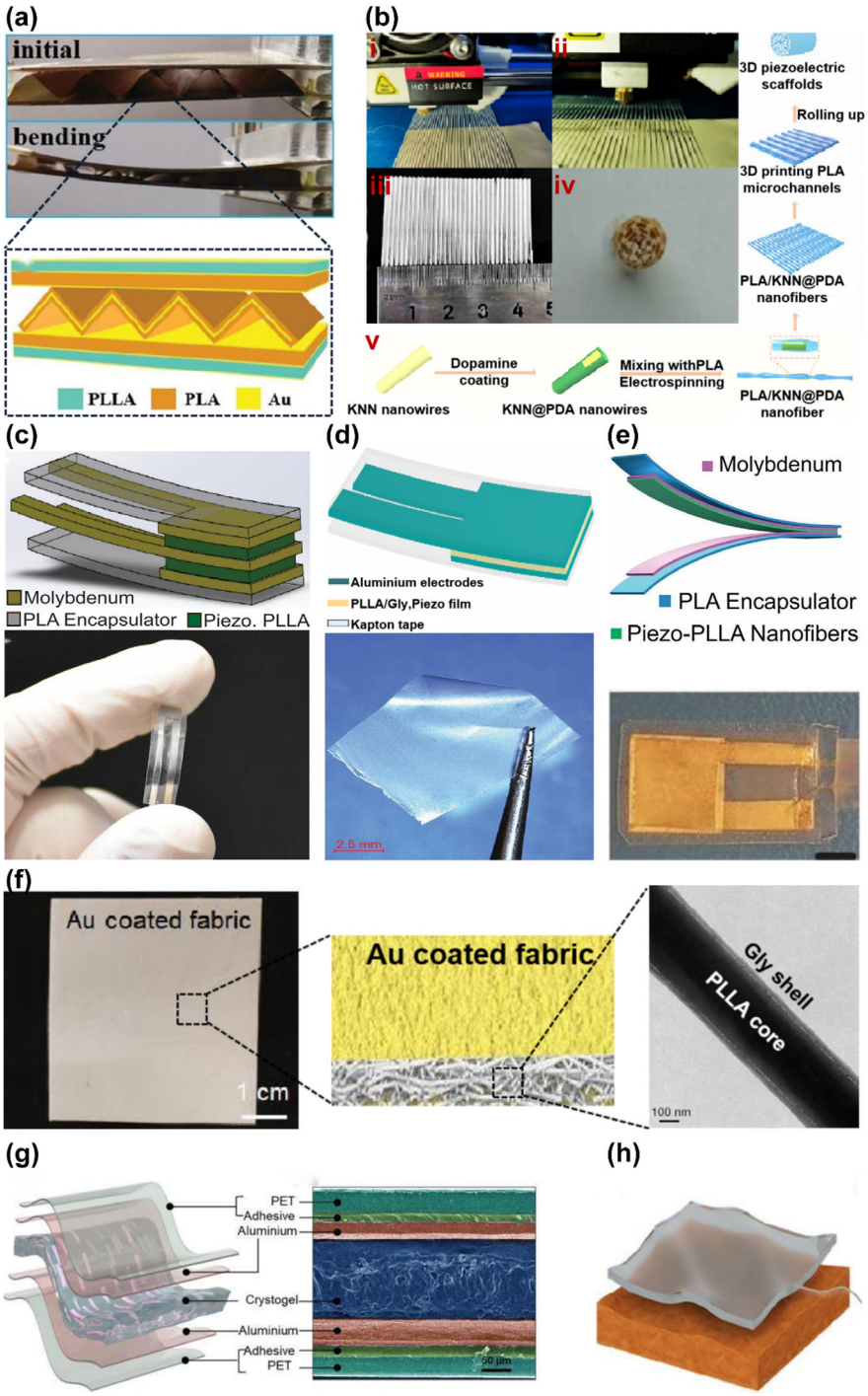

Figure 7. Various piezoelectric devices based on synthetic materials. a) Optical diagram of the hybrid NG device in its initial state and bent state, along with its structural schematic. Reproduced with permission.[101] Copyright 2020, John Wiley and Sons. b) Preparation process of 3D piezoelectric scaffolds. b-i, ii) Fabrication of highly oriented PLA microstrips on PLA/KNN@PDA nanofiber films via 3D printing technology. b-iii) Optical photograph of PLA/KNN@PDA nanofiber film with scale bar. b-iv) Optical photograph of the 3D piezoelectric scaffold device. b-v) Schematic illustration of the preparation process for the 3D piezoelectric PLA/KNN@PDA nanofiber scaffold. Reproduced with permission.[102] Copyright 2022, American Chemical Society. c) Simplified schematic diagram and optical image of a biodegradable PLLA piezoelectric sensor. Reproduced with permission.[103] Copyright 2018, Published under the PNAS. d) Simplified schematic diagram and optical image of a biodegradable PLLA/Gly piezoelectric sensor. Reproduced with permission.[104] Copyright 2023, John Wiley and Sons. e) The schematic of a biodegradable pressure sensor and ultrasound transducer, and the optical images of a typical biodegradable US transducer. Reproduced with permission.[105] Copyright 2020, Published under the PNAS. f) Optical image (left) and schematic diagram (center) of PLLA/Gly nonwoven fibers with gold sputtered electrodes, along with TEM image (right) showing the core–shell structure of PLLA/Gly nanofibers. Reproduced with permission.[106] Copyright 2024, The American Association for the Advancement of Science. g) Schematic diagram of the device's layered structure and cross-sectional SEM image. Reproduced with permission.[107] Copyright 2025, Wiley. h) Schematic illustration of a BS-TENG based on PEGDA/Lap hydrogel. Reproduced with permission.[108] Copyright 2023, American Chemical Society.

mV kPa^{-1} with a response time of 10 ms and good mechanical stability.

As an attractive technology, electrospinning provides another method for fabricating the PLLA nanofiber. Some researchers have fabricated the PLLA nanofibers films via electrospinning but struggled with a few limitations.[109–111] Like lacking appropriate materials to stability nanomaterial or utilize the shear-piezoelectric mode (i.e., d_{14}) of PLLA to get the best piezoelectricity or generating the triboelectric effect during the measurement. Curry et al.[105] achieved new piezoelectric PLLA nanofibers with highly controllable, efficient, and stable properties, and Figure 7e illustrates these biodegradable piezoelectric devices made up by this powerful nanomaterial. Compared to the previously reported thermally stretched PLLA bulk films,[103] this PLLA nanofiber film exhibited higher sensitivity and flexibility while maintaining a similar degradation rate. And in this study, they made it into a biodegradable and highly efficient piezoelectric US transducers to promote the blood-brain barrier (BBB) opening for the drugs delivery into the brain. Li et al.[106] reported another kind of interfacial anchoring strategy in their study. They fabricated core/shell PLLA/GLY nanofibers (NFs) (Figure 7f) by electrospinning under this strategy and result in a high ratio of piezoelectric β phase and excellent orientation alignment. Moreover, the core/shell NFs show high piezoelectric property and outstanding stability, and it fit well to heavily wrinkled surfaces so that it could exactly detect the sign of complex physiological motions in organs.

Polyhydroxyalkanoates (PHAs), as a kind of natural storage polyesters, are formed by microorganisms, with biocompatibility and biodegradability.[112] More specifically, among the PHAs, PHB is known by its higher biocompatibility and biodegradability, acceptable mechanical properties, and minimal tissue toxicity.[113] Notably, the piezoelectric properties of PHB were first systematically characterized by Fukada et al.,[114,115] who identified shear piezoelectricity arising from the material's orthorhombic α-crystalline phase featuring chiral helical molecular conformations. Subsequently, through the stretched PHB films, Ort et al[116] found another crystalline structure (β-phase) which presented the zigzag chain conformation between the α-crystal lamellae phase due to its presence of the orthorhombic α-crystalline phase (the chiral helix). The crystal structure of the PHB was similar to quartz, leading to possess normal and bending piezoelectricity.[117] Despite PHB shows biocompatibility, biodegradability, and piezoelectricity, compared with other piezoelectric polymers like PVDF, it exhibits lower piezoelectricity and poorer electric and makes it difficult for applications of implantable devices.[118] In this case, the incorporation of the nonpiezoelectric nanofibers like reduced graphene oxide (rGO), has been proved that its functions in enhancing the piezoelectric response of polymers.

Based on developed biocompatible piezoelectric PHB and rGO flakes, Chernozem et al.[119] designed a novel hybrid biodegradable 3D scaffold. When such a PHB-rGO scaffold was immersed in PBS solution (37 °C, pH = 7.4) containing 0.25 mg mL^{-1} lipase for 30 days, its relative mass loss ranged from ≈2% to 4.5%, and its degradation rate was closely related to its initial molecular weight. The addition of the rGO further promoted the formation of the zigzag chain between paired lamellae in PHB fibers. When the rGO content reached to 0.7%, such a scaffold could be detected the maximum effective piezoelectric response, and showed 2.5 and 1.7 times higher than the pure PHB fibers in out-of-plane and in-plane values, respectively. This work provided a promising method for enhancing the piezoelectric response of the PHB fibers. Besides, Sheng et al.[120] demonstrated enhanced piezoelectric performance in PHB through the incorporation of reduced graphene oxide (rGO) and polyaniline (PANi). The study revealed that introducing these conductive fillers reduced average fiber diameters and lowered hydrophobicity in PHB fibers. Comparative analysis identified 0.2 wt.% rGO loading as optimal for piezoelectric enhancement, yielding superior piezoelectric response relative to pristine PHB and other composite formulations. Cytocompatibility assessments indicated preserved adhesion densities of bone marrow-derived mesenchymal stem cells (BMSCs) at concentrations up to 1 wt.% rGO and 3 wt.% PANi, confirming biocompatibility within these thresholds. Therefore, how to further enhance the piezoelectric response of the PHB is a critical point for its applications.

Moreover, there is still a main demand in further developing the sensors with highly flexible, stretchable, and self-powered properties. Subsequently, the hydrogels as a novel material were found and attracted intentions.[121–123] Hydrogels are flexible and biocompatible material with 3D polymericstructures build of cross-linked hydrophilic networks and are appropriate for flexible electronics.[124,125] Additionally, it's water-rich, breathable, and soft, and can mimic the natural tissue extracellular matrix (ECM) so that it's easy to detect mechanical and suitable for cell signaling.[126–128] Recently, the combination of hydrogels with piezoelectricity (i.e., PiezoGel) has attracted a number of attention in wearable healthcare piezoelectric devices. The structure of PiezoGel is really similar to hydrogel and its major composition is water molecules within their interlocked, therefore PiezoGel could be recognized as a special kind of hydrogel. Compared with other kinds of hydrogels, the advantages of PiezoGels are ordered crystalline and acentric structural features, which are essential for energy harvestors or sensors.[129,130]

Unfortunately, wearable and implantable electronic devices often face the risk of damage due to mechanical deformation. Therefore, developing a piezoelectric material that simultaneously possesses stretchability, degradability, and self-healing capability still remains a significant challenge. Ghosh et al.[107] incorporated dl-alanine amino acid crystals into their self-developed biocompatible and biodegradable ionically crosslinked hydrogel, thereby developing a composite hydrogel that simultaneously exhibits superior extensibility, self-healing capability, biocompatibility, and biodegradability. The dl-Alanine grew during gelation, enabling the polarization axes of dl-alanine to align, thereby significantly enhancing the piezoelectric response coefficient of this composite hydrogel (Figure 7g). It exhibited the highest piezoelectric voltage coefficient and figure-of-merit (FoM) among reported biodegradable piezoelectric films. The piezoelectric coefficient d_{33} of the polarized composite gel was 35 pC N^{-1} and after undergoing 21 cycles of mechanical damage and repair over 21 days, its piezoelectric properties still exhibit excellent stability and recovery efficiency. Furthermore, it demonstrated superior performance compared to most biodegradable self-healing piezoelectric materials—57.6 pm^2 N^{-1}—making it a promising

candidate for high-performance energy harvesters. After polarization, the composite gel prototype energy harvester containing 15% dl-alanine exhibited a voltage output of 9.3 V and a current output of 638 nA. When the device's surface area was increased to 25 cm^2 and subjected to a force of 13–14 N, it stably delivered a high voltage of 492 V, a current of 153 μA, and an output power of 75.3 mW over an extended period. By tapping such a device to generate electricity, it can illuminate 520 blue light-emitting diodes (LEDs) or three 110V bulbs of different colors.

Another example was that Sun et al.[131] using PVA as the matrix, bacterial cellulose as reinforcement, MXene as the conductive material and filler, and borax as the crosslinking agent. Through a simple repeated freeze-thaw method, they combined and crosslinked these components to prepare a multifunctional hydrogel (PBM hydrogel) sensor exhibiting self-healing, biocompatibility, and degradability. The PBM hydrogel exhibited a fast response time (10 ms) alongside high self-healing efficiency (97.8%). Furthermore, it degraded over 56 days in PBS solution and achieved complete degradation within 53 min in 3% H_2O_2 solution. Biocompatibility tests demonstrated that the device not only exhibited no cytotoxicity but also promoted cell adhesion and proliferation.

Li et al.[108] applied polyethylene glycol (ethylene glycol) diacrylate (PEGDA) hydrogels and Laponite nanocomposites (Lap) as the raw materials to fabricate PEGDA/Laponite (PEDGA/Lap) composite hydrogels (Figure 7h) and made into a flexible biodegradable single-electrode TENG (BS-TENG). Through their study, it was found that the composite hydrogels were with the optimal electrical and mechanical properties when the dosage of Laponite is 10 wt.%. The strain of the composite hydrogels is ≈1001.8%, and the resistance is ≈10.8 Ω. And the developed BS-TENG exhibits a Voc of ≈10.4 V and can perform stably for 106 cycles with a size of 25 mm × 15 mm. Additionally, the device exhibits a sensitivity of 49.48 mV N^{-1} and a fastest response time of 0.5 ms, enabling effective and accurate monitoring of human motion signals. These materials possess excellent biocompatible property and can facilitate cell adhesion. Degradation experiments conducted by immersing the device in PBS solution (25 °C, containing 0.01% lipase) and PBS solution (37 °C) revealed degradation cycles of 90 and 60 days at 25 and 37 °C, respectively. This demonstrated that the degradation rate of the device can be regulated by adjusting conditions such as temperature or adding lipase. Furthermore, during degradation, the encapsulation layer was compromised, leading to a significant decline in the device's output performance.

4. Summary

In the preceding sections, we have provided a detailed overview of various materials and summarized them in Table 1. While they demonstrate significant potential for biomedical applications, translating them into practical clinical applications requires addressing the challenge of balancing key performance parameters, including the piezoelectric coefficient (dictating energy conversion efficiency), degradation rate (determining functional lifetime), and mechanical properties (influencing tissue integration). In this section, we will systematically compare and discuss the trade-offs between core properties of different materials based on the various materials described earlier.

4.1. Piezoelectric Properties and Degradation Rate

This is a key relationship that must be carefully considered. The high piezoelectric coefficient stems from the highly ordered crystal structure and the orientable ferroelectric domains,[142] which often conflict with the requirement for rapid degradation.[143] These materials can be categorized into two typical scenarios: 1) High output performance and slow degradation: Represented by polymers (such as PLLA), which have a relatively high piezoelectric coefficient and rank in the upper-middle range among biodegradable polymers, but require months to years for complete degradation in the body.[88–90,103] Consequently, they are suitable for the situation requiring medium-to-long-term electrical stimulation, such as bone repair[144] and nerve repair;[145] 2) Low output performance and fast degradation: This category includes most natural biomolecules (e.g., peptide-based materials, unmodified polysaccharides). For instance, silk exhibits a low piezoelectric coefficient, but its degradation rate can be controlled from weeks to months through processing techniques,[136] making it suitable for short-term implants or biocompatible scaffolds.

Integrating superior piezoelectric performance with controllable degradability remains a key challenge in the field of applications of biodegradable piezoelectric materials. For example, amino acids and self-assembling peptides offer potential solutions, exhibiting high piezoelectric coefficients alongside excellent biocompatibility. However, they dissolve too rapidly in physiological environments—often within minutes or hours. Thus, through encapsulating them with various polymers can extend their functional lifespan to days or weeks.

4.2. Mechanical Properties and Biocompatibility and Piezoelectric Properties

The mechanical properties (Young's modulus) of implants must match those of the target tissue to avoid stress shielding effects[146] and mitigate inflammatory responses.[147] This demand needs to form a balanced relationship with the biocompatibility and piezoelectric performance of the material. Rigid materials, such as pure amino acid crystals and peptide crystals typically exhibit ceramic-like brittleness and high Young's moduli (e.g., glycine with E >25 GPa[40]), resulting in severe mismatch with the mechanics of soft tissues (Young's moduli typically ranging from 0.1 kPa to 20 MPa[148]). Despite their favorable output performance, these materials risk mechanical failure or tissue damage upon implantation. Conversely, flexible materials like hydrogels and most polysaccharide-based materials possess excellent flexibility and tunable moduli, effectively mimicking soft tissue mechanics.[77,107] However, their piezoelectric properties are generally weak, often requiring composites with high-piezo fillers to enhance performance.[72,74] To address this contradiction, composite strategies offer a promising approach by combining high-performance piezoelectric fillers with flexible, biodegradable polymer matrices. This ap-

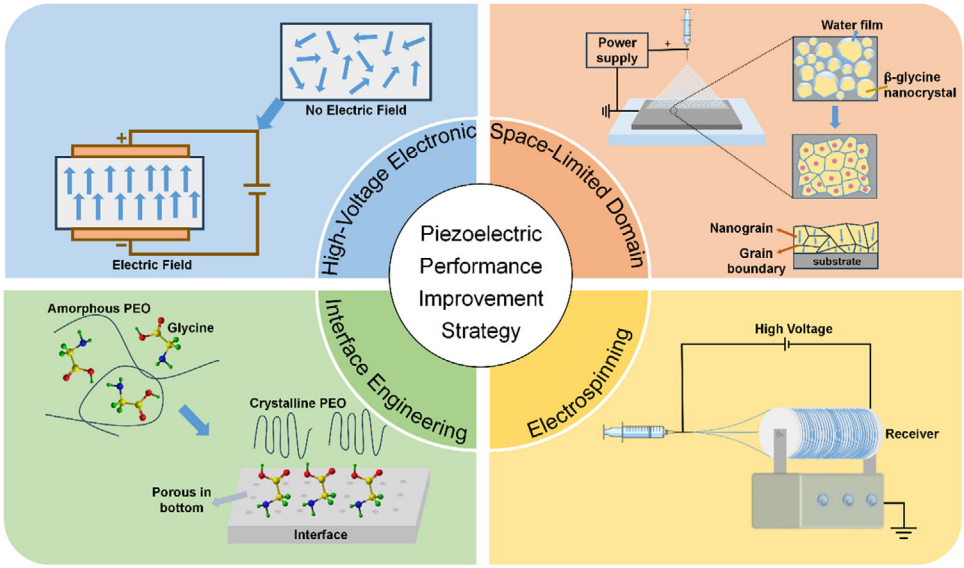

Figure 8. The schematic of the piezoelectric performance improvement strategy, including a) High-Voltage Electronic;[43] b) Space-limited Domain;[39] c) Interface Engineering;[48,50] d) Electrospinning.[41,65]

proach preserves substantial piezoelectric output while imparting the desired flexibility and biodegradability to the composite material.

4.2.1. Strategies for Enhancing Piezoelectric Performance

The translational development of biodegradable piezoelectric materials for biomedical applications depends on complex design strategies to coordinately address the fundamental performance indicators: robust piezoelectric performance, controllable biodegradation kinetics, tissue-compatible mechanical adaptability, and biomimetic structure integration. As shown in **Figure 8**, this section synthesizes four key strategies for enhancing piezoelectric performance: 1) Interface Engineering; 2) Space-limited Domain; 3) High-Voltage Electronic; 4) Electrospinning. The purpose of this section is to provide systematic strategies for researchers, which is crucial for translating laboratory breakthroughs into clinical applications.

Precise regulation of the molecular crystallization process is the key to enhancing piezoelectric performance. The above-mentioned strategies achieve crystal orientation control and performance optimization through different mechanisms. For example, the self-assembly technology under interface induction plays a key regulatory role in the directional growth of unstable γ-glycine.[14,49] Furthermore, space-limited methods such as using nanoconfinement, like constructing nanoscale crystallization chambers on silicon-based substrates,[39] polymer matrix constraints such as the 3D network structure of chitosan,[40] and surface curvature adjustment[48] can precisely control the nucleation and growth paths of crystals. The assistance of a high-voltage electronic field also promotes molecular crystallization. Applying a high-voltage electronic field can induce the dipoles of crystal molecules to align along the electric field direction and preferentially form the nuclei of one of the crystal forms in the electric field direction.[43] The electrospinning strategy mainly utilizes good tensile properties. Charged droplets are stretched into fine streams in the electric field, and stretching can promote the high orientation of molecular chains and crystals, forming a highly ordered dipole structure.[41,63] The tensile force can also refine the fiber diameter and form a porous structure, enabling the material to generate a larger deformation during the stretching and compression processes and enhancing the stress-charge conversion efficiency.[112,113] Combining multiple strategies can better enhance the piezoelectric performance. For example, by simulating the sintering and polarization processes in the manufacture of piezoelectric ceramics, when preparing crystals, the Space-limited Domain and High-Voltage Electronic strategies are combined. The electric field induces the orientation of molecular dipoles in the nanoscale space, and the nanoconfinement limits the crystal growth dimension.[38] This multi-strategy integration not only breaks through the performance bottleneck of a single method but also enhances tissue compatibility through biomimetic structure integration, forming a synergistic optimization system of "performance-structure-biocompatibility".

For future research aiming at performance improvement, in addition to continuously optimizing the existing strategies for enhancing piezoelectric performance, the synergistic mechanism between the piezoelectric effect and drug controlled release, such as the piezoelectric-driven local drug sustained-release system,[112,144] and the combined application of piezoelectric materials with physical fields such as ultrasound, magnetic fields, and photothermal fields, such as constructing an ultrasound-activated piezoelectric-electrical stimulation composite system,[40,41] can also be explored. Through the systematic integration and synergistic optimization of multiple strategies, the translation process of degradable piezoelectric materials from laboratory prototypes to clinical applications will be effectively accelerated, providing a new diagnostic and treatment platform integrating biocompatibility, piezoelectric performance, and intelligent response for the field of regenerative medicine.

5. Applications of Biodegradable Piezoelectric Materials in Biotherapy

Multidisciplinary knowledges including materialogy, electronics, and mechanics are involved for the studying of the piezoelectric effect, and it promotes the cross-fertilization of these disciplines in turn. This discovery holds profound scientific and technological significance, leading to the emergence of self-powered technology and overcoming the limitations of traditional electrical stimulation medical devices, completely transforming the landscape of electrical stimulation medical devices.[149] The emergence of piezoelectric materials provides another new idea for fabricating biomedical implantable devices. For these biomedical implantable devices including energy harvestors,[150] bio-physiological signals collecting sensors,[151] drug delivery systems,[152] and so on, which are exposed to the biological environment and stay in it, or contact with external of internal tissues. Therefore, it's necessary to consider that the biomaterials should possess nontoxic, biocompatible, and biodegradable properties.

5.1. Bone Repair

The skeletal system, as one of the largest organ systems in the human body, account for ≈15% of the total body weight.[153] Bones are not only a kind of internal support system of the human body, but also take a vital part in protecting the organs and nervous system, and play an important role in our movement.[154] Bone defects are typically observed in patients with severe trauma (like fractures in a car accident or falls), osteitis, or bone tumors.[155] Thus, how to achieve the highly efficient repairing of bone defects is still a challenging issue right now.

The natural osseous microenvironment exhibits a hierarchically organized architecture comprising collagen fibrils and hydroxyapatite (HA), synergistically optimized for mechanical integrity, ionic homeostasis, and electrical properties. This composite structure functions not only support a certain mechanical strength but also as a dynamic ionic reservoir regulating mineral metabolism during regeneration processes.[156] What's more, the asymmetric molecular structure of collagen makes natural bone be with unique piezoelectricity.[157] Some researchers have certified the regulation of osteogenic differentiation is driven by the piezoelectricity of natural bone through activating cell membrane calcium channels, surface receptor redistribution, and signaling pathways.[158–160] Additionally, the processing of the natural bone regeneration is regulated by innervation, where early-phase neural innervation facilitates osteogenesis and vascularization through spatiotemporal release of neurokines including nerve growth factor (NGF) and brain-derived neurotrophic factor (BDNF). Therefore, in a word, the supplement of the piezoelectric signal is a key point to regulate bone regeneration.

Inspired by nature, based on mimicking the structure and chemistry of bone, Cui et al.[144] developed a piezocatalytically regulated mineralization strategy through the design of a biomimetic poly-L-lactic acid (PLLA)-based scaffold (pcm-PLLA) (**Figure 9**a, middle). Such a scaffold was fabricated via assembly of piezoelectric PLLA fibers into ordered micro-nano architectures, mimicking the structural and chemical microenvironment of osseous tissue. Ultrasound-activated piezoelectric signals from the scaffold were shown to rapidly recruit endogenous stem cells, triggering the opening of calcium channels in the cell membrane and PI3K pathway activation to drive osteogenic differentiation. The processing of migration of endogenous stem cells to the apart of bone defects is considered as a critical step in bone repair,[161,162] and owing to the porous structure of the pcm-PLLA scaffold and suitable chemical environment, the pcm-PLLA group recruited more endogenous cells. Besides that, it also provided the appropriate microenvironment for facilitating macrophage M2 polarization and angiogenesis, resulting in enhancing bone regeneration in the skull of defects of rats. Such a scaffold was not only loose and porous, but also possessed bone-like chemical compositions and piezoelectricity, and the degradation rate of this scaffold aligned with the rate of bone regeneration completely.

As the one of the most important biophysical level regulator and a nonpharmaceutical intervention in clinical practice, the electrical stimulation has shown a significant effect on modulating cell activity and facilitating tissue regrowth,[165] not only for facilitating bone regeneration and but also effected the cartilage repair,[166,167] which means the applications of piezoelectric materials are not limited to bone tissue engineering, but also shows potential in the field of cartilage regeneration. For instance, another common joint disease is called osteoarthritis (OA) which leads to a huge deterioration and damage of cartilage tissue and makes excruciating pain and severe limitations of daily functioning to those affected.[168,169] Vinikoor et al.[163] reported a pioneered a minimally invasive therapeutic strategy for cartilage regeneration through the development of an injectable piezoelectric hydrogel composite, comprising cryosectioned electrospun poly-L-lactic acid (PLLA) nanofibers (NF-sPLLA) embedded within a hydrogel matrix (Figure 9b). This biodegradable composite material enabled ultrasound-activated electrical stimulation at osteochondral (OC) defect sites, and it was implanted into the defect via injection, which circumvented the need for surgical implantation. Mechanistically, the piezoelectric nanofiber network transduces US energy into localized ES, and the previous evidence have demonstrated ES-mediated chondrogenic enhancement via TGF-β1 secretion and progenitor cell recruitment.[170,171] In vivo evaluation using a rabbit OC defect model revealed superior regenerative outcomes in the hydrogel-treated cohort, characterized by seamless integration of neocartilage with native tissue and elevated repair quality scores.

Besides, Liu et al.[172] combined a piezoelectric cartilage-decellularized extracellular matrix (dECM) and piezoelectric-conductive modified gelatine (Gel-PC) to manufacture a degradable piezoelectric-conductive scaffold. The piezoelectricity and conductive properties of the scaffold were achieved by FF assembly in the pore surface and the incorporating poly(3,4-ethylenedioxythiophene), respectively. Notably, when the scaffold was exposed to the external force, it would generate deformation and a subsequent electric potential difference. The upper layer of the scaffold accumulated the positive charges to attract bone marrow mesenchymal stem cells (BMSCs), facilitating its migration and chondrogenic differentiation, while the negative charges accumulated on the lower layer to induce the osteogenic differentiation of BMSCs. Meanwhile, the in vivo experiments in the Parma pig model of osteochondral defects proved that

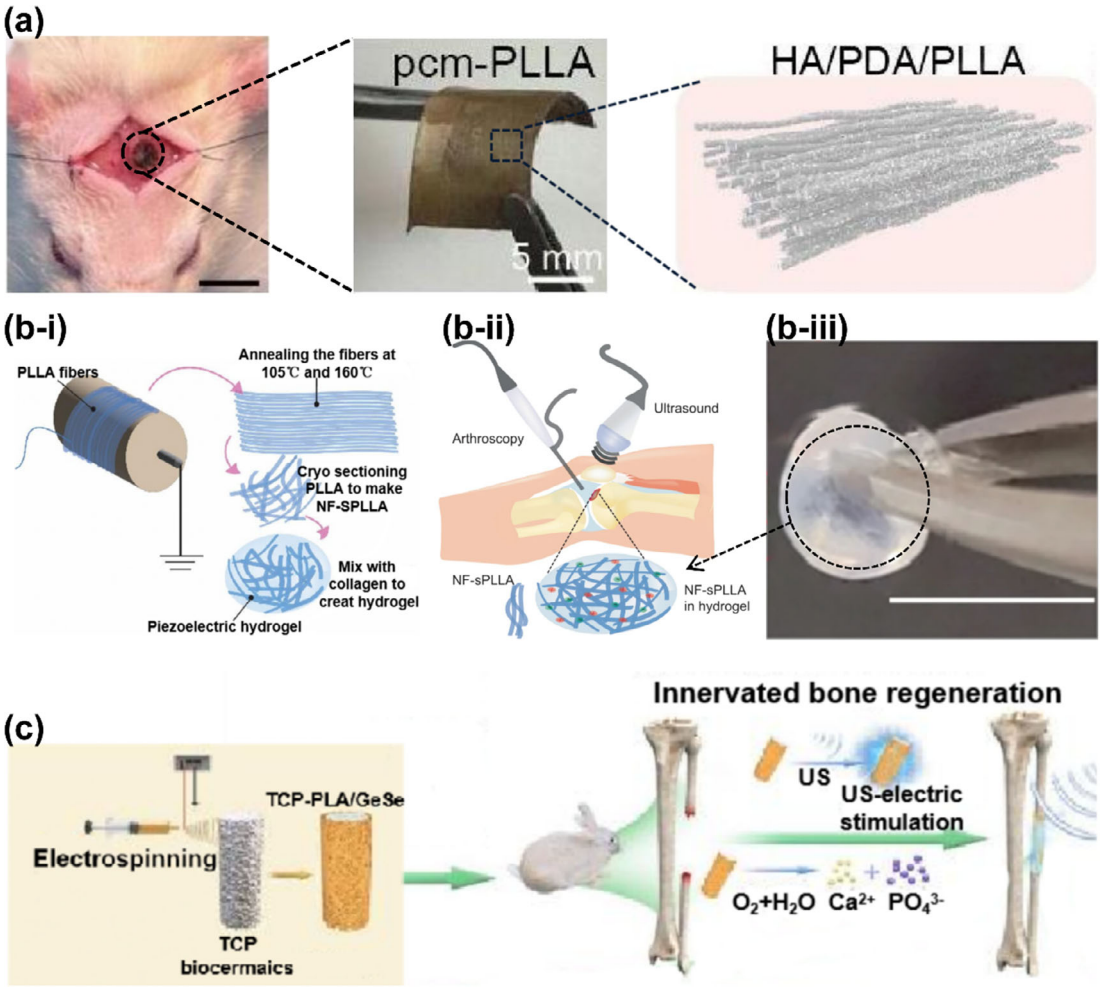

Figure 9. A variety of piezoelectric devices for bone repair. a) The pcm-PLLA scaffold implantation site (left), optical image of the pcm-PLLA piezoelectric bracket (middle), and schematic diagram of HA/PDA/PLLA nanofibers (right). Reproduced with permission.[144] Copyright 2024, Elsevier. b-i) Schematic diagram of the preparation process for hydrogels doped with piezoelectric nano-PLLA fibers. b-ii) Schematic illustration of the use of a piezoelectric hydrogel for OA patients. The piezoelectric hydrogel contains piezoelectric short nanofibers of PLLA (NF-sPLLA) and a hydrogel matrix of collagen, which could be injected into knee joints by arthroscopy or X-ray guidance. b-iii) Optical image of a piezoelectric hydrogel (Scale bar: 1 cm). Reproduced with permission.[163] Copyright 2023, Springer Nature. c) Schematic illustration of the fabrication of TCP-PLA/GeSe scaffolds and the schematic illustration of the Piezoelectric biomimetic bone-periosteum scaffold (TCP-PLA/GeSe) for spatiotemporal innervated bone regeneration and tumor ablation. Reproduced with permission.[164] Copyright 2024, Springer Nature.

such a piezoelectric scaffold showed outstandingly reparative efficacy. Wu et al.[173] designed another kind of hydrogel, which was made by incorporating polydopamine-modified ceramic hydroxyapatite (PDA-hydroxyapatite, PHA) and PDA-modified barium titanate (PDA-$BaTiO_3$, PBT) nanoparticles into a chitosan/gelatin (Cs/Gel) matrix. The function of $BaTiO_3$ was that it enhanced the mechanical properties for the scaffold and added self-generated electricity into it. Owing to the endogenous piezoelectric stimulation and bioactive properties of the Cs/Gel/PHA/PBT hydrogel, it showed significant biocompatibility and immunomodulatory as well as angiogenic and osteogenic abilities. Through the experiment in vivo, these multifunctional PiezoGel outstandingly accelerated new bone formation in a large-sized cranial injury model.

More and more evidences illustrate that the early innervation is significant for initiating bone regeneration and the piezoelectric materials can cooperatively promote nerve regeneration and osteogenesis by simulating the electric microenvironment. The bone generation starts from innervation that releases neurotransmitters and neuron trophic factors which stimulate osteoblast differentiation and angiogenesis.[174–179] Among these, Schwann cells (SCs) critically orchestrate neural regenerative processes through the mechanisms of myelination and paracrine release of neurotrophic factors.[180] Xu et al.[164] reported a multifunctional piezoelectric composite through electrospinning poly-L-lactic acid/germanium selenide (PLA/GeSe) nanofibers onto β-tricalcium phosphate (TCP) scaffolds (TCP-PLA/GeSe) (Figure 9c), designed to synergize innervated bone regeneration with photothermal osteosarcoma treatment. According to some studies, Germanium selenide (GeSe) possess high piezoelectricity and can enhance the piezoelectric coefficient of organic polymers like PLA through doping GeSe nanosheets. There is no doubt that PLA is fully biodegradable, and the degradation

products of TCP bioceramics—phosphate and calcium ions, which can promote bone formation. In vitro evaluation employing PC12 neuronal precursors cultured in SC-conditioned medium demonstrated ultrasound-activated TCP-PLA/GeSe scaffolds significantly potentiated neuritogenesis, with quantified axonal elongation exceeding control groups. Subsequently, they produced a length of 15 mm segmental bone defect in the middle radius of New Zealand rabbits as the bone defect model, where the scaffolds were implanted. It could be obviously observed that, after 6 weeks, all groups showed new bone growth. However, the more important thing was the TCP-PLA/GeSe groups uniquely demonstrated the ability of the newly formed bone to connect the upper and lower parts of the radius surrounding the defect.

Aseptic loosening is mainly caused by abnormal bone resorption and inflammatory responses triggered by micro-particles produced by implant wear, forming a vicious cycle and resulting in a high rate of secondary surgeries. Cui et al.[181] proposed an innovative strategy based on the composite coating of piezoelectric polylactic acid (PLLA) and zoledronic acid (ZA). By introducing ZA as a nucleating agent into PLLA, the dual functional synergy of enhancing the piezoelectric properties of the material and sustained drug release was achieved. Experiments showed that the addition of ZA significantly increased the crystallinity of PLLA (from 21.65% to 37.89%), and its piezoelectric coefficient rised to 8.02 pC N^{-1}, which far exceeding that of pure PLLA (2.24 pC N^{-1}). The in vivo rat femoral implantation experiment further verified the superiority of the coating: The coating promoted osteogenic differentiation of mesenchymal stem cells (MSCs) through piezoelectric signals generated by mechanical deformation, and at the same time, the sustained-release ZA effectively inhibited osteoclast activity and reduced bone resorption. In addition, the coating demonstrated excellent biocompatibility and degradability, and can function continuously without external intervention.

5.2. Nerve Repair

The hierarchical regulation of physiological systems in an organism is controlled through neural networks comprising the central (CNS) and peripheral (PNS) nervous systems. Especially for the vulnerable PNS, possessing the absence of osseous encasement and blood-brain barrier (BBB) protection, was more prone to trauma.[182–185] Peripheral nerve injuries (PNIs) often result in sensorimotor deficits and irreversible functional impairment due to the limited regenerative capacity of mature neuronal populations. Current clinical interventions predominantly employ autologous nerve grafts, harvesting donor tissue from the patient for transplantation at injury sites. While this approach remains the therapeutic gold standard, it still falls short for ideal expectations. The appearance of piezoelectric polymers made by biomaterials provides a new platform for nerve regeneration. Under the guidance of neural tissue engineering, these piezoelectric polymers could be processed into nerve guidance conduits (NGCs).[186,187]

Currently, electrical stimulation has been widely accepted and applied in the repair of injured tissues, including nerves, muscles, skin, and bones. Research indicates that for nerve repair, the combination of poly pyrrole/sericin conductive nerve conduits with electrical stimulation can promote axonal and myelin regeneration while stimulating the activation of the MAPK signaling pathway. In this case, Wu et al.[145] prepared high-performance piezoelectric composite films using poly(3-hydroxybutyrate-co-3-hydroxyvalerate) (PHBV) and PLLA as substrates, KNN nanowires as conductive dopants, and surface modification of KNN nanowires with PDA (optimal mass ratio of KNN@PDA being 50%) (**Figure 10**a). Under ultrasonic drive, the device exhibited voltage and current outputs of 12 V and 36 μA, respectively, which increased with rising ultrasonic power. Subsequently, they established a rat sciatic nerve injury model. Experimental results demonstrated that the PHBV/PLLA/KNN nanogenerator, as a minimally invasive implantable neurostimulator, can significantly stimulate nerve regeneration while simultaneously monitoring nerve repair status. After encapsulation with PLA (≈200 μm thick), the nano-piezoelectric generator implanted in mice fully degraded by week 12 while providing stable electrical output for two weeks. In contrast, the nanogenerator encapsulated with PCL (≈500 μm thick) maintained its structural integrity and delivered stable output in PBS solution (37 °C) for 12 weeks. However, its output decreased to 80% of the initial value by week 12, and the device largely disappeared after 32 weeks.

Among the strategies of nerve repair, the combination of piezoelectric materials and drugs is an effective strategy. Both in vitro and in vivo experiments clarified that Curcumin possesses neuroprotective properties and the ability to facilitate nerve regeneration.[188] Nevertheless, its therapeutic application is constrained by pharmacokinetic limitations including rapid metabolic clearance and low water solubility.[189] To slowly release this therapeutic agent, Delavar et al.[190] encapsulated the Curcumin into Algae particles and made it with controlled drug release and great stability. The hollow piezoelectric conductive conduit was manufactured via electrospinning: the inner layer was poly(ϵ-caprolactone)/barium titanate (PCL/$BaTiO_3$) and the outer layer was poly-L-lactic acid/polyaniline-graphene-chitosan/gelatin (PLLA/PAG-CS/Gel). This structural configuration encapsulated curcumin-loaded Algae particles within the lumen, achieving sustained drug release over extended therapeutic windows. Due to its abilities to maintain drug release for a long time and transmit self-stimulated electrical signals between cells, such conduits showed extremely high-performance for repairing injured nerve tissues.

Except for conventional physicochemical modulation strategies, biomimetic approaches replicating natural ontogenetic processes have emerged as innovative paradigms for neural regeneration. Drawing inspiration from natural embryonic neurogenesis, Shan et al.[191] engineered a biohybrid neurodevelopmental self-evolving scaffold (ND-SENS) (Figure 10b) through synergistic integration of hierarchically ordered micro-nano architectures, extracellular matrix-mimetic hydrogels, and stem cell populations. The entire scaffold system can fully degrade within 12 months. This construct uniquely contained dual embryonic developmental mechanisms: 1) establishment of endogenous bioelectrical microenvironments through precisely aligned nanostructures to direct mesenchymal stem cell differentiation, and 2) dynamic biochemical regulation via paracrine signaling cascades from differentiated cells that induced the

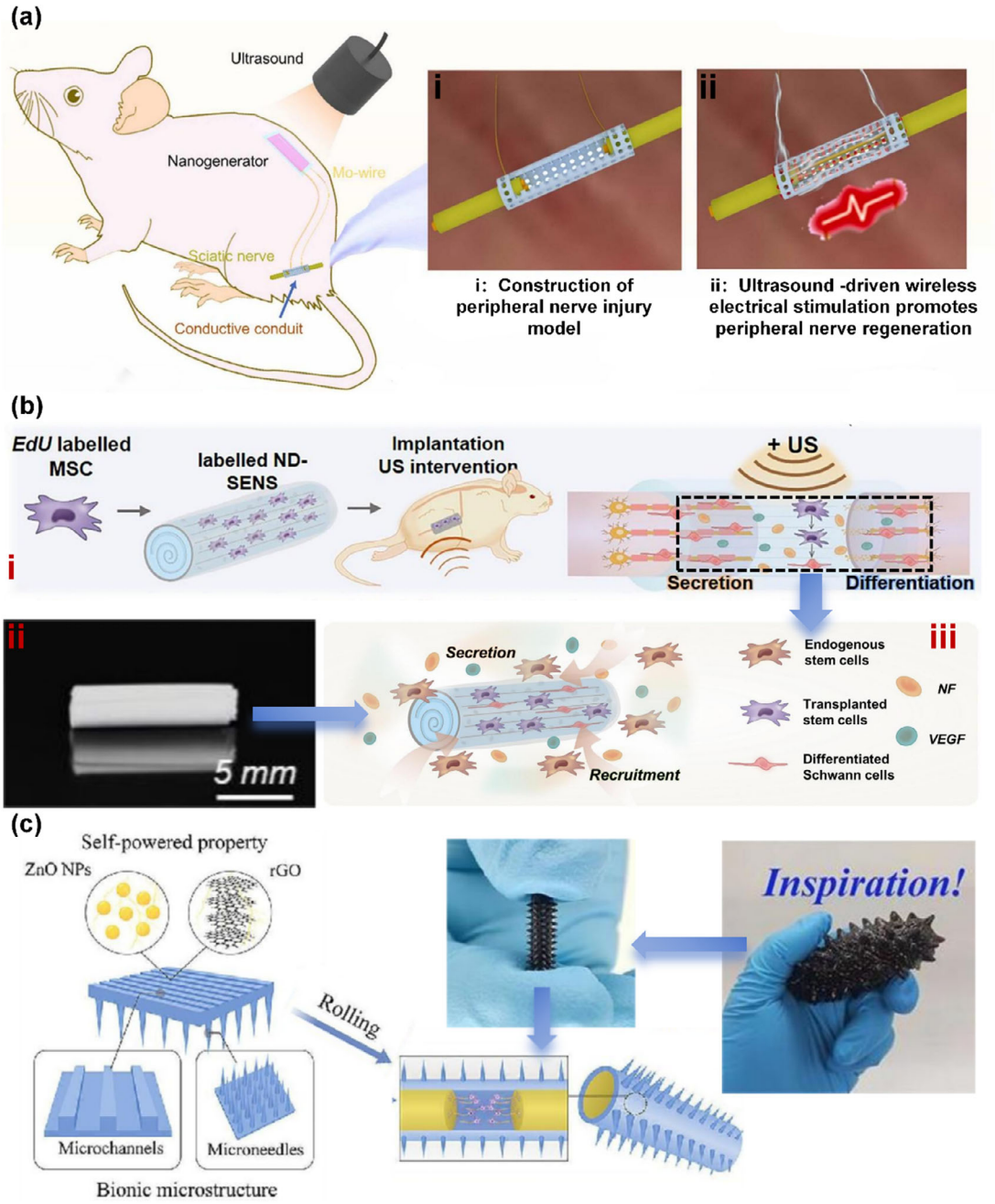

Figure 10. A variety of piezoelectric devices for nerve repair. a) Ultrasound-driven implantable PHBV/PLLA/KNN thin-film nanogenerator delivers drugs to promote nerve injury repair. Reproduced with permission.[145] Copyright 2022, Elsevier. b) Photographs of the BTNPs/P(VDF-TrFE) nanofibers derived hydrogel NGC and the schematic diagram of the US-responsive aligned piezoelectric nanofibers derived hydrogel conduits for peripheral nerve regeneration. Reproduced with permission.[191] Copyright 2024, John Wiley and Sons. c) Schematic of PZG-MNGCs and the digital photos of sea cucumbers and MNGCs. Reproduced with permission.[192] Copyright 2024, American Chemical Society.

recruitment and differentiation of endogenous stem cells, finally achieving self-evolving axonal outgrowth. In both the dorsal root ganglion explant growth model and rat sciatic nerve injury model, the ND-NENS exhibited remarkable neurorestorative effects.

The combination of biomimetic structures and drug delivery is also a new and effective platform for neural repair. Inspired by the structure of the sea cucumber, Hu et al.[192] proposed a bionic microneedle NGCs (MNGCs) integrated microneedles (MNs) and microchannel technology, which simulated the structure and piezoelectric of sea cucumbers (Figure 10c). The manufactures of such MNGCs were combined micro/nanomanufacturing and 3D printing technology. Morphologically, the outer layer of MNGCs is an outward-pointing array of MN tips. And the inner layer con-

tains microchannels which are produced by 3D printing technology. These microchannels work for regulating the directed migration of SCs to promote nerve fibers regeneration. Subsequently, in order to improve piezoelectricity and conductivity of the MNGCs to facilitate SCs' migration and restoration of neuromoscular function, they utilized doping the conductive reduced graphene oxide (rGO) and piezoelectric zinc oxide nanoparticles (ZnO NPs) into the polycaprolactone (PCL) scaffold. This made MNGCs generate microcurrent to stimulate ES to the muscles which have lost nerve innervation by the needle tips so that it could protect the muscle from atrophy. Thus, all these effects work together and finally lead to the inhibition of muscle atrophy and the restoration of nerve function.

The above studies show that piezoelectric materials offer new possibilities for PNI repair beyond autologous transplantation through bionic design, multi-mechanism collaboration (electrical stimulation/drug release/cell regulation), and advanced manufacturing techniques (electrospinning/3D printing).

5.3. Skin-Wound Repair

As the largest organ of the human body, skin plays an important role in protecting the internal tissues and organs. Therefore, when a skin wound occurs, it is extremely important and urgent to repair the injured area to a normal state. At the wound site, an endogenous electric field (EF) is usually generated,[193] and then triggers a series of physiological reactions to heal the wound. Owing to the existence of the endogenous electric field, it could generate a positive effect on all stages of wound healing. Subsequently, according to some studies, researchers have proved that wound healing could be facilitated by the existence of bioelectricity via speeding the migration of critical cells.[194] Based on this, researchers further explored the effect of exogenous electrical stimulation on wound healing, and achieved some good results. For wounds that cannot heal themselves, exogenous electric fields can usually be used for adjuvant treatment.[194] Thus, the devices made of piezoelectric materials play a certain role in the intervention of wound healing.

EF is generated by the differences in ionic gradients and acts as a decisive role in the processing of wound healing. Inspired by this, Luo et al.[195] presented a self-manipulating sodium ion gradient-based endogenic electrical stimulation dressing (smig-EESD) to achieve non-invasive and endogenic electrical stimulation of wound healing. Such smig-EESD could eventually enhance the wound endogenous EF through reducing the potential at the center of the wound via absorbing Na^+ and leading to facilitate the tissue repair process by converting the active transport dependent on Na^+/K^+-ATPase into passive diffusion under saving ATP consumption situation. Meanwhile, the formation of scar and injury-associated inflammatory responses could be inhibited by upregulating the secretion of multiple cytokines to regulate innate and adaptive immune responses.

During wound healing, the timely dynamic regulation of immune responses and angiogenesis plays a crucial role in subsequent tissue repair, scar formation, and regeneration at the injured site. Yan et al.[196] combined natural collagen matrix with amino acid-modified barium titanate (BTN) nanoparticles, using oxidized konjac gum (OG) as a crosslinker, to prepare a tilapia collagen-based piezoelectric hydrogel scaffold (Col/OG/BTN) (**Figure 11a**), proposing a novel wireless immunomodulation strategy. The 3D porous structure of this hydrogel scaffold supported cell migration and preferential transmission. Under ultrasonic (US) drove, the phosphoinositide 3-kinase (PI3K)/protein kinase B (Atk) and tumor necrosis factor (TNF) signaling pathways were modulated by the hydrogel scaffold, enabling the reprogramming of pro-inflammatory M1 macrophages into pro-healing M2 macrophages. Experimental results from rat full-thickness excision wound models demonstrated that this hydrogel scaffold significantly promotes angiogenesis, collagen deposition, stimulates hair follicle regeneration, reduces inflammation, and ultimately achieves high-quality wound healing and functional recovery. Compared to other hydrogel scaffolds, the Col/OG/BTn hydrogel scaffold exhibited the highest retention rate after 14 days of in vivo implantation, demonstrating excellent stability.

Contemporary wound management strategies require synergistic integration of bioelectrical stimulation and antimicrobial intervention to address both tissue regeneration and infection control. Sonodynamic therapy (SDT) has emerged as a precision antimicrobial modality, leveraging ultrasound-activated sonosensitizers to generate cytotoxic reactive oxygen species (ROS) with deep tissue penetration while circumventing bacterial resistance mechanisms.[197] Wang et al.[198] presented an electroactive multifunctional device through lithium-doped ZnO/PLLA (Li-ZnO/PLLA) microfibers functionalized with 4-octyl itaconate (4OI) antioxidant coatings. Lithium doping induced lattice expansion in wurtzite-structured ZnO nanorods, synergistically amplifying piezoelectric output and ROS generation to potentiate SDT efficacy. This device can slowly degrade in PBS solution and release zinc ions, which participate in subsequent processes such as antibacterial activity and tissue repair. Systematic evaluation of this piezoelectric device employed a Sprague-Dawley rat full-thickness dorsal wound model (Figure 11b), with commercial Atrauman AgTM dressing serving as the positive control (POS). Histopathological analysis revealed differential suppuration patterns: while the 1.25 ZnLiPOI US+ group and Atrauman AG group maintained microbial suppression, other experimental groups exhibited progressive Staphylococcus aureus colonization by days 3–6 post-injury. Quantitative wound closure metrics demonstrated superior regenerative performance in the 1.25 ZnLiPOI US+ group, achieving near-complete epithelialization (99.0%) with scar-free restoration—a significant improvement over conventional antimicrobial dressings.

Complementing existing therapeutic modalities, Das et al.[199] presented an innovative biodegradable piezoelectric wound scaffold with the capability of self-charged (Figure 11c). PLLA nanofibers are prepared by electrospinning, and then a Teflon sheet is placed on the top and bottom respectively. The film was immersed in PBS solution (37, and 70 °C) and simulated body fluid (SBF) (37, and 70 °C) respectively, and after fourteen days, the film completely disintegrated in both the 70 °C PBS and SBF solutions. Such unique piezoelectric scaffolds were drove by the external ultrasound that generated well-controlled surface charges with different polarities. Therefore, it could show

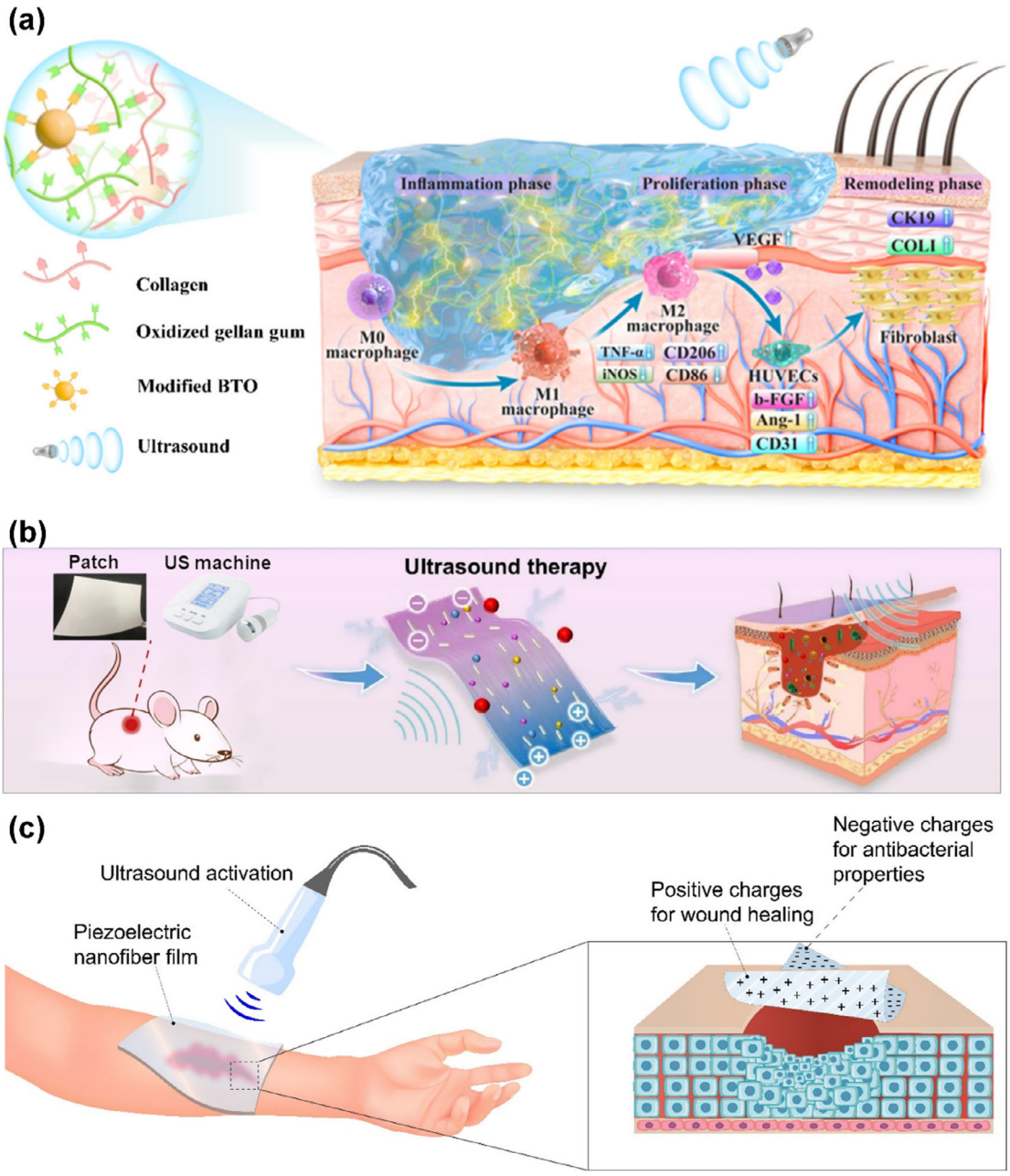

Figure 11. A variety of piezoelectric devices for skin-wound repair. a) Schematic of the mechanism by which Col/OG/BTN piezoelectric hydrogel scaffolds promote wound repair and healing. Reproduced with permission.[196] Copyright 2025, Elsevier. b) Schematic illustration of the mechanism of piezoelectric microfibers for wound healing under stepwise US therapy. Reproduced with permission.[197] Copyright 2025, Elsevier. c) The biodegradable piezoelectric PLLA nanofibers applied to the wound site generate controllable surface charges under ultrasonic drive to promote wound healing and prevent bacterial infection. Reproduced with permission.[198] Copyright 2023, Elsevier.

the dual therapeutic functionality—bactericidal activity through negative surface charge and pro-regenerative effects via positive surface charge. The experiments in vivo had certified the scaffolds were activated by low-frequency/intensity US could make it equip the abilities of suppressing the growth of S. aureus and P. aeruginosa bacteria, promoting the proliferation of fibroblast/epithelial cells as well as improving the expression of genes like collagen I, III, and fibronectin, which are typical for the processing of skin-wound repair.

5.4. Tumor Therapy

As one of the three major killers, cancer has extremely threatened human health today. In recent years, electrical stimulation therapy as one potential area of research attracted a lot of attention. It includes direct ES like irreversible electroporation (IRE), tumor treating fields (TTFields), and direct ES therapy based on self-powered devices (nanogenerator, etc.) or electrically responsive nanomaterials (piezoelectric nanomaterials,

electrocatalytic nanomaterials and etc.), and some of them have been applied in clinical practice widely.[200] Additionally, 1) Catalyzing the production of reactive oxide species (ROS) to eliminate the tumor cells. 2) Promoting the apoptosis of tumor cells through the biological activities influenced by the electrical signals generated. which are two of the main mechanisms of mechanical stimulation of piezoelectric nanomaterials for tumor therapy.

Unlike tissue regeneration, tumor therapy requires higher electrical signals to generate reactive oxygen species and induce apoptosis, thus, improving the piezoelectric properties of piezoelectric materials is necessary. Zhang et al.[141] presented an ideal transient implantable piezoelectric material for tumor therapy. They found that, without poling conditions, the piezoelectric constant of molecular crystal $HOCH2(CF_2)_3CH_2OH$ [2,2,3,3,4,4-hexafluoropentane-1,5-diol (HFPD)] (**Figure 12a**) could reach to ≈138 pC N^{-1}, which has exceeded 100 pC N^{-1}. Besides the strong piezoelectric response, it also shows excellent biocompatibility, biodegradability, and biosafety.

High-voltage nanosecond pulses (hvNPs) can penetrate the membrane and directly affect the intracellular components, resulting in DNA damage, organelle membrane perforation, etc., which would induce apoptosis in cancer cells. Xu et al.[201] developed a Schottky nanodiode-enabled triboelectric nanosecond pulse generator (st-NPG) through integration of wafer-scale TiO_2 nanotube (TNT) arrays with titanium substrates. This architecture synergistically enhanced interfacial charge accumulation while achieving optimal electrochemical compatibility, characterized by low impedance, elevated capacitance, and maximized surface charge density. The optimized st-NPG demonstrated exceptional electromechanical performance, generating output parameters of 10 kV peak voltage, 60 ns pulse duration, 17 MW peak power, 0.6 J single-pulse energy, and sustained operational stability over 7 days. Meanwhile, they also proved its potential for medical applications by generating hvNPs to achieve immunogenic death of tumor cells and pulsed ablation for tumor treatment.

Except for the direct electrical stimulation, the synergistic effect of piezoelectric materials and ultrasound can achieve precise strikes on deep tumors. Ultrasound has excellent tissue penetration ability as well, which has inherent advantages in the non-invasive treatment of deep and solid tumors. Cai et al.[202] proposed a new method called the one-step method to synthesize hollow ZnO (HZnO). Subsequently, black phosphorus quantum dots (BPQDs) were attached to the surface of HZnO by electrostatic adsorption. For improving tumor-targeting ability and water solubility, X-PEG [poly (ethylene glycol)]-COOH [X = RGD (arginine-glycine-aspartic acid peptide)/FITC, 1/1] was modified on the surface of HZnO-BPODs (Figure 12b). The piezoelectric constant of HZnO was enhanced almost four times than the common solid ZnO NPs. When the HZnO-BPQDs was irradiated by US, due to its peculiar hollow morphologies and heterostructures, it could generate ROS more effectively. The function of ROS generated is to heighten autophagy efficiently, causing in ferroptosis. Meanwhile, under an acidic tumor microenvironment, HZnO-BPQDs could degrade completely to release Zn^{2+} and PO_4^{3-} ions respectively, and all of them could induce autophagy in tumor cells. The inhibition rate of HZnO-BPQDs/US group could reach up to 90%, and the inhibition rate of HZnO-BPQDs/US group was significantly higher than any other groups. As so far, HZnO-BPQDs could be thought as the first example of a completely degradable piezoelectric sonosensitizer at the tumor site.

Today, an increasing number of piezoelectric materials are being developed as sonosensitizers for sonodynamic therapy (SDT) targeting tumors. Consequently, demands on sonosensitizers are growing more stringent: they must generate sufficient reactive oxygen species (ROS) to induce pyroptosis while also degrading in vivo and exhibiting excellent biocompatibility. Therefore, Cai et al.[203] constructed biodegradable Mn-doped hydroxyapatite (Mn-HAP) based on hydroxyapatite (HAP) for SDT (Figure 12c). Although HAP has been reported for SDT, its low piezoelectricity results in low ROS generation efficiency, limiting its application. Cai et al. doped Mn^{2+} into HAP to introduce oxygen vacancies (Ov), enhancing the piezoelectric coefficient of HAP by 1.7-fold. Additionally, Mn^{2+} activated the cGAS-STING signaling pathway and stimulated dendritic cell (DC) maturation, demonstrating additional therapeutic advantages. Experimental results indicated that Mn^{2+} doping effectively enhances ROS generation. Under ultrasonic cavitation, bubble rupture created high pressure, inducing HAP deformation and generating an internal electric field. This process produces O_2^- and ·OH, activating cell membrane-associated ion channels and inducing Ca^{2+} influx. Subsequently, Mn-HAP began degradation in the weakly acidic tumor microenvironment (TME). The synergistic effects of Ca^{2+} released during degradation, generated ROS, and Mn^{2+} activate the cGAS-STING pathway, enhancing pyroptosis-induced immunotherapy against tumors. Mn-HAP achieves complete degradation after 96 h of incubation in a weakly acidic TME.

Unfortunately, the blood-brain barrier (BBB) is a significant pharmacological challenge, which severely restricting therapeutic efficacy by impeding drug penetration and limiting conventional delivery systems. This biological interface fundamentally constrains treatment modalities for intracranial malignancies. Emerging piezoelectric biomaterials offer potential for transient BBB modulation to facilitate targeted neurotherapeutic delivery. Like we mentioned before in this article, Chorsi et al.[41] adopted glycine-embedded poly(ϵ-caprolactone) (PCL) nanofibers via electrospinning, achieving large-scale alignment of glycine crystals within the polymeric matrix. These nanostructured fibers exhibited superior actuation performance (i.e., the ability to convert electricity into motion) compared to solvent-cast glycine films, demonstrating enhanced efficiency in mechano-electrical energy transduction. The optimized glycine-PCL composite was integrated into ultrasonic transducers capable of generating ultrasound stimulation, enabling transient blood-brain barrier (BBB) permeability for targeted CNS drug delivery. Moreover, the glycine-PCL-based US transducers can be controlled and optimized the functional lifetime by tailoring the encapsulation layer, to meet all kinds of different needs for various implantable applications. In their study, they used it to assist the delivery of formulated paclitaxel (PTX; it's known to all that this chemotherapeutic drug is challenging for bypassing the BBB) for treating mice bearing an orthotopic gliolastoma (GBM) tumor model. Such a device enhanced the animal survival time (two-fold) in mice-bearing orthotopic glioblastoma models notably.

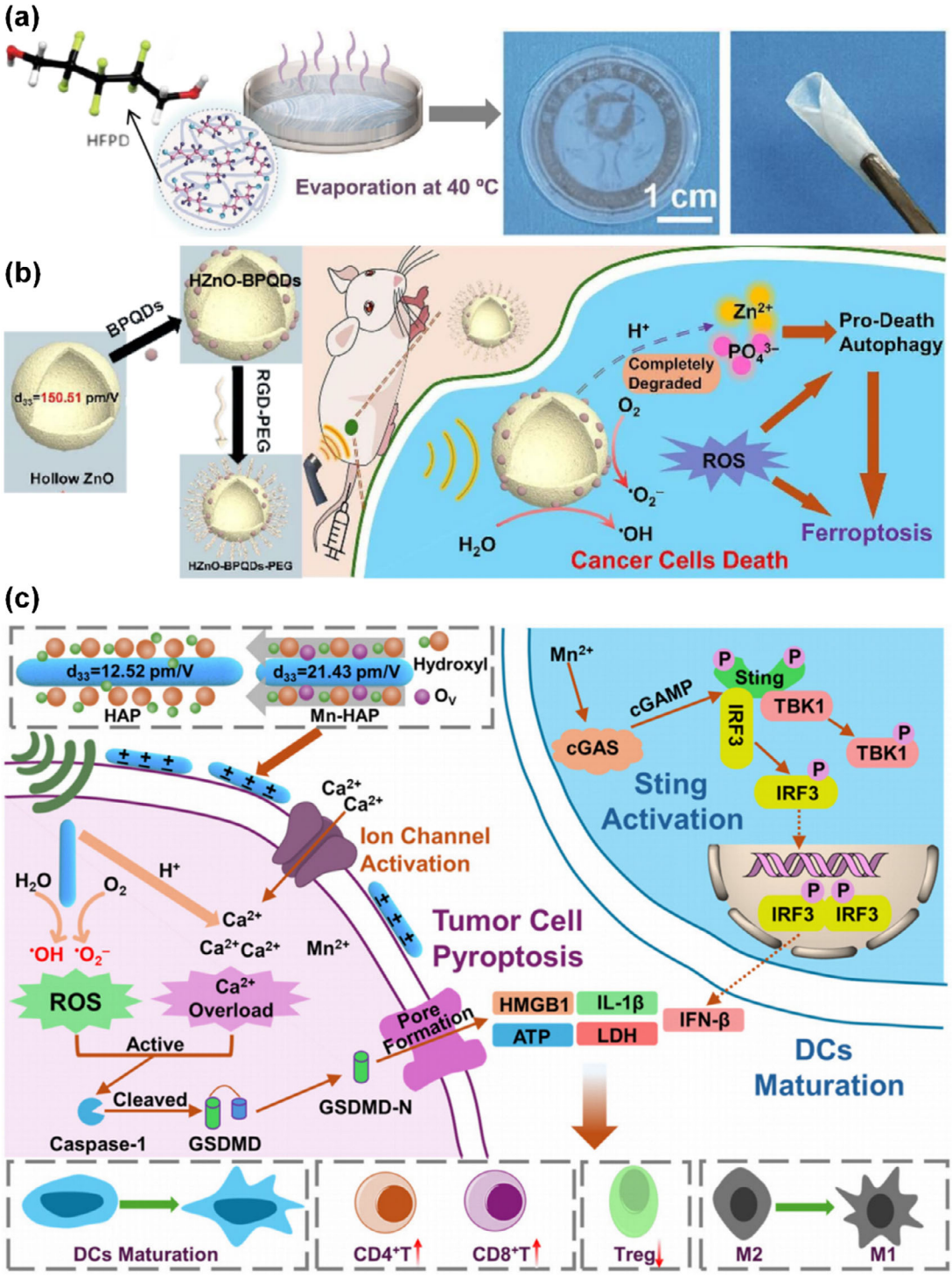

Figure 12. Various piezoelectric devices are used for tumor therapy. a) The left side shows a schematic diagram of the solvent evaporation method for preparing PVA-HFPD films, while the right side displays optical images of the PVA-HFPD film and its curled state. Reproduced with permission.[141] Copyright 2024, The American Association for the Advancement of Science. b) Schematic of the Synthesis of HZnO-BPQDs-PEG and the Anti-Tumor Process through Zn^{2+}/PO_4^{3-} Ions-Induced Pro-Death Autophagy and ROS. Reproduced with permission.[202] Copyright 2024, American Chemical Society. c) Schematic of the Antitumor Process of Mn-HAP and the Mechanism of Tumor Cell Pyroptosis, Activation of cGAS-STING Pathway, and following Immune Responses. Reproduced with permission.[203] Copyright 2025, American Chemical Society.

5.5. Others

Biodegradable piezoelectric materials, as a kind of multifunctional material with good biocompatibility and biodegradability, have been applied in various biomedicine fields such as bone repair, nerve damage repair, skin-wound repair, and tumor treatment. Without any doubt, these materials also show unlimited potential in many other biomedical applications. In this section, we will briefly introduce some other applications, including drug release,[204] device power supply,[205,206] and flexible sensing devices.

The self-powered devices such as nanogenerators (NGs) which could transform biomechanical energy into electricity and power for the long-term drug release. And it plays an important role in precision medicine which is a kind of highly effective therapy requires precise regulation of drugs in terms of time, space, and dosage. Compared with conventional power supply equipment, the NGs overcome the limitations of short-lifetime battery, large size, toxic elements, etc., which were major challenges in the wearable and implantable controlled drug release devices.

Piezoelectric Catalytic Therapy (PCT), based on an ultrasound-activated piezoelectric catalyst, has emerged as a novel reactive oxygen species-driven therapeutic strategy. The high precision of piezoelectric nanoparticles (PNPs) in PCT offers broad application prospects. However, conventional PNP delivery via injection may cause undesirable tissue damage. To address this, Xue et al.[204] proposed a minimally invasive approach (**Figure 13a**): creating microchannels with a soluble microneedle (MN) patch that allows drug-loaded PNPs to act locally on superficial tumors or enter systemic circulation. This wearable flexible ultrasound microneedle patch (wf-UMP) comprised three components: 1) A stretchable, lead-free ultrasonic transducer array for ultrasound emission 2) A biocompatible hydrogel containing N-hydroxy succinimide (NHS) for adhesion 3) A PNP-loaded, soluble hyaluronic acid (HA) microneedle patch for minimally invasive, pain-free drug delivery. This microneedle exhibited a more focused beam with a penetration depth of ≈100 mm, enabling more efficient diffusion and activation of PNPs. Notably, the MN patch possessed excellent solubility to ensure rapid dissolution and drug release post-application. Moreover, under 30 min of US stimulation, the MN delivered drugs to a depth of 4.6 mm within the agarose hydrogel—twice deeper than the control group without US stimulation. Subsequently, in vivo anticancer experiments were conducted using a 4T1 subcutaneous tumor model. Results demonstrated that wf-UMP significantly inhibited tumor growth and prolonged mouse survival without observable toxic side effects.

Piezoelectric materials, attributing to their unique mechanical energy-electrical conversion properties, provide a subversive solution for the treatment of cardiovascular diseases. Compared to the conventional cardiovascular electronic devices (CIEDs) which are limited by bottlenecks such as battery dependence, non-degradable materials, and invasive electrodes, the piezo-driven self-powered energy systems can generate electricity independently through biomechanical stimulation (such as heartbeat, blood flow) and also achieve precise electrophysiological regulation and controlled degradation, thereby avoiding the risk of secondary surgery. In recent years, through material innovation and structural design, researchers have successfully developed piezoelectric intervention devices with efficient energy conversion, tissue compatibility, and therapeutic functions, opening up a non-invasive and intelligent new path for cardiac pacing and myocardial repair. Lv et al.[205] extracted silk sericin (SS) from Bombyx mori cocoons as a fundamental material to develop functionalized SS (F-SS) materials and designed an F-SS-based energy-generating device (EG device) (Figure 13b). The SS was functionalized with aminated reduced graphene oxide (A-rGO), resulting in the crystallization of the SS structure and enhancing its charge storage capacity. Subsequently, the F-SS-based piezoelectric film was prepared by integration of a self-assembly approach and a chemical crosslinking method involving F-SS, PVA, and ZnO nanorods. Due to doping piezoelectric and anti-inflammatory ZnO nanorods into the F-SS and PVA mixture, the piezoelectric coefficient d_{33} of the film could reach to 12.1 pC N^{-1}, over than the most of reported bio-organic films. Moreover, under manual pressing, the EG device could generate sufficiently instantaneous energy power density (218.5 μW m^{-2}) for delivering effective pacing to restart a non-beating heart or normalize an atrioventricular block in a preclinical model. Such a film can fully degrade within 20 days in PBS solution (37 °C, pH = 7.4). When devices encapsulated with PET were immersed in PBS solution, their output remained stable at ≈847 mV for the first and two days. On the third and fourth days, the output decreased by 24.5% and 75.2%, respectively, until complete failure occurred on the fifth day.

However, the percutaneous leads of the pacemakers and pacing therapy devices which commonly need invasive electrode implantation, resulting in enhancing a risk of infection.[207] Zhao et al.[206] designed a wireless ES system based on lead-free, biodegradable PLLA piezoelectric nanofibers. The PLLA nanofiber membrane began degrading after two months of immersion in PBS solution (37 °C, pH = 7.4), breaking down into smaller fragments by the third month. Following implantation in mice, small fragments of the implant remained adhered to the heart surface after three months. Upon removal, these fragments retained piezoelectric response under ultrasonic stress. In their study, they proved that such an ultrasound-driven wireless ES system could conspicuously improve mitochondria function and angiogenesis and promoted the structural and functional recovery of cardiac tissue in murine myocardial infarction model both in vivo and in vitro experiments. As shown in Figure 13c-ii, after 28 days of ultrasound-driven wireless ES therapy treatment (PLLA-US group), the representative echocardiographic images and statistical analysis results illustrated a remarkable improvement in myocardial systolic function. Moreover, the ES system also played a role in regulating intracellular calcium ion concentration and cardia tissue contraction rhythm of isolated neonatal rat.

The conventional energy storage devices (commonly, batteries and supercapacitors) are rigid, non-degradable, non-recyclable, short-lifetime, low biocompatible, and even contain toxic elements. Thus, for the long-time development of wearable and implantable electronics, the development direction of next-generation bioelectronics requests such energy storage devices are soft, flexible, biocompatible, and biodegradable. Lee et al.[208] demonstrated the M13 bacteriophage (phage) could generate electrical energy due to its piezoelectricity and liquid-crystallinity, and then used piezoresponse force microscopy to characterize the structure-based piezoelectricity of the phage at the molecular

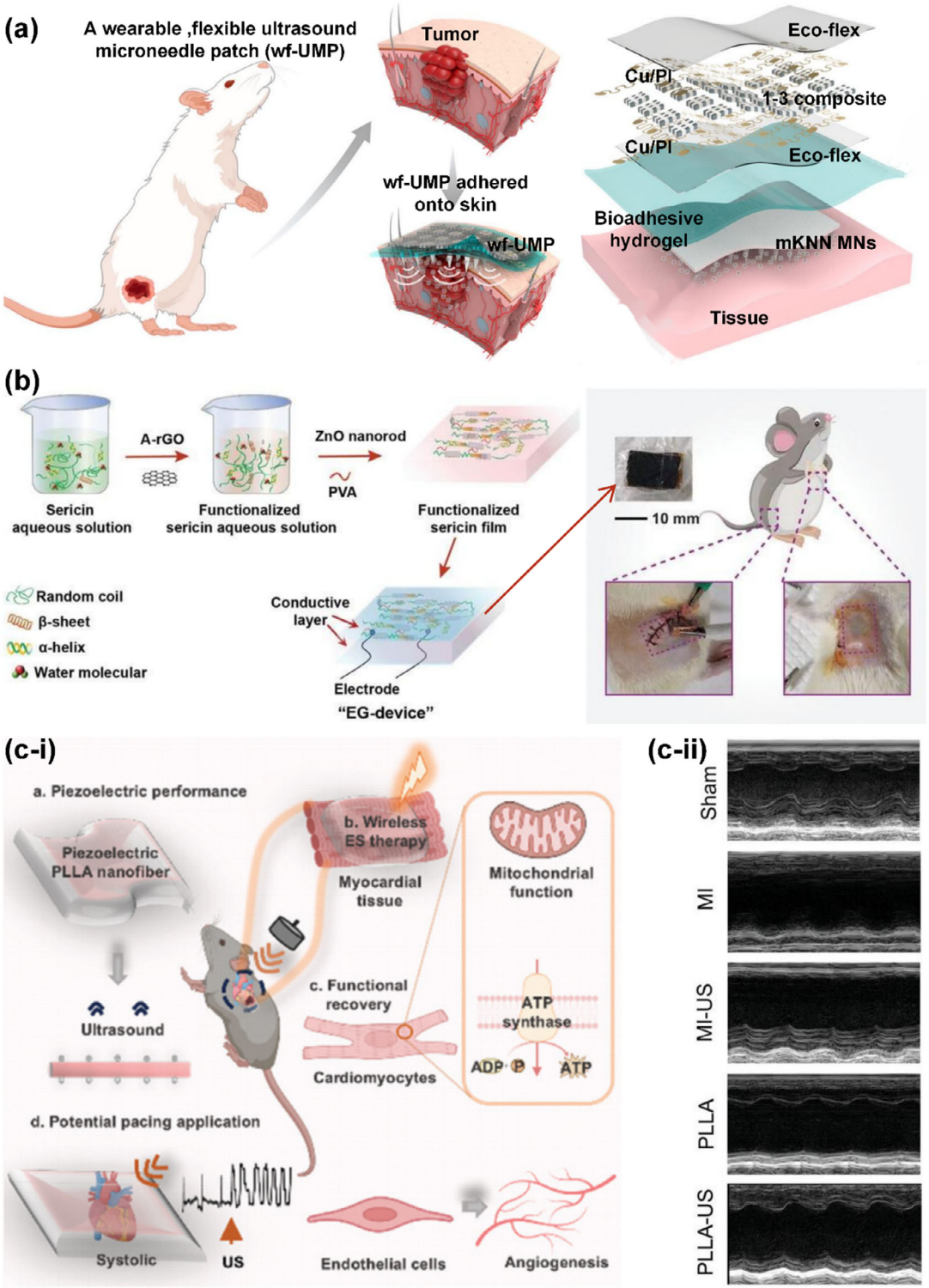

Figure 13. A variety of piezoelectric devices for precise drug release and delivery, as well as cardiac pacing. a) Schematic diagram of wf-UMP for superficial tumor treatment and structural diagram of wf-UMP integrated electronic devices. Reproduced with permission.[204] Copyright 2025, Nature Communications. b) Scheme of the preparation process of sericin-based piezoelectric device and the schematic image and digital photographs of the implantations of packaged EG-device in the thigh and chest areas of SD rats. Reproduced with permission.[205] Copyright 2025, John Wiley and Sons. c-i) Schematic of an ultrasonically driven wireless ES system for treating myocardial infarction and serving as a potential cardiac pacemaker. PLLA piezoelectric nanofibers, under ultrasonic drive, deliver therapeutic agents to mouse myocardial tissue, improve mitochondrial function, promote angiogenesis, effectively treat myocardial infarction, and possess potential pacing capabilities. c-ii) Representative echocardiography images of mice in five groups on day 28 after MI. Reproduced with permission.[206] Copyright 2025, John Wiley and Sons.

level. The piezoelectric constant of self-assembled thin films has been tested and reaches up to 7.8 pm V^{-1}. They observed that the piezoelectric response was regulated by the dipole strength which depended on genetically engineering the major coat proteins (pVIII) of the phage. Subsequently, they utilized a variable number of the negatively charged amino-acid glutamate (E) to design the pVIII N-terminus. The residues [from one (1E) to four (4E)] were inserted between the first (Ala) and fifth (Asp) amino acids of the wild-type pVIII major coat sequence. And this meant that the 4E-phage shows two additional negative charges than the wild-type phage which contains two negative charges without the insert region. Based on such 4E-phage films, researchers dropcast the spontaneously ordered multilayer phage between two gold electrodes. Its piezoelectric coefficient was roughly estimated of 11.2 ± 0.7 pm V^{-1}, and the open-circuit voltage and current were 400 mV and 6 nA, respectively, and it could be used to operate a liquid-crystal display. The development of degradable nanogenerators (BD-NGs) provided another promising and safe method for biotransient medical electronics. Nevertheless, because of the low output performance of BD-NGs, it faces a huge challenge during the rapid development phase.

To enhance the output performance of nanogenerators, researchers have developed a piezoelectric-triboelectric hybrid strategy. Liu et al.[209] assembled PVA/Gy (γ-Glycine)/PVA to fabricate an excellent performance and completely biodegradable piezo-triboelectric hybrid nanogenerator (FB-HNG) with a sandwich-like heterostructured through an electric field-assisted water evaporation method (**Figure** 14a-i). The inner Gy bulk layer was designed to provide highly piezoelectric output, while the outer PVA layer formed the triboelectric part by rub against a PLGA film. Thus, such films finally achieved a maximum piezoelectric coefficient d_{33} of 9 pC N^{-1} and maximum output voltage and current of 94 V and 2.3 μA, respectively. In addition, as shown in Figure 14a-iii, among all the reported BD-NGs, this film also showed the highest current density of 1.53 μA cm^{-2} and charge density of 6.53 nC cm^{-2}.

Additionally, beyond amino acid crystals, vitamin crystals can also be utilized to fabricate piezoelectric nanogenerators. Hu et al.[210] conducted the first systematic investigation into the piezoelectric properties of vitamins. They discovered that vitamin molecules can self-assemble into diverse supramolecular structures, with density functional theory (DFT) calculations revealing that the piezoelectric coefficient of vitamins can vary within the range of 3.8 to 42.8 pC N^{-1}. Notably, they observed that vitamin B_7 D-biotin (D-BIO) (Figure 14b) exhibited an exceptionally high piezoelectric coefficient d_{36} of 42.8 pC N^{-1} due to its low symmetry and sophisticated supramolecular arrangement. Subsequently, when fabricated into a piezoelectric nanogenerator, it generated an open-circuit voltage of 0.8 V under an external mechanical force of 47 N. It maintained stable output after 5400 cycles and for at least three months.

Moreover, for the development of fully biodegradable flexible supercapacitors (BFSC), Wang et al.[214] presented a BFSC designed for in vivo applications. The BFSC integrated MXene nanosheet electrodes, a ChCl/PVA hydrogel electrolyte, and a PLGA encapsulation layer, enabling high electrochemical performance (0.36 F cm^{-2} surface capacitance, 73.1 μWh cm^{-2} energy density) alongside complete biodegradability within 120 days post-implantation. Such BFSC showed outstanding performances include a month operational lifespan in vivo (70% capacitance retention), 20 000-cycle stability, and the ability to power bioelectronic circuits for neural excitation/inhibition and cardiac pacing in animal models.

The flexible wearable devices can collect various stimulations from the environment and convert it into electrical signals. Thus, for sensing purposes, it is required to achieve high flexibility of sensors to fit human skin and enhance the fidelity of signal acquisition. Not only that, but the piezoelectric materials used to fabricate sensors are predominantly non-biodegradable. Therefore, there is an urgent need to develop environmentally friendly, low-cost devices that combine high sensing performance with the simplicity of preparation and use of biodegradable materials. As a recently recognized potential sensing material for flexible pressure sensors—MXene—Su et al.[211] employed a simple hydrazine-induced foaming method. They utilized 1D cellulose nanofibers (CNF) to combine multiple layers of adjacent MXene nanosheets, increasing the distance between MXene layers and forming a well-developed porous structure (Figure 14c). The reducing environment in hydrazine also prevented MXene oxidation, significantly improving the sensor's performance. The MXene/CNF foam-based piezoresistive sensor developed by Su et al. exhibits exceptional performance due to its unique microstructure: a wide sensing range, high sensitivity (419.7 kPa^{-1} at 0–8.04 kPa and 649.3 kPa^{-1} at 8.04–20.55 kPa), low detection limit (4 Pa), fast response/recovery times (123/139 ms), and outstanding durability (10 000 cycles). In the 1 wt.% H_2O_2 solution, the device degraded almost completely within 12 days, with MXene film degradation consistently preceding CNF degradation.

Gelatin has emerged as a candidate material for sustainable transient electronics due to its biocompatibility, ambient-temperature processability, and environmental benignity. However, its practical application has been limited by suboptimal electromechanical properties (low piezoelectric coefficient and pyroelectric coefficient) and hydrolytic instability. Addressing these limitations, Ghosh et al.[212] developed a fully biodegradable epidermal sensor (Figure 14d-ii) mimicking the hierarchical interlocking microstructures of dermal-epidermal junctions. The system combined porcine-derived gelatin matrices with magnesium electrodes, achieving 6-fold and 11.8-fold enhancements in piezoelectric (d_{33} = 24 pC N^{-1}) and pyroelectric (13 μC m^{-2} K^{-1}) coefficients relative to planar gelatin films. Besides, this bioinspired architecture demonstrated unprecedented multimodal sensitivity, exhibiting a pressure detection threshold of 0.005 Pa (41 MV Temperature detection limit of 0.04 K, which performance metrics surpassing all reported ferroelectric biosensors. According to the proof-of-concept tests, this device proved that it had the ability to sense the spatially resolved pressure, temperature, and surface texture in an unknown object.

Bacterial cellulose (BC) hydrogel as a natural polysaccharide polymer cellulose consists of β-1,4 glucosidic linkages with β-D-glucose and is produced by microorganisms which belongs to Gluconacetobacter xylinus.[215] Except for the biocompatibility, biodegradability, and renewable property, BC also exhibited high crystallinity, water uptake capacity, and ionic exchangeability compared to the plants or Cladophora cellulose. Lu et al.[213] presented a sensor composed of a matrix of the BC hydrogel and a functional element of the imidazolium perchlorate ($ImClO_4$) molecular ferroelectric (Figure 14e-i), exhibiting an excellent sen-

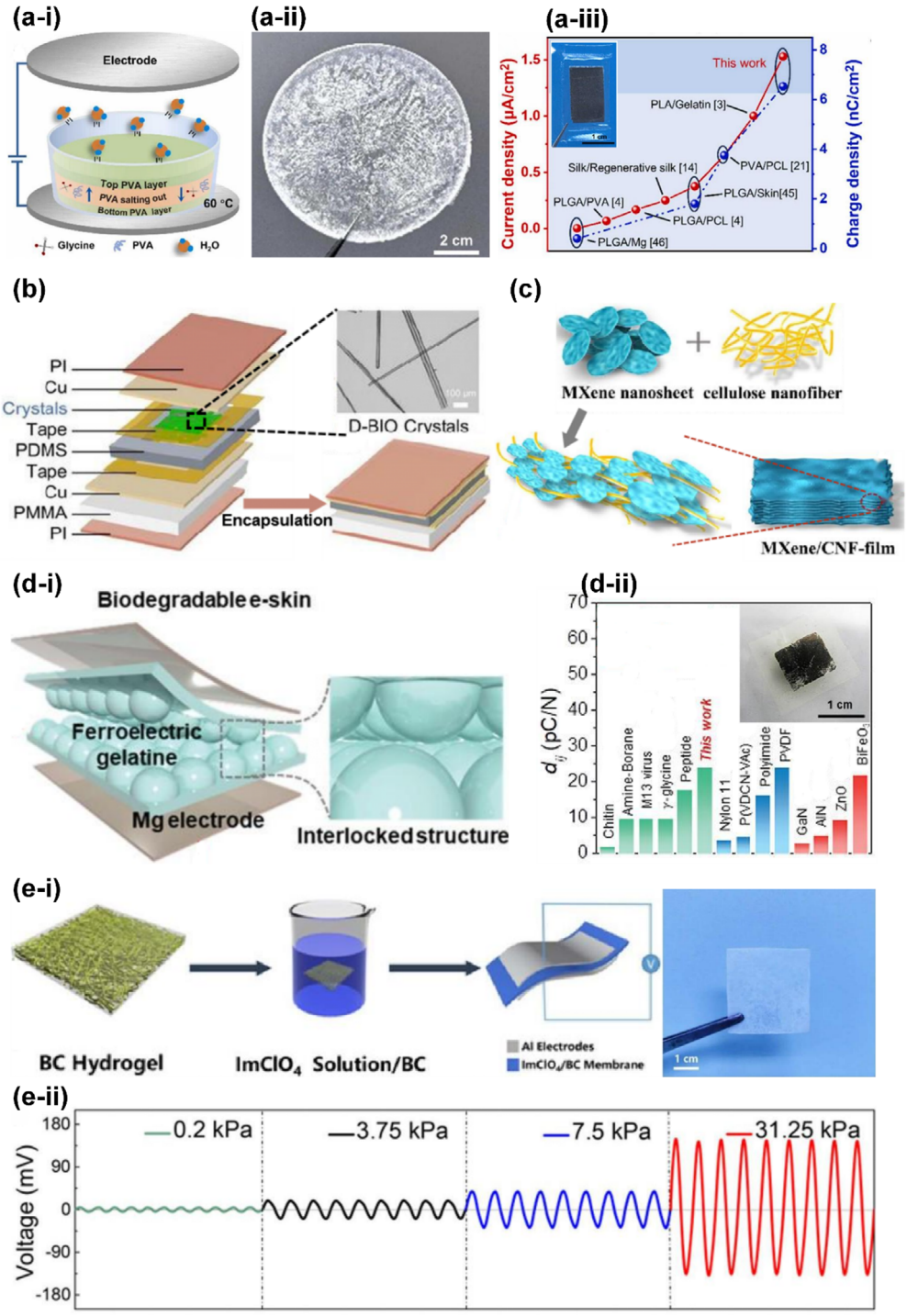

Figure 14. A variety of piezoelectric devices used for power generation, energy storage, and sensing. a-i) Schematic diagram of the preparation process of PVA/Gy/PVA piezoelectric film using the electric field-assisted evaporation method. a-ii) Optical image of a wafer-scale PVA/Gy/PVA piezoelectric film with a diameter of 9 cm. a-iii) Optical image of an FB-HNG (upleft) and a systematically comparison of the output current density (red) and charge density (blue) between previous reported FB-NGs and our FB-HNG. Reproduced with permission.[209] Copyright 2024, Elsevier. b) Schematic diagram of the layered structure of the D-BIO device and transmission electron microscopy image of the D-BIO crystal. Reproduced with permission.[210] Copyright 2025, Wiley. c) Schematic Diagram of the Preparation Process for MXene/CNF Foam. Reproduced with permission.[211] Copyright 2021, Elsevier. d-i) Schematic of the concept of gelatine-based transient "green" electronics. d-ii) corresponding photographs of the e-skin (upright) and comparison of the piezoelectric strain coefficient (d_{ij}) of the interlocked microdome gelatine with various biodegradable (green) and non-biodegradable organic (blue) and inorganic (red) materials. Reproduced with permission.[212] Copyright 2021, John Wiley and Sons. e-i) Schematics of the fabrication process to prepare the molecular ferroelectric/BC hybrid sensor and the optical images of a flexible molecular ferroelectric/BC hybrid. e-ii) The piezoelectric voltage waveforms under various out-of-plane compression pressures of 0.2, 3.75, 7.5, and 31.25 kPa. Reproduced with permission.[213] Copyright 2022, American Chemical Society.

sitivity of 4 mV kPa^{-1} and a wide operational range from 0.2 to 31.25 kPa (Figure 14e-ii).

In this review, a lot of advanced applications of biodegradable materials have been introduced. Attributed to the excellent biodegradability, biocompatibility, and biosafety of these materials, obtained from nature or synthesis, they have rapidly emerged and developed in the medical fields. However, there are still some non-negligible challenges we need to face and solve, including achieving long-term stability, higher piezoelectricity, more suitable to the different situations and requirements, etc. Additionally, another major challenge we face is how to transition these biodegradable piezoelectric device technologies from the laboratory to clinical practice, including addressing deeper immunotoxicity concerns, further optimizing ultrasound delivery, and standardizing synthesis steps. Although these studies are still in their early stages, these materials demonstrate significant potential and market applications in biomedical fields.[216] As long as we can further overcome these difficulties, the potential and application of this material will be further amplified.

6. Discussion and Prospects

The emergence of degradable piezoelectric materials signifies a transformative shift in bioelectronic medicine, creating unprecedented opportunities to bridge endogenous bioelectric phenomena with clinical therapies. Replacing the traditional implantable medical electronic devices (IMEDS) with the developed implantable biodegradable medical electronic devices (IBMEDs) exhibits great significance in monitoring the human physical signals and the treatment of various serious diseases.[217] However, translating these materials from fundamental research to clinical applications faces multifaceted challenges rooted in scientific limitations and engineering constraints. Based on the advancements reviewed herein, we critically analyze unresolved questions and propose actionable strategies for future development.

Central to progress is the optimization of material design to reconcile piezoelectric performance, controlled degradation, and biocompatibility. Natural biomaterials, despite their inherent biocompatibility, exhibit significantly lower piezoelectric coefficients compared to synthetic polymers such as PLLA or inorganic ceramics. This inherent "piezoelectricity-biodegradability trade-off" necessitates innovative engineering strategies, including interface engineering, spatial confinement of polar domains, and advanced processing techniques like electrospinning. Nevertheless, mismatched degradation kinetics—where materials persist beyond therapeutic windows—remain a critical issue. Future designs should prioritize stimuli-responsive degradation mechanisms triggered by pH, enzymatic activity, or ultrasound. Furthermore, integrating piezoelectric systems with transient electronics, such as magnesium-based circuits, could enable self-powered biointerfaces for real-time tissue monitoring and adaptive stimulation.

In clinical translation, early successes in wound healing and bone regeneration highlight the potential of degradable piezoelectrics. Expanding these applications requires addressing unaddressed medical need. Critical barriers include the lack of standardized evaluation frameworks capable of assessing dynamic interactions between piezoelectric materials and biological systems, as well as insufficient long-term biosafety data. Current ISO standards fail to account for time-varying electrical properties during material degradation, while chronic immune responses to degradation byproducts, such as lactic acid from polylactic acid (PLA), demand systematic investigation.

Looking beyond conventional therapeutic paradigms, future opportunities lie in merging piezoelectric materials with synthetic biology and intelligent systems. Electrogenetic interfaces, for instance, could translate mechanical energy into direct-current fields to modulate voltage-sensitive ion channels without genetic modification. Concurrently, closed-loop biohybrid systems integrating degradable piezoelectrics with AI-driven biosensors may enable adaptive tissue remodeling, such as scaffolds that dynamically adjust mechanical properties based on physiological cues.

In conclusion, degradable piezoelectric materials lie at the intersection of biomimetics, electronics, and regenerative medicine. Realizing their full potential requires interdisciplinary collaboration spanning materials science, computational modeling, and clinical trial design. By harmonizing material innovation with a deeper understanding of bioelectrical pathophysiology, this field could deliver intelligent electrostimulation therapies capable of restoring the body's intrinsic electrical balance, thereby revolutionizing treatments for neurological, cardiovascular, and degenerative disorders.

Acknowledgements

This work was supported by Beijing Natural Science Foundation (L245015; Z240022); National Natural Science Foundation of China (No. T2125003); The Fundamental Research Funds for the Central Universities and National Natural Science Foundation of China (NO: 32571629).

Conflict of Interest

The authors declare no conflict of interest.

Author Contributions

Z.W. and C.C. contributed equally to this work.

Keywords

biodegradable, biomaterials, medical applications, piezoelectricity

Received: July 28, 2025
Revised: October 18, 2025
Published online:

[1] B. Jaffe, R. S. Roth, S. Marzullo, *J. Appl. Phys.* **1954**, *25*, 809.
[2] V. S. Bystrov, I. K. Bdikin, A. Heredia, R. C. Pullar, E. D. Mishina, A. S. Sigov, A. L. Kholkin, in *Piezoelectric Nanomaterials for Biomedical Applications*, Springer, Berlin, Heidelberg **2012**, pp. 187.
[3] R. Patel, S. McWilliam, A. A. Popov, *Smart Mater. Struct.* **2014**, *23*, 085002.
[4] K. G. Aktas, I. Esen, *Eng. Technol. Appl. Sci. Res.* **2020**, *10*, 6549.
[5] M. Gebhardt, S. Kurz, F. Grundmann, T. Klink, V. Slowik, C.-E. Heyde, H. Steinke, *bioRxiv* **2024**, *1*, 586492.

[6] D. J. Riemersma, H. C. Schamhardt, *Res. Vet. Sci.* **1985**, *39*, 263.
[7] X. Li, X. Liao, Z. Jia, S. Liu, P. Li, L. Li, W. Zhang, X. Niu, Y. Fan, *Compos. Part B Eng.* **2024**, *283*, 111603.
[8] V. J. González, A. M. Rodríguez, I. Payo, E. Vázquez, *Nanoscale Horiz.* **2020**, *5*, 331.
[9] L. Csoka, I. C. Hoeger, O. J. Rojas, I. Peszlen, J. J. Pawlak, P. N. Peralta, *ACS Macro Lett.* **2012**, *1*, 867.
[10] J. Xia, J. Huang, Y. Zhao, C.-l. Feng, *ACS Nano* **2023**, *17*, 10280.
[11] T. Zheng, Y. Yu, Y. Pang, D. Zhang, Y. Wang, H. Zhao, X. Zhang, H. Leng, X. Yang, Q. Cai, *Compos. Part B Eng.* **2022**, *234*, 109734.
[12] M. Yan, S. Liu, Q. Xu, Z. Xiao, X. Yuan, K. Zhou, D. Zhang, Q. Wang, C. Bowen, J. Zhong, Y. Zhang, *Nano Energy* **2023**, *106*, 108096.
[13] Z. H. Liu, C. T. Pan, L. W. Lin, J. C. Huang, Z. Y. Ou, *Smart Mater. Struct.* **2014**, *23*, 025003.
[14] S.-M. Chang, S. Hur, J. Park, D.-G. Lee, J. Shin, H. S. Kim, S. E. Song, J. M. Baik, M. Kim, H.-C. Song, C.-Y. Kang, *Addit. Manuf.* **2023**, *67*, 103470.
[15] P. Martins, A. Lasheras, J. Gutierrez, J. M. Barandiaran, I. Orue, S. Lanceros-Mendez, *J. Phys. D: Appl. Phys.* **2011**, *44*, 495303.
[16] J. Curie, P. Curie, *Bull. Minéral.* **1880**, *3*, 90.
[17] L. Jiang, B. Wu, X. Wei, X. Lv, H. Xue, G. Lu, Y. Zeng, J. Xing, W. Wu, J. Wu, *Mater. Horiz.* **2022**, *9*, 2180.
[18] B. Yaghootkar, S. Azimi, B. Bahreyni, *IEEE Sens. J.* **2017**, *17*, 4005.
[19] K. Parida, V. Bhavanasi, V. Kumar, R. Bendi, P. S. Lee, *Nano Res.* **2017**, *10*, 3557.
[20] R. E. JAEGER, L. EGERTON, *J. Am. Ceram. Soc.* **1962**, *45*, 209.
[21] Z. L. Wang, J. Song, *Science* **2006**, *312*, 242.
[22] S. Guerin, A. Stapleton, D. Chovan, R. Mouras, M. Gleeson, C. McKeown, M. R. Noor, C. Silien, F. M. F. Rhen, A. L. Kholkin, N. Liu, T. Soulimane, S. A. M. Tofail, D. Thompson, *Nat. Mater.* **2018**, *17*, 180.
[23] S. Trolier-McKinstry, in *Piezoelectric and Acoustic Materials for Transducer Application*, Springer US, Boston, MA, USA **2008**, p. 39.
[24] T. Someya, Permanent Polarity and Piezoelectricity of Electrospun α-Helical Poly(α-Amino Acid) Fibers, John Wiley & Sons, Hoboken, NJ, USA **2012**.
[25] J. Kim, K. J. Loh, J. P. Lynch, presented at Proc. of the ASME 2008 Conf. on Smart Materials, Adaptive Structures and Intelligent Systems. Smart Materials, Adaptive Structures and Intelligent Systems, Ellicott City, MD, USA, October **2008**.
[26] H. Liu, X. Bi, H. Lu, R. Hu, T. Lan, X. Wang, M. Huang, *J. Asian Earth Sci.* **2018**, *161*, 35.
[27] C. Chang, V. H. Tran, J. Wang, Y.-K. Fuh, L. Lin, *Nano Lett.* **2010**, *10*, 726.
[28] K. Refson, P. R. Tulip, S. J. Clark, *Phys. Rev. B* **2006**, *73*, 155114.
[29] R. M. F. Baptista, B. Silva, J. Oliveira, B. Almeida, C. Castro, P. V. Rodrigues, A. Machado, E. d. M. Gomes, M. Belsley, *Micro* **2024**, *4*, 196.
[30] P. R. Tulip, S. J. Clark, *J. Chem. Phys.* **2004**, *121*, 5201.
[31] Y. Zhang, Y. Bao, D. Zhang, C. R. Bowen, *J. Am. Ceram. Soc.* **2015**, *98*, 2980.
[32] Y. Bai, H. Meng, Z. Li, Z. L. Wang, *Med Mat* **2024**, *1*, 40.
[33] D. Farrar, K. Ren, D. Cheng, S. Kim, W. Moon, W. L. Wilson, J. E. West, S. M. Yu, *Adv. Mater.* **2011**, *23*, 3954.
[34] H.-Y. Son, S.-S. Park, *Mater. Today Sustain.* **2024**, *25*, 100689.
[35] D. Vasilescu, R. Cornillon, G. Mallet, *Nature* **1970**, *225*, 635.
[36] G. S. Ducker, J. D. Rabinowitz, *Cell Metab.* **2017**, *25*, 27.
[37] V. V. Lemanov, *Ferroelectrics* **2000**, *238*, 211.
[38] Z. Zhang, X. Li, Z. Peng, X. Yan, S. Liu, Y. Hong, Y. Shan, X. Xu, L. Jin, B. Liu, X. Zhang, Y. Chai, S. Zhang, A. K. Y. Jen, Z. Yang, *Nat. Commun.* **2023**, *14*, 4094.
[39] E. Seyedhosseini, K. Romanyuk, D. Vasileva, S. Vasilev, A. Nuraeva, P. Zelenovskiy, M. Ivanov, A. N. Morozovska, V. Y. Shur, H. Lu, A. Gruverman, A. L. Kholkin, *ACS Appl. Mater. Interfaces* **2017**, *9*, 20029.
[40] E. S. Hosseini, L. Manjakkal, D. Shakthivel, R. Dahiya, *ACS Appl. Mater. Interfaces* **2020**, *12*, 9008.
[41] M. T. Chorsi, T. T. Le, F. Lin, T. Vinikoor, R. Das, J. F. Stevens, C. Mundrane, J. Park, K. T. M. Tran, Y. Liu, J. Pfund, R. Thompson, W. He, M. Jain, M. D. Morales-Acosta, O. R. Bilal, K. Kazerounian, H. Ilies, T. D. Nguyen, *Sci. Adv.* **2023**, *9*, adg6075.
[42] Q. Lin, Y. Zhang, L. Chen, H. Zhang, C. An, C. Li, Q. Wang, J. Song, W. He, H. Wang, *Regen. Biomater.* **2024**, *11*, rbae047.
[43] Z. Wang, Z. Zhang, Z. Peng, X. Yang, X. Li, Y. Shan, B. Liu, X. Xu, Y. Gao, Z. Yang, *Nano Mater. Sci.* **2025**, *7*, 113.
[44] Q. Jiang, M. D. Ward, *Chem. Soc. Rev.* **2014**, *43*, 2066.
[45] I. S. Lee, K. T. Kim, A. Y. Lee, A. S. Myerson, *Cryst. Growth Des.* **2008**, *8*, 108.
[46] E. Seyedhosseini, M. Ivanov, V. Bystrov, I. Bdikin, P. Zelenovskiy, V. Y. Shur, A. Kudryavtsev, E. D. Mishina, A. S. Sigov, A. L. Kholkin, *Cryst. Growth Des.* **2014**, *14*, 2831.
[47] S. Ukasi, P. Jutapukti, C. Ninthub, N. Pinpru, P. Pakawanit, W. Vittayakorn, S. Pongampai, N. Vittayakorn, T. Charoonsuk, *Nano Energy* **2024**, *119*, 109045.
[48] F. Yang, J. Li, Y. Long, Z. Zhang, L. Wang, J. Sui, Y. Dong, Y. Wang, R. Taylor, D. Ni, W. Cai, P. Wang, T. Hacker, X. Wang, *Science* **2021**, *373*, 337.
[49] J. Sui, J. Li, L. Gu, C. A. Schmidt, Z. Zhang, Y. Shao, E. Gazit, P. U. P. A. Gilbert, X. Wang, *J. Mater. Chem. B* **2022**, *10*, 6958.
[50] Q. Yu, Y. Bai, Z. Li, F. Jiang, R. Luo, Y. Gai, Z. Liu, L. Zhou, Y. Wang, C. Li, K. Ren, D. Luo, H. Meng, Z. Li, *Nano Energy* **2024**, *121*, 109196.
[51] S. Guerin, J. O'Donnell, E. U. Haq, C. McKeown, C. Silien, F. M. F. Rhen, T. Soulimane, S. A. M. Tofail, D. Thompson, *Phys. Rev. Lett.* **2019**, *122*, 047701.
[52] B. Jeon, D. Han, G. Yoon, *iScience* **2023**, *26*, 105768.
[53] J. Li, C. Carlos, H. Zhou, J. Sui, Y. Wang, Z. Silva-Pedraza, F. Yang, Y. Dong, Z. Zhang, T. A. Hacker, B. Liu, Y. Mao, X. Wang, *Nat. Commun.* **2023**, *14*, 6562.
[54] C. Cai, J. Lin, Y. Lu, Q. Zhang, L. Wang, *Chem. Soc. Rev.* **2016**, *45*, 5985.
[55] C. A. Petroff, G. Cassone, J. Šponer, G. R. Hutchison, *Adv. Mater.* **2021**, *33*, 2007486.
[56] K. Tao, W. Hu, B. Xue, D. Chovan, N. Brown, L. J. W. Shimon, O. Maraba, Y. Cao, S. A. M. Tofail, D. Thompson, J. Li, R. Yang, E. Gazit, *Adv. Mater.* **2019**, *31*, 1807481.
[57] K. Ryan, J. Beirne, G. Redmond, J. I. Kilpatrick, J. Guyonnet, N.-V. Buchete, A. L. Kholkin, B. J. Rodriguez, *ACS Appl. Mater. Interfaces* **2015**, *7*, 12702.
[58] J. Anderson, P. T. Lake, M. McCullagh, *J. Phys. Chem. B* **2018**, *122*, 12331.
[59] J. Zhao, Q. Liu, X. Tong, Y. Wang, K. Cai, W. Ji, *Adv. Funct. Mater.* **2024**, *34*, 2401466.
[60] H. Park, Y. Kim, Y. Kim, C. Lee, H. Park, H. Joo, J. Hun Lee, J.-H. Lee, *Appl. Surf. Sci.* **2023**, *618*, 156588.
[61] Y. Kim, H. Park, Y. Kim, C. Lee, H. Park, J.-H. Lee, *ACS Appl. Mater. Interfaces* **2022**, *14*, 38778.
[62] K. Jenkins, S. Kelly, V. Nguyen, Y. Wu, R. Yang, *Nano Energy* **2018**, *51*, 317.
[63] Z. Tao, H. Yuan, S. Ding, Y. Wang, W. Hu, R. Yang, *Nano Energy* **2021**, *88*, 106229.
[64] J.-H. Lee, K. Heo, K. Schulz-Schönhagen, J. H. Lee, M. S. Desai, H.-E. Jin, S.-W. Lee, *ACS Nano* **2018**, *12*, 8138.
[65] J. Ma, L. Qian, F. Jin, W. Zheng, T. Li, Z. Wei, T. Wang, Z.-Q. Feng, *Adv. Fiber Mater.* **2025**, *7*, 338.
[66] H. Yuan, P. Han, Z. Tao, B. Xue, Y. Guo, D. Levy, W. Hu, Y. Wang, Y. Cao, E. Gazit, R. Yang, *ACS Appl. Mater. Interfaces* **2022**, *14*, 6538.
[67] Y. Hwang, Y. Je, D. Farrar, J. E. West, S. M. Yu, W. Moon, *Polymer* **2011**, *52*, 2723.
[68] E. N. Harvey, *Science* **1939**, *89*, 460.

[69] Y. Guo, X.-S. Zhang, Y. Wang, W. Gong, Q. Zhang, H. Wang, J. Brugger, *Nano Energy* **2018**, *48*, 152.
[70] I. Chiesa, C. De Maria, M. R. Ceccarini, L. Mussolin, R. Coletta, A. Morabito, R. Tonin, M. Calamai, A. Morrone, T. Beccari, L. Valentini, *ACS Appl. Mater. Interfaces* **2022**, *14*, 19253.
[71] S. K. Ghosh, D. Mandal, *ACS Sustain. Chem. Eng.* **2017**, *5*, 8836.
[72] L. Wang, T. Cheng, W. Lian, M. Zhang, B. Lu, B. Dong, K. Tan, C. Liu, C. Shen, *Carbohydr. Polym.* **2022**, *275*, 118740.
[73] S. K. Ghosh, F. Matino, F. L. Favrin, I. Tonazzini, R. D'Orsi, J. G. de la Ossa, A. Camposeo, J. Li, W. Liu, T. A. Hacker, D. Pisignano, A. Operamolla, X. Wang, L. Persano, *Sci. Adv.* **2025**, *11*, ads0778.
[74] T. Wu, Y. Song, Z. Shi, D. Liu, S. Chen, C. Xiong, Q. Yang, *Nano Energy* **2021**, *80*, 105541.
[75] N. Sriplai, R. Mangayil, A. Pammo, V. Santala, S. Tuukkanen, S. Pinitsoontorn, *Carbohydr. Polym.* **2020**, *231*, 115730.
[76] G. Zhang, Q. Liao, Z. Zhang, Q. Liang, Y. Zhao, X. Zheng, Y. Zhang, *Adv. Sci.* **2016**, *3*, 1500257.
[77] Y. Luo, H. Luo, X. Yang, X. Ding, K. Wang, M. Zhang, J. Wei, Y. An, J. Xu, H. He, J. Wu, *Int. J. Biol. Macromol.* **2024**, *282*, 136486.
[78] D. Denning, J. I. Kilpatrick, E. Fukada, N. Zhang, S. Habelitz, A. Fertala, M. D. Gilchrist, Y. Zhang, S. A. M. Tofail, B. J. Rodriguez, *ACS Biomater. Sci. Eng.* **2017**, *3*, 929.
[79] E. Fukada, *Wood Sci. Technol.* **1968**, *2*, 299.
[80] E. Fukada, *J. Phys. Soc. Jpn.* **1955**, *10*, 149.
[81] Y. Song, Z. Shi, G.-H. Hu, C. Xiong, A. Isogai, Q. Yang, *J. Mater. Chem. A* **2021**, *9*, 1910.
[82] Y. Song, T. Wu, J. Bao, M. Xu, Q. Yang, L. Zhu, Z. Shi, G.-H. Hu, C. Xiong, *Carbohydr. Polym.* **2022**, *288*, 119407.
[83] B. Duan, Y. Huang, A. Lu, L. Zhang, *Prog. Polym. Sci.* **2018**, *82*, 1.
[84] D. Lingait, R. Rahagude, S. S. Gaharwar, R. S. Das, M. G. Verma, N. Srivastava, A. Kumar, S. Mandavgane, *Int. J. Biol. Macromol.* **2024**, *257*, 128676.
[85] J. Li, S. Zhuang, *Eur. Polym. J.* **2020**, *138*, 109984.
[86] A. Verlee, S. Mincke, C. V. Stevens, *Carbohydr. Polym.* **2017**, *164*, 268.
[87] R. M. Street, T. Huseynova, X. Xu, P. Chandrasekaran, L. Han, W. Y. Shih, W.-H. Shih, C. L. Schauer, *Carbohydr. Polym.* **2018**, *195*, 218.
[88] E. Capuana, F. Lopresti, M. Ceraulo, V. L. Carrubba, *Polymers* **2022**, *14*, 1153.
[89] D. Shi, Y. Kang, G. Zhang, C. Gao, W. Lu, C. Yang, H. Zou, H. Jiang, *Polym. Degrad. Stab.* **2018**, *158*, 148.
[90] R. Fitzgerald, L. M. Bass, D. J. Goldberg, M. H. Graivier, Z. P. Lorenc, *Aesthet. Surg. J.* **2018**, *38*, S13.
[91] P. Simamora, W. Chern, *J. Drugs Dermatol.* **2006**, *5*, 436.
[92] Y. Wu, Y. Ma, H. Zheng, S. Ramakrishna, *Mater. Des.* **2021**, *211*, 110164.
[93] Y. Dai, T. Lu, M. Shao, F. Lyu, *Front. Bioeng. Biotechnol.* **2022**, *10*, 1011783.
[94] Y. Tajitsu, *Ferroelectrics* **2015**, *480*, 32.
[95] D. da Silva, M. Kaduri, M. Poley, O. Adir, N. Krinsky, J. Shainsky-Roitman, A. Schroeder, *Chem. Eng. J.* **2018**, *340*, 9.
[96] S. Lee, M. K. Joshi, A. P. Tiwari, B. Maharjan, K. S. Kim, Y.-H. Yun, C. H. Park, C. S. Kim, *Chem. Eng. J.* **2018**, *347*, 771.
[97] S. Farah, D. G. Anderson, R. Langer, *Adv. Drug Deliv. Rev.* **2016**, *107*, 367.
[98] Y. Tajitsu, *IEEE Trans. Ultrason. Ferroelectr. Freq. Control* **2013**, *60*, 1625.
[99] M. Ando, H. Kawamura, H. Kitada, Y. Sekimoto, T. Inoue, Y. Tajitsu, *Jpn. J. Appl. Phys.* **2013**, *52*, 09KD17.
[100] M. Ando, H. Kawamura, H. Kitada, Y. Sekimoto, T. Inoue, Y. Tajitsu, presented at *2013 Joint IEEE Int. Symposium on Applications of Ferroelectric and Workshop on Piezoresponse Force Microscopy (ISAF/PFM)*, Trague, Czech Republic, July **2013**.
[101] S. Gong, B. Zhang, J. Zhang, Z. L. Wang, K. Ren, *Adv. Funct. Mater.* **2020**, *30*, 1908724.
[102] P. Chen, C. Xu, P. Wu, K. Liu, F. Chen, Y. Chen, H. Dai, Z. Luo, *ACS Nano* **2022**, *16*, 16513.
[103] E. J. Curry, K. Ke, M. T. Chorsi, K. S. Wrobel, A. N. Miller, A. Patel, I. Kim, J. Feng, L. Yue, Q. Wu, C.-L. Kuo, K. W.-H. Lo, C. T. Laurencin, H. Ilies, P. K. Purohit, T. D. Nguyen, *Proc. Natl. Acad. Sci. USA* **2018**, *115*, 909.
[104] M. Ali, S. M. Hoseyni, R. Das, M. Awais, I. Basdogan, L. Beker, *Adv. Mater. Technol.* **2023**, *8*, 2300347.
[105] E. J. Curry, T. T. Le, R. Das, K. Ke, E. M. Santorella, D. Paul, M. T. Chorsi, K. T. M. Tran, J. Baroody, E. R. Borges, B. Ko, A. Golabchi, X. Xin, D. Rowe, L. Yue, J. Feng, M. D. Morales-Acosta, Q. Wu, I.-P. Chen, X. T. Cui, J. Pachter, T. D. Nguyen, *Proc. Natl. Acad. Sci. USA* **2020**, *117*, 214.
[106] T. Li, Y. Yuan, L. Gu, J. Li, Y. Shao, S. Yan, Y. Zhao, C. Carlos, Y. Dong, H. Qian, X. Wang, W. Wu, S. Wang, Z. Wang, X. Wang, *Sci. Adv.* **2024**, *10*, adn8706.
[107] S. K. Ghosh, S. Pal, K. Roy, W. Yue, Y. Gao, F. Xia, P. He, S. Sarkar, M. Teng, J. Park, P. Tsao, X. Li, S. A. M. Tofail, P. B. Messersmith, L. Lin, *Adv. Mater.* **2025**, *37*, 2507859.
[108] Z. Li, C. Li, W. Sun, Y. Bai, Z. Li, Y. Deng, *ACS Appl. Mater. Interfaces* **2023**, *15*, 12787.
[109] G. Zhao, B. Huang, J. Zhang, A. Wang, K. Ren, Z. L. Wang, *Macromol. Mater. Eng.* **2017**, *302*, 1600476.
[110] A. Sultana, S. K. Ghosh, V. Sencadas, T. Zheng, M. J. Higgins, T. R. Middya, D. Mandal, *J. Mater. Chem. B* **2017**, *5*, 7352.
[111] S. J. Lee, A. P. Arun, K. J. Kim, *Mater. Lett.* **2015**, *148*, 58.
[112] V. A. Zhuikov, A. P. Bonartsev, D. V. Bagrov, S. G. Yakovlev, V. L. Myshkina, T. K. Makhina, I. V. Bessonov, M. N. Kopitsyna, A. S. Morozov, A. A. Rusakov, A. S. Useinov, K. V. Shaitan, G. A. Bonartseva, *Mol. Cryst. Liq. Cryst.* **2017**, *648*, 236.
[113] H. Vieyra, E. Juárez, U. F. López, A. G. Morales, M. Torres, *Biomed. Mater.* **2018**, *13*, 045011.
[114] Y. Ando, E. Fukada, *J. Polym. Sci.: Polym. Phys. Ed.* **1984**, *22*, 1821.
[115] E. Fukada, Y. Ando, *Int. J. Biol. Macromol.* **1986**, *8*, 361.
[116] W. J. Orts, R. H. Marchessault, T. L. Bluhm, G. K. Hamer, *Macromolecules* **1990**, *23*, 5368.
[117] P. J. Dobson, *Phys. Bullet.* **1985**, *36*, 506.
[118] I. S. Vatlin, R. V. Chernozem, A. S. Timin, A. P. Chernova, E. V. Plotnikov, Y. R. Mukhortova, M. A. Surmeneva, R. A. Surmenev, *Polymers* **2020**, *12*, 240.
[119] R. V. Chernozem, K. N. Romanyuk, I. Grubova, P. V. Chernozem, M. A. Surmeneva, Y. R. Mukhortova, M. Wilhelm, T. Ludwig, S. Mathur, A. L. Kholkin, E. Neyts, B. Parakhonskiy, A. G. Skirtach, R. A. Surmenev, *Nano Energy* **2021**, *89*, 106473.
[120] R. Sheng, J. Mu, R. V. Chernozem, Y. R. Mukhortova, M. A. Surmeneva, I. O. Pariy, T. Ludwig, S. Mathur, C. Xu, R. A. Surmenev, H. H. Liu, *ACS Appl. Mater. Interfaces* **2023**, *15*, 3731.
[121] H. Li, L. Zhao, J. Meng, C. Pan, Y. Zhang, Y. Zhang, Z. Liu, Y. Zou, Y. Fan, Z. L. Wang, Z. Li, *Nano Today* **2020**, *33*, 100873.
[122] J. Bian, N. Wang, J. Ma, Y. Jie, J. Zou, X. Cao, *Nano Energy* **2018**, *47*, 442.
[123] Y. Long, Y. Chen, Y. Liu, G. Chen, W. Guo, X. Kang, X. Pu, W. Hu, Z. L. Wang, *Nanoscale* **2020**, *12*, 12753.
[124] E. M. Ahmed, *J. Adv. Res.* **2015**, *6*, 105.
[125] Y. S. Zhang, A. Khademhosseini, *Science* **2017**, *17*, eaaf3627.
[126] C. Wang, T. Yokota, T. Someya, *Chem. Rev.* **2021**, *121*, 2109.
[127] T. Jungst, W. Smolan, K. Schacht, T. Scheibel, J. Groll, *Chem. Rev.* **2016**, *116*, 1496.
[128] S. Correa, A. K. Grosskopf, H. L. Hernandez, D. Chan, A. C. Yu, L. M. Stapleton, E. A. Appel, *Chem. Rev.* **2021**, *121*, 11385.
[129] Y. Du, W. Du, D. Lin, M. Ai, S. Li, L. Zhang, *Micromachines* **2023**, *14*, 167.

[130] B. X. Wang, W. Xu, Z. Yang, Y. Wu, F. Pi, *Macromol. Rapid Commun.* **2022**, *43*, 2100785.
[131] S. Sun, R. Yuan, S. Ling, T. Zhou, Z. Wu, M. Fu, H. He, X. Li, C. Zhang, *ACS Appl. Mater. Interfaces* **2024**, *16*, 7826.
[132] S. Liu, F. Manshaii, J. Chen, X. Wang, S. Wang, J. Yin, M. Yang, X. Chen, X. Yin, Y. Zhou, *Nano-Micro Lett.* **2024**, *17*, 44.
[133] S. Guerin, T. A. M. Syed, D. Thompson, *Nanoscale* **2018**, *10*, 9653.
[134] P. Zelenovskiy, I. Kornev, S. Vasilev, A. Kholkin, *Phys. Chem. Chem. Phys.* **2016**, *18*, 29681.
[135] E. Fukada, *IEEE Trans. Ultrason. Ferroelectr. Freq. Control* **2000**, *47*, 1277.
[136] R. L. Horan, K. Antle, A. L. Collette, Y. Wang, J. Huang, J. E. Moreau, V. Volloch, D. L. Kaplan, G. H. Altman, *Biomaterials* **2005**, *26*, 3385.
[137] J. Wang, C. Carlos, Z. Zhang, J. Li, Y. Long, F. Yang, Y. Dong, X. Qiu, Y. Qian, X. Wang, *ACS Appl. Mater. Interfaces* **2020**, *12*, 26399.
[138] E. Praveen, S. Murugan, K. Jayakumar, *RSC Adv.* **2017**, *7*, 35490.
[139] N. A. Hoque, P. Thakur, P. Biswas, M. M. Saikh, S. Roy, B. Bagchi, S. Das, P. P. Ray, *J. Mater. Chem. A* **2018**, *6*, 13848.
[140] J. Zhang, S. Gong, C. Wang, D.-Y. Jeong, Z. L. Wang, K. Ren, *Macromol. Mater. Eng.* **2019**, *304*, 1900259.
[141] H.-Y. Zhang, Y.-Y. Tang, Z.-X. Gu, P. Wang, X.-G. Chen, H.-P. Lv, P.-F. Li, Q. Jiang, N. Gu, S. Ren, R.-G. Xiong, *Science* **2024**, *383*, 1492.
[142] E. A. Neppiras, *J. Sound Vib.* **1972**, *20*, 562.
[143] H. Tsuji, *Macromol. Biosci.* **2005**, *5*, 569.
[144] X. Cui, L. Xu, Y. Shan, J. Li, J. Ji, E. Wang, B. Zhang, X. Wen, Y. Bai, D. Luo, C. Chen, Z. Li, *Sci. Bull.* **2024**, *69*, 1895.
[145] P. Wu, P. Chen, C. Xu, Q. Wang, F. Zhang, K. Yang, W. Jiang, J. Feng, Z. Luo, *Nano Energy* **2022**, *102*, 107707.
[146] M. Niinomi, *J. Mech. Behav. Biomed. Mater.* **2008**, *1*, 30.
[147] R. Sridharan, A. R. Cameron, D. J. Kelly, C. J. Kearney, F. J. O'Brien, *Mater. Today* **2015**, *18*, 313.
[148] Y.-C. Fung, in *Biomechanics: Mechanical Properties of Living Tissues*, Springer, New York **1993**, pp. 500.
[149] X. Cui, L. Wu, C. Zhang, Z. Li, *Adv. Sci.* **2025**, *12*, 2412044.
[150] A. Kaynak, A. Zolfagharian, *Polymers* **2020**, *12*, 1569.
[151] C.-Y. Hsu, C.-C. Chiang, H.-Y. Wen, J.-J. Weng, J.-L. Chen, T.-H. Chen, Y.-H. Chen, *Polymers* **2020**, *12*, 2023.
[152] O. Cegielska, P. Sajkiewicz, *Polymers (Basel)* **2019**, *11*, 1742.
[153] Y. Han, X. You, W. Xing, Z. Zhang, W. Zou, *Bone Res.* **2018**, *6*, 16.
[154] B. Clarke, *Clin. J. Am. Soc. Nephrol.* **2008**, *3*, S131.
[155] Y. Yang, L. Chu, S. Yang, H. Zhang, L. Qin, O. Guillaume, D. Eglin, R. G. Richards, T. Tang, *Acta Biomater.* **2018**, *79*, 265.
[156] Z. Yang, H. Yuan, W. Tong, P. Zou, W. Chen, X. Zhang, *Biomaterials* **1996**, *17*, 2131.
[157] M. Minary-Jolandan, M.-F. Yu, *ACS Nano* **2009**, *3*, 1859.
[158] J. Fu, X. Liu, L. Tan, Z. Cui, Y. Zheng, Y. Liang, Z. Li, S. Zhu, K. W. K. Yeung, X. Feng, X. Wang, S. Wu, *ACS Nano* **2019**, *13*, 13581.
[159] R. Siddappa, A. Martens, J. Doorn, A. Leusink, C. Olivo, R. Licht, L. van Rijn, C. Gaspar, R. Fodde, F. Janssen, C. van Blitterswijk, J. de Boer, *Proc. Natl. Acad. Sci. USA* **2008**, *105*, 7281.
[160] Z. Tang, S. Chen, Y. Ni, R. Zhao, X. Zhu, X. Yang, X. Zhang, *Acta Biomater.* **2021**, *129*, 293.
[161] M. Bez, D. Sheyn, W. Tawackoli, P. Avalos, G. Shapiro, J. C. Giaconi, X. Da, S. B. David, J. Gavrity, H. A. Awad, H. W. Bae, E. J. Ley, T. J. Kremen, Z. Gazit, K. W. Ferrara, G. Pelled, D. Gazit, *Sci. Transl. Med.* **2017**, *9*, aal3128.
[162] X. Zhang, W. Jiang, C. Xie, X. Wu, Q. Ren, F. Wang, X. Shen, Y. Hong, H. Wu, Y. Liao, Y. Zhang, R. Liang, W. Sun, Y. Gu, T. Zhang, Y. Chen, W. Wei, S. Zhang, W. Zou, H. Ouyang, *Nat. Commun.* **2022**, *13*, 5211.
[163] T. Vinikoor, G. K. Dzidotor, T. T. Le, Y. Liu, H.-M. Kan, S. Barui, M. T. Chorsi, E. J. Curry, E. Reinhardt, H. Wang, P. Singh, M. A. Merriman, E. D'Orio, J. Park, S. Xiao, J. H. Chapman, F. Lin, C.-S. Truong, S. Prasadh, L. Chuba, S. Killoh, S.-W. Lee, Q. Wu, R. M. Chidambaram, K. W. H. Lo, C. T. Laurencin, T. D. Nguyen, *Nat. Commun.* **2023**, *14*, 6257.
[164] Y. Xu, C. Xu, H. Song, X. Feng, L. Ma, X. Zhang, G. Li, C. Mu, L. Tan, Z. Zhang, Z. Liu, Z. Luo, C. Yang, *J. Nanobiotechnol.* **2024**, *22*, 250.
[165] S. Yao, X. Cui, C. Zhang, W. Cui, Z. Li, *Biomaterials* **2025**, *320*, 123288.
[166] M. Griffin, A. Bayat, *Eplasty* **2011**, *11*, 34.
[167] G. Victoria, B. Petrisor, B. Drew, D. Dick, *Indian J. Orthop.* **2009**, *43*, 117.
[168] A. Cui, H. Li, D. Wang, J. Zhong, Y. Chen, H. Lu, *eClinicalMedicine* **2020**, *29–30*, 100587.
[169] J. Lin, W. Zhang, A. Jones, M. Doherty, *BMJ* **2004**, *329*, 324.
[170] S. H. Bhang, W. S. Jang, J. Han, J.-K. Yoon, W.-G. La, E. Lee, Y. S. Kim, J.-Y. Shin, T.-J. Lee, H. K. Baik, B.-S. Kim, *Adv. Funct. Mater.* **2017**, *27*, 1603497.
[171] M. Wu, Z. Zhang, Z. Liu, J. Zhang, Y. Zhang, Y. Ding, T. Huang, D. Xiang, Z. Wang, Y. Dai, X. Wan, S. Wang, H. Qian, Q. Sun, L. Li, *Nano Today* **2021**, *37*, 101104.
[172] D. Liu, X. Wang, C. Gao, Z. Zhang, Q. Wang, Y. Pei, H. Wang, Y. Tang, K. Li, Y. Yu, Q. Cai, X. Zhang, *Adv. Mater.* **2024**, *36*, 2409400.
[173] P. Wu, L. Shen, H. F. Liu, X. H. Zou, J. Zhao, Y. Huang, Y. F. Zhu, Z. Y. Li, C. Xu, L. H. Luo, Z. Q. Luo, M. H. Wu, L. Cai, X. K. Li, Z. G. Wang, *Mil. Med. Res.* **2023**, *10*, 35.
[174] A. Marrella, T. Y. Lee, D. H. Lee, S. Karuthedom, D. Syla, A. Chawla, A. Khademhosseini, H. L. Jang, *Mater. Today* **2018**, *21*, 362.
[175] X.-D. Wang, S.-Y. Li, S.-J. Zhang, A. Gupta, C.-P. Zhang, L. Wang, *Theranostics* **2020**, *10*, 4839.
[176] Z. Zhang, F. Wang, X. Huang, H. Sun, J. Xu, H. Qu, X. Yan, W. Shi, W. Teng, X. Jin, Z. Shao, Y. Zhang, S. Zhao, Y. Wu, Z. Ye, X. Yu, *Adv. Sci.* **2023**, *10*, 2206155.
[177] Y. X. Ma, K. Jiao, Q. Q. Wan, J. Li, M. Y. Liu, Z. B. Zhang, W. Qin, K. Y. Wang, Y. Z. Wang, F. R. Tay, L. N. Niu, *Bioact Mater* **2022**, *9*, 475.
[178] Z. Li, C. A. Meyers, L. Chang, S. Lee, Z. Li, R. Tomlinson, A. Hoke, T. L. Clemens, A. W. James, *J. Clin. Invest.* **2019**, *129*, 5137.
[179] L. Leitão, E. Neto, F. Conceição, A. Monteiro, M. Couto, C. J. Alves, D. M. Sousa, M. Lamghari, *Bone Res.* **2020**, *8*, 20.
[180] F. Rao, Y. Wang, D. Zhang, C. Lu, Z. Cao, J. Sui, M. Wu, Y. Zhang, W. Pi, B. Wang, Y. Kou, X. Wang, P. Zhang, B. Jiang, *Theranostics* **2020**, *10*, 1590.
[181] X. Cui, Y. Shan, J. Li, M. Xiao, Y. Xi, J. Ji, E. Wang, B. Zhang, L. Xu, M. Zhang, Z. Li, Y. Zhang, *Adv. Funct. Mater.* **2024**, *34*, 2403759.
[182] S. Lee, M. Patel, R. Patel, *Eur. Polym. J.* **2022**, *181*, 111663.
[183] P. Zarrintaj, E. Zangene, S. Manouchehri, L. M. Amirabad, N. Baheiraei, M. R. Hadjighasem, M. Farokhi, M. R. Ganjali, B. W. Walker, M. R. Saeb, M. Mozafari, S. Thomas, N. Annabi, *Appl. Mater. Today* **2020**, *20*, 100784.
[184] S. Behtaj, J. A. K. Ekberg, J. A. St John, *Pharmaceutics* **2022**, *14*, 219.
[185] S. Houshyar, A. Bhattacharyya, R. Shanks, *ACS Chem. Neurosci.* **2019**, *10*, 3349.
[186] C. Ribeiro, V. Sencadas, D. M. Correia, S. Lanceros-Méndez, *Colloids Surf. B Biointerfaces* **2015**, *136*, 46.
[187] Y. Ma, H. Wang, Q. Wang, X. Cao, H. Gao, *Chem. Eng. J.* **2023**, *452*, 139424.
[188] Z. Zhao, X. Li, Q. Li, *Biomed. Pharmacother.* **2017**, *92*, 1103.
[189] A. E. Krausz, B. L. Adler, V. Cabral, M. Navati, J. Doerner, R. A. Charafeddine, D. Chandra, H. Liang, L. Gunther, A. Clendaniel, S. Harper, J. M. Friedman, J. D. Nosanchuk, A. J. Friedman, *Nanomedicine* **2015**, *11*, 195.
[190] F. Delavar, M. Mohseni, A. Jahandideh, M. Khajehmohammadi, N. Najmoddin, *Int. J. Biol. Macromol.* **2025**, *286*, 137833.
[191] Y. Shan, L. Xu, X. Cui, J. Zhang, H. Ouyang, X. Wang, J. Huang, J. Xue, K. Wang, D. Wang, E. Wang, K. Ren, D. Luo, Z. Li, *Cell Biomater.* **2025**, *1*, 100006.

[192] C. Hu, B. Liu, X. Huang, Z. Wang, K. Qin, L. Sun, Z. Fan, *ACS Nano* **2024**, *18*, 14427.
[193] C. D. McCaig, A. M. Rajnicek, B. Song, M. Zhao, *Physiol. Rev.* **2005**, *85*, 943.
[194] M. Zhao, B. Song, J. Pu, T. Wada, B. Reid, G. Tai, F. Wang, A. Guo, P. Walczysko, Y. Gu, T. Sasaki, A. Suzuki, J. V. Forrester, H. R. Bourne, P. N. Devreotes, C. D. McCaig, J. M. Penninger, *Nature* **2006**, *442*, 457.
[195] R. Luo, J. Dai, J. Zhang, Z. Li, *Adv. Healthcare Mater.* **2021**, *10*, 2100557.
[196] P. Yan, H. Zheng, P. Liu, C. Yan, M. Zhao, S. Ling, Z. Wang, C. Liu, S. H. Tan, K. Liang, S. H. Teoh, *Acta Biomater.* **2025**, *204*, 216.
[197] X. Wang, K. Sun, C. Wang, M. Yang, K. Qian, B. Ye, X. Guo, Y. Shao, C. Chu, F. Xue, J. Li, J. Bai, *Biomaterials* **2025**, *313*, 122803.
[198] R. Das, T. T. Le, B. Schiff, M. T. Chorsi, J. Park, P. Lam, A. Kemerley, A. M. Supran, A. Eshed, N. Luu, N. G. Menon, T. A. Schmidt, H. Wang, Q. Wu, M. Thirunavukkarasu, N. Maulik, T. D. Nguyen, *Biomaterials* **2023**, *301*, 122270.
[199] Y. Xiang, J. Lu, C. Mao, Y. Zhu, C. Wang, J. Wu, X. Liu, S. Wu, K. Y. H. Kwan, K. M. C. Cheung, K. W. K. Yeung, *Sci. Adv.* **2023**, *9*, adf0854.
[200] S. Xie, J. Huang, A. T. Pereira, L. Xu, D. Luo, Z. Li, *BMEMat* **2023**, *1*, 12038.
[201] L. Xu, E. Wang, Y. Kang, D. Fu, L. Luo, Y. Quan, Y. Xi, J. Huang, X. Cui, J. Zeng, D. Jiang, B. Shi, H. Feng, H. Ouyang, C. Chen, Z. Li, *Device* **2025**, *6*, 100721.
[202] L. Cai, T. Sun, F. Han, H. Zhang, J. Zhao, Q. Hu, T. Shi, X. Zhou, F. Cheng, C. Peng, Y. Zhou, S. Long, W. Sun, J. Fan, J. Du, X. Peng, *J. Am. Chem. Soc.* **2024**, *146*, 34188.
[203] L. Cai, F. Han, J. Ding, X. Zhou, T. Shi, F. Cheng, C. Peng, S. Long, W. Sun, J. Fan, J. Du, X. Peng, *ACS Nano* **2025**, *19*, 24067.
[204] H. Xue, J. Jin, X. Huang, Z. Tan, Y. Zeng, G. Lu, X. Hu, K. Chen, Y. Su, X. Hu, X. Peng, L. Jiang, J. Wu, *Nat. Commun.* **2025**, *16*, 2650.
[205] Q. Lv, S. Chen, D. Luo, H. Liu, Y. Song, M. Liu, F. Xiao, Z. Wang, L. Wang, *Adv. Mater.* **2025**, *37*, 2413610.
[206] X. Zhao, J. Li, J. Dai, Z. Qu, X. Li, Y. Wu, S. Hu, J. Fang, Z. Shen, M. Xiao, M. Tang, *Adv. Funct. Mater.* **2025**, *35*, 2418708.
[207] A. Cafarelli, A. Marino, L. Vannozzi, J. Puigmartí-Luis, S. Pané, G. Ciofani, L. Ricotti, *ACS Nano* **2021**, *15*, 11066.
[208] B. Y. Lee, J. Zhang, C. Zueger, W.-J. Chung, S. Y. Yoo, E. Wang, J. Meyer, R. Ramesh, S.-W. Lee, *Nat. Nanotechnol.* **2012**, *7*, 351.
[209] J. Liu, S. Li, S. Zhou, Z. Chen, J. Xu, N. Cui, M. Yuan, B. Li, L. Gu, *Nano Energy* **2024**, *122*, 109310.
[210] J. Hu, S. Liu, Y. Huo, B. Yang, Y. Yin, M.-L. Tan, P. Liu, K. Cai, W. Ji, *Adv. Mater.* **2025**, *37*, 2417409.
[211] T. Su, N. Liu, Y. Gao, D. Lei, L. Wang, Z. Ren, Q. Zhang, J. Su, Z. Zhang, *Nano Energy* **2021**, *87*, 106151.
[212] S. K. Ghosh, J. Park, S. Na, M. P. Kim, H. Ko, *Adv. Sci.* **2021**, *8*, 2005010.
[213] J. Lu, S. Hu, W. Li, X. Wang, X. Mo, X. Gong, H. Liu, W. Luo, W. Dong, C. Sima, Y. Wang, G. Yang, J.-T. Luo, S. Jiang, Z. Shi, G. Zhang, *ACS Nano* **2022**, *16*, 3744.
[214] E. Wang, M. Wu, L. Luo, X. Cui, L. Xu, R. Luo, Y. Zou, T. Le, Y. Shan, Y. Quan, Y. Bai, L. Wu, Y. Hu, S. Cheng, J. Yang, C. Zhu, D. Yu, J. Ji, Y. Ren, D. Jiang, B. Shi, H. Feng, W. Hua, Z. Li, H. Ouyang, *Device* **2025**, *3*, 100724.
[215] Y. Z. Wan, H. Luo, F. He, H. Liang, Y. Huang, X. L. Li, *Compos. Sci. Technol.* **2009**, *69*, 1212.
[216] A. Marino, A. Bargero, G. Ciofani, *Nanomedicine* **2024**, *19*, 1029.
[217] H. Meng, Q. Yu, Z. Liu, Y. Gai, J. Xue, Y. Bai, X. Qu, P. Tan, D. Luo, W. Huang, K. Nie, W. Bai, Z. Hou, R. Tang, H. Xu, Y. Zhang, Q. Cai, X. Yang, Z. L. Wang, Z. Li, *Matter* **2023**, *6*, 4274.

Zijian Wang received his bachelor's degree in Biomedical Engineering from Shenyang Pharmaceutical University in 2024, and is currently pursuing a master's degree in Biomedical Engineering at Shenyang Pharmaceutical University. His research interests mainly focus on novel piezoelectric materials.

Changxu Chen received his Bachelor-s degree from Southern Medical University in 2025. He is currently a Ph.D. student in Biophysics at the School of Nanoscience and Engineering, University of Chinese Academy of Sciences. His research interests mainly focus on piezoelectric bone materials.

Hongyu Meng received his Ph.D. degree from Institute of Chemistry, Chinese Academy of Sciences. Now he is an assistant professor at Beijing Institute of Nano Energy and Systems, Chinese Academy of Sciences. His research interests include biodegradable electronic medical devices, bio-polymer and composite materials.

He Lian received his Ph.D. in Pharmaceutics at Shenyang Pharmaceutical University in 2014. She is currently an Associate professor at School of Medical Devices, Shenyang Pharmaceutical University. Her scientific interests are focused on development of novel electroactive material, drug delivery, and cancer treatment.

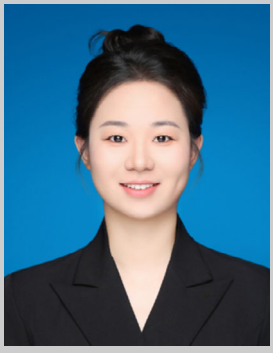

Xi Cui received her Ph.D. degree at Beijing Institute of Nanoenergy and Nanosystems, Chinese Academy of Sciences, Beijing, China, in 2024. Her research mainly focuses on piezoelectric bone implant materials.

Chao Zhang received his Ph.D. degree and bachelor's degree from Wuhan University, China, in 2005. Dr. Zhang currently works as the Professor and Deputy Dean at the School of Biomedical Engineering, Sun Yat-Sen University. He does research in Biomaterials, Tissue Engineering, and Materials Chemistry. His current project is 'Implantable biomaterials for bone repair/regeneration.

Zhou Li is a professor in Tsinghua Changgung Hospital, School of Clinical Medicine, School of Biomedical Engineering, Tsinghua University. He received his Ph.D. from Peking University in Department of Biomedical Engineering in 2010, and Bachelor's Degree from Wuhan University in 2004. His research interest focused on bioelectronics, self-powered medical system, nanogenerators, implantable energy harvesting devices, single cell mechanics and nano-biosensors.